JMeXFRI

Journal of the Mexican Federation of Radiology and Imaging

J Mex Fed Radiol Imaging

Volume 2. Number 2, April-June 2023

ISSN: 2938-1215

eISSN: 2696-8444

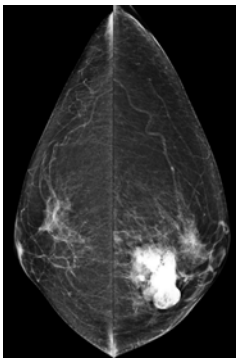

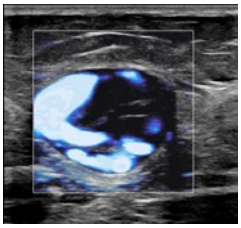

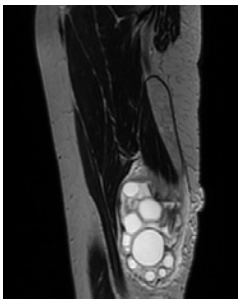

PERMANYER
www.permanyer.com

Official Journal of the

FEDERACIÓN MEXICANA DE RADIOLOGÍA E IMAGEN, A.C

WWW.JMeXFRI.COM

Carestream

Meet the **NEW** member of the family

DRX-Rise

It's amazing!

We have **EQUIPMENT for all YOUR NEEDS**

Right for **Today...** *Ready for Tomorrow.*

Scan the QR and visit the Virtual Hospital

JMeXFRI

Journal of the Mexican Federation of Radiology and Imaging

J Mex Fed Radiol Imaging

Volume 2. Number 2, April-June 2023

ISSN: 2938-1215

eISSN: 2696-8444

The *Journal of the Mexican Federation of Radiology and Imaging* (JMeXFRI) is the official journal of the Federacion Mexicana de Radiologia e Imagen. The aim of the journal is to disseminate scientific knowledge and technological developments for innovation in diagnostic and therapeutic radiology with original articles on basic and clinical aspects of modern radiology in an international context with global impact. JMeXFRI is published in American English with 4 issues per year (print and online) and the first issue was published in the first quarter of 2022. Articles undergo a rigorous, double-blind peer-review process. Publication of articles in JMexFRI is free of charge and all published articles are open access.

The journal publishes the following types of manuscripts: *Full Research Article, Pictorial Essay, Brief Research Article, Technical Note, In-Depth Review, Case Report, Images in Radiology, and Editorial.*

EDITORIAL BOARD

Original papers should be deposited in their electronic version through the following URL:

https://publisher.jmexfri.permanyer.com

PERMANYER
www.permanyer.com

Permanyer Mexico
Temistocles, 315
Col. Polanco, Del. Miguel Hidalgo
11560 Ciudad de Mexico
Tel.: +52 55 2728 5183
mexico@permanyer.com

Permanyer
Mallorca, 310 – Barcelona (Cataluña), España
permanyer@permanyer.com

ISSN: 2696-8444
Ref.: 7608AX232

www.permanyer.com

JMeXFRI

Journal of the Mexican Federation of Radiology and Imaging

Check for updates

EDITORIAL

Radiologists' empowerment through artificial intelligence

Guillermo Elizondo-Riojas

Department of Radiology, University Hospital, Universidad Autonoma de Nuevo Leon, Monterrey, Nuevo Leon, Mexico

ORCID: 0000-0002-9555-430X

On March 5th there was an article in the New York Times[1], and an interview in CNN[2] on March 7th, informing that an artificial intelligence (AI) algorithm detected a breast cancer 4 years before that a radiologist on a mammogram. This is a little misleading since this was a retrospective study and with the "retroscope", as we usually say in medicine, it's very easy to see if something was there. The point is that the computed assisted detection (CAD) system found this without knowing that the images were from the same patient!. It´s not the point to discuss the paper here, but the concept that sooner rather than later, AI will be part of our normal practice. As a matter of fact, on one interview, one of the authors says: *"I'm dreaming about the day when women are going to a breast cancer center and they are asking, 'Do you have A.I. or not?"*.

On March 14th, the "*Pi* Day" (3.14), GPT4 was announced and made public. It has now more contextual features, more processing power, voice recognition, but more importantly for us, the capabilities to process and analyze imaging and contextualize them, let´s say, with the electronic medical record of each patient.

But let´s contextualize this. Radiology is a critical field in modern medicine with medical imaging playing an essential role in the diagnosis and treatment of various diseases. One of the most significant challenges we are facing today is the growing workload and pressure to process large volumes of medical images. AI algorithms have demonstrated an ability to quickly and accurately analyze these images, allowing us to process more cases in less time. By automating routine and repetitive tasks, AI can reduce our workload, freeing up us to focus on more complex cases or engage in direct patient care. Additionally, AI can help to prevent us for the burnout, which is becoming a common issue in our field due to the high and demanding workload.

For example, in busy radiology departments, prioritizing cases based on severity or the likelihood of a critical condition is crucial to ensure that patients with urgent needs are attended promptly. AI can be used to triage cases automatically, evaluating the urgency of each case and flagging those that require immediate attention. This will enable us to focus on the most critical cases first, potentially saving lives and improving patient outcomes, and reducing workload and anxiety associated with the triage process.

Every day, more and more research papers are published describing that the new deep learning and generative transformer algorithms can be trained to recognize subtle patterns and abnormalities in medical images that may be difficult for the human eye to detect. By augmenting our capabilities as radiologists, AI can help us to improve our diagnostic accuracy and minimize the risk of missed or misinterpreted findings. This has the potential to significantly impact patient care, as early and accurate diagnosis is crucial for optimal treatment and prognosis, as the case of breast cancer that was discussed above. Moreover, AI algorithms can continuously learn and improve, resulting in ever-increasing levels of accuracy over time. With the use of ChatGPT-like algorithms, we can even learn from "them," as they now explain why they categorized the findings as they did or why they suggested certain actions for a particular patient[3].

In this context, AI's ability to identify patterns and correlations in large datasets can contribute to the

Corresponding author:
Guillermo Elizondo-Riojas
E-mail: guillermo.elizondorj@uanl.edu.mx

Received for publication: 15-03-2023
Accepted for publication: 22-03-2023
DOI: 10.24875/JMEXFRI.M23000044

Available online: 13-07-2023
J Mex Fed Radiol Imaging. 2023;2(2):79-81
www.JMeXFRI.com

development of personalized medicine. By integrating radiology findings with other patient information, such as electronic medical records, genomics, and other biomarkers, AI can provide a more holistic view of a patient's health. This can help us and other medical specialists develop tailored treatment plans based on each patient's unique needs and circumstances, ultimately leading to better patient outcomes.

In our everyday practice, we are often faced with complex cases and challenging diagnostic dilemmas. AI-driven decision support tools can assist us in making more informed decisions by providing us with relevant clinical information, contextual data, and evidence-based recommendations. This can help improve patient outcomes by ensuring that we have access to the most up-to-date information and can make well-informed decisions regarding diagnosis and treatment.

Besides the patient care and imaging workflow capabilities, AI can also be an important aid for teaching and medical education. The rapid advancements in medical imaging techniques and the increasing complexity of cases necessitate continuous learning and skill development for radiologists. AI-powered teaching tools can help us learn and improve our skills by providing instant feedback, simulating complex cases, and tracking progress over time. These tools can be particularly valuable for trainees and residents, allowing them to learn from real-life cases and receive immediate feedback on their performance. Furthermore, AI-driven education platforms can adapt to the individual learner's needs, identifying areas of weakness and providing targeted training materials, leading to more efficient and effective learning. Some of these "apps" are actually being used by some of our residents in several institutions around the world.

AI also has the potential to facilitate the discovery of new imaging biomarkers (Radiomics), disease associations, and predict treatment outcomes, which can drive the development of new imaging techniques and therapies. By analyzing large datasets and identifying patterns and correlations, AI can uncover previously unrecognized relationships between radiomic and imaging findings and clinical outcomes. This can help to do research on designing more targeted studies, accelerate the development of novel imaging techniques, and ultimately improve patient care.

As radiology is increasingly becoming a multidisciplinary field, with radiologists collaborating with other healthcare professionals, such as oncologists, surgeons, and pathologists to provide comprehensive patient care, AI-powered platforms can help connect us with other specialists, facilitating collaboration on complex cases and fostering a multidisciplinary approach to patient care. By enabling a better communication and data sharing, these platforms can facilitate the diagnostic process and ensure that all patient´s doctors have access to the information they need to make informed decisions.

Last but not least, in the age of patient-centered care, it is essential for patients to understand their medical imaging results and be actively involved in their care. AI-driven tools can help patients better understand their imaging findings by providing clear, easy-to-understand explanations and visualizations. AI tools can empower patients to take an active role in managing their health and make informed decisions about their care. Furthermore, enhanced patient engagement has been linked to improved patient satisfaction and better health outcomes.

In summary, I am sure that AI will revolutionize the field of radiology by augmenting our capabilities and improving our efficiency, accuracy, and patient care. While AI is not intended to replace us, it can support and enhance our work, allowing us to focus on complex cases, engage in direct patient care, and collaborate more effectively with other medical professionals. By combining the strengths of both human and machine intelligence, the integration of AI into radiology has the potential to transform our practice and ultimately lead to better patient outcomes. It is essential for the radiology community to embrace AI and actively participate in its development and implementation to ensure its responsible and ethical use in our specialty[4].

Funding

Not applicable.

Conflicts of interest

No potential conflicts of interest are disclosed by the author.

Ethical disclosures

Protection of Individuals. Not applicable.

Confidentiality of data. Not applicable.

Right to privacy and informed consent. The author declares that there are no ethical responsibilities, since

handling human beings' confidential information was not presented.

REFERENCES

1. Satariano A, Metz C. Using A.I. to Detect Breast Cancer That Doctors Miss. The New York Times. 2023 March; Sect. A:1 www.nytimes.com/2023/03/05/technology/artificial-intelligence-breast-cancer-detection.html.
2. Images show AI detecting breast cancer 4 years before it developed (Video). In: CNN Health. Harlow P. 2023 [accessed 2023, March 14]. Available from: https://edition.cnn.com/videos/health/2023/03/07/artificial-intelligence-breast-cancer-detection-mammogram-cnntm-vpx.cnn.
3. Shen Y, Heacock L, Elias J, Hentel KD, Reig B, Shih G, et al. ChatGPT and Other Large Language Models are Double-edged Swords. Radiology. 2023; 230163. doi:10.1148/radiol.230163.
4. Kitamura FC, do Nascimento FBP, Elizondo-Riojas G, Chavez H, Henriquez Leighton H, Salinas-Miranda E, et al. Forging Connections in Latin America to Advance AI in Radiology. Radiol Artif Intell. 2022;4(5): e220125. doi:10.1148/ryai.220125.

JMeXFRI

Journal of the Mexican Federation of Radiology and Imaging

Check for updates

IN-DEPTH REVIEW

Imaging evaluation of congenital pediatric neck pathologies

Nitesh Shekhrajka[1,a], Felice D'Arco[2], Richard Wiggins[3], and Amy Juliano[1]*

[1]Department of Radiology, Massachusetts Eye and Ear Infirmary, Boston MA, USA; [2]Department of Radiology, Great Ormond Street Hospital, London, UK; [3]Department of Radiology, Health Sciences Center, University of Utah, Salt Lake City, UT, USA

ORCID: [a]0000-0001-5173-8492

ABSTRACT

Diagnosing congenital neck masses in the pediatric population can be challenging, since the differential diagnosis often includes rare or unfamiliar entities, and there is overlap in clinical presentation and imaging findings. A thorough understanding of embryology, anatomy, and common lesions in the pediatric neck, along with the typical location, clinical presentation, and imaging findings of commonly encountered pediatric neck masses significantly decreases unnecessary testing and delay in diagnosis and treatment. The purpose of this article is to present congenital lesions of the pediatric neck with pertinent embryology, clinical presentation, and imaging considerations.

Keywords: *Branchial cleft. Branchial arch. Thyroglossal duct cyst. Thymus. Lymphatic malformation. Dermoid.*

INTRODUCTION

Neck masses are not infrequently encountered in the pediatric population and comprise a wide spectrum of benign and, less commonly, malignant entities. Etiologies include congenital and anomalous developmental lesions, nodal pathology, infectious/inflammatory processes, and tumors, among others. In this article, we focus on congenital entities, a lesion category that is particularly important to bear in mind among the pediatric population.

Branchial apparatus anomalies

The branchial apparatus has a major contribution to the development of the head and neck. There are six pairs of branchial arches that form at the fifth and sixth week of gestation. The fifth arch regresses in humans, and the sixth arch is often small, and discussed in combination with the fourth arch, leaving 4 main arches that are commonly discussed with congenital pediatric lesions. On each side, there are four branchial (or pharyngeal) arches separated from one another externally by grooves (or clefts) and internally by pouches[1]. Between the cleft and the pouch at each level is the respective branchial plate[2,3]. The outer surface of the branchial apparatus, including the clefts, is lined by ectoderm, and the inner surface of the branchial apparatus, including the pouches, is lined by endoderm. The branchial plate is made of mesoderm[3]. A neurovascular component supplies each arch which also contains cartilage.

Between the third and seventh weeks of gestation, the branchial apparatus undergoes complex morphological changes and differentiation, resulting in gradual obliteration of the clefts and pouches via "invasion", or filling-in, by surrounding mesenchyme, and subsequent maturation of various portions into the different head

***Corresponding author:**
Nitesh Shekhrajka
E-mail: nshekhrajka@meei.harvard.edu

Received for publication: 23-01-2023
Accepted for publication: 22-02-2023
DOI: 10.24875/JMEXFRI.23000003

Available online: 13-07-2023
J Mex Fed Radiol Imaging. 2023;2(2):82-97
www.JMeXFRI.com

Table 1. Branchial apparatus and derivatives

Arch number	Pouch derivatives (endoderm)	Arch derivatives (mesoderm)					Cleft derivatives (ectoderm)
		Cartilage	Bone/ cartilage derivatives	Muscle	Connective tissue	Nerve	
First (mandibular)	Middle ear Eustachian tube	Meckel's	Maxilla Mandible Zygoma Temporal bone Malleus Incus	Muscles of mastication Mylohyoid Anterior belly of digastric Tensor veli palatini Tensor tympani	Anterior ligament of malleus Sphenomandibular ligament	Trigeminal (CN V)	External auditory canal
Second (hyoid)	Palatine tonsil	Reichert's	Styloid process Lesser horn and upper body of hyoid Stapes	Facial muscles (incl. Buccinator, platysma, posterior Belly of digastric) Stylohyoid Stapedius	Stylohyoid ligament	Facial (CN VII)	Sinus of His
Third	Inferior parathyroid Thymus pyriform fossa	None	Greater horn and lower body of hyoid	Stylopharyngeus	None	Glossopharyngeal (CN IX)	Sinus of His
Fourth	Superior parathyroid Apex of pyriform sinus Ultimobranchial body	None	Thyroid cartilage Corniculate cartilage Cuneiform cartilage	Pharyngeal and extrinsic laryngeal muscles Levator veli palatini	None	Vagus (CN X)	Sinus of His

CN: cranial nerve.

and neck structures[2-4]. The mature head and neck cartilages, bones, muscles, ligaments, and associated neurovascular structures derived from each of the branchial arches, clefts, and pouches are listed in Table 1.

Branchial apparatus anomalies are thought to occur by either the persistence of vestigial cellular remnants within solid neck tissue, or incomplete obliteration of clefts and pouches during morphological evolution of the apparatus. Depending on the location of the vestigial remnants or the extent of failed obliteration, anomalies may manifest as cysts, sinuses, or fistulae. A cyst is a focal fluid collection lined by epithelium surrounded by soft tissue. A sinus is a blind-ending tubular or saccular structure with communication either to the skin externally or to the pharyngeal lumen internally. A fistula connects to both the skin externally and the pharyngeal lumen internally and is thought to arise secondary to persistence of a portion of the branchial cleft with concomitant rupture of the branchial membrane, resulting in a complete external-internal communication[2,5,6].

In general, the treatment of all branchial apparatus anomalies is complete surgical excision of the lesion with its associated sinus or fistulous tract. In cases of third and fourth arch anomalies, cannulation and chemo-cauterization of the internal opening in the pyriform sinus and associated fistulous tract may be done, however long-term efficacy of this method is not well-documented[7]. If a fourth arch anomaly is found, an ipsilateral hemithyroidectomy should be performed.

First branchial cleft anomalies

First branchial cleft anomalies (BCA) are rare and account for less than 10% of all branchial apparatus anomalies and are more common in females[8,9]. Most of these anomalies present as cysts, but a minority of cases can also present as sinuses or fistulae[9]. They may communicate with the external auditory canal or, rarely, the middle ear.[3] Based on the clinical and histopathological features, the first BCA were classified into two groups by Work[10].

Work type I anomalies are duplications of the membranous external auditory canal and are composed of ectoderm/keratinized stratified squamous epithelium. These lesions manifest as cystic masses near the ear, medial to the conchal cartilage and superficial to the facial nerve and may extend to the postauricular region[10].

Work Type II anomalies contain ectodermal and mesodermal elements and can manifest as a cyst, sinus, fistula, or any combination of these[10]. They manifest as

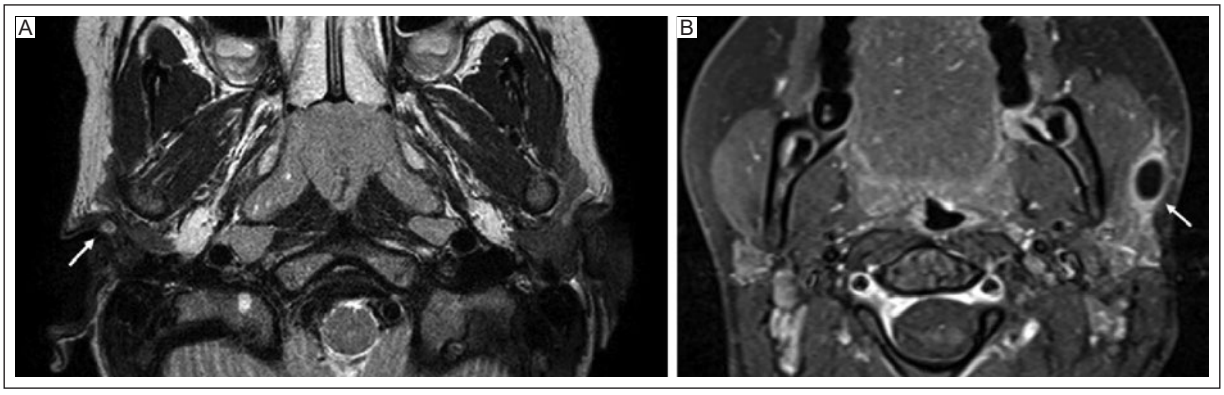

Figure 1. First branchial cleft cyst. **A:** axial T2-weighted image shows a Work type I first branchial cleft cyst along the external auditory canal (arrow). **B:** axial post-contrast fat-suppressed T1-weighted image shows a Work type II first branchial cleft cyst (arrow). Notice the central cystic component with peripheral enhancement that may represent mild inflammatory change.

a swelling or mass in the pre-, infra-, or postauricular region at or below the mandibular angle. In cases where there is an associated sinus or fistula, the external opening is near the angle of the mandible and the internal opening is inferior to or in the membra-nous external auditory canal, typically at the bony-cartilaginous junction. The tract is closely associated with or deep to the facial nerve[4,10]. Clinical presentations vary and patients may present with swelling near the ear, parotid, or mandibular angle with cervical and/or auricular symptoms. Auricular symptoms may include recurrent otorrhea which may be mucoid or, if infected, purulent. Cervical signs may include a pit near the mandibular angle with mucoid or purulent drainage, and recurrent unilateral parotitis.

In general, ultrasound is the first-line modality of choice in the evaluation of superficial head and neck masses, especially in the pediatric population. Ultrasound is quick and cost-effective and provides information about the size, shape, location, vascularity, and internal content of the lesion and its relationship with the surrounding structures[11]. On ultrasound, a first branchial cleft cyst is a well-circumscribed rounded or oval anechoic cystic structure with posterior acoustic enhancement. A complex cystic structure with internal septations and peripheral hypervascularity can be seen in the setting of superimposed infection (Figure 1). For delineation of a potential concurrent sinus or fistulous tract, a high-resolution magnetic resonance imaging (MRI), conventional fluoroscopy, or computed tomography (CT) fistulogram may be helpful, as resection of the tract is necessary to prevent future recurrence[12]. A fistulous tract between the lesion and external auditory canal may been seen on heavily T2-weighted MR imaging, which would confirm the diagnosis of a first BCA.

The differential diagnosis of a first branchial cleft cyst includes other cystic lesions near the external auditory canal and in or adjacent to the parotid: lymphatic malformation (often multicystic, transpatial, and with fluid-fluid levels), cystic node (including benign etiologies such as mycobacterium infection and malignant etiologies such as metastatic papillary thyroid carcinoma, so the clinical context is important), pilomatricoma (especially if close to the skin surface), and sialocele, lymphoepithelial cyst, and cystic primary salivary tumor (if in the parotid gland). Dermoid and epidermoid cysts would show low-level echoes within the lesion on ultrasound and different signal (e.g., diffusion weighted imaging (DWI) hyperintensity) on MRI.

Second branchial cleft anomalies

The second branchial apparatus anomalies are most frequent, accounting for as many as 67% to 93% of all branchial anomalies[13-15]. They are the second-most commonly identified congenital head and neck malformations after thyroglossal duct anomalies[4]. Second branchial cleft cysts are three times more common than second branchial sinuses and fistulae. Second branchial cleft cysts present at a later age, compared to sinuses and fistulae, usually in the second to the fourth decade of life with the mean age being 40 years[16-18]. Caution should be taken when considering a second branchial cleft cyst as a potential diagnosis in any adult patient, as cystic/necrotic lymph nodes from metastatic squamous cell carcinoma are much more common than the second branchial cleft cysts in the adult population. Less than 3% of all second branchial cleft lesions are seen in adults over 40[19].

The external opening of the second branchial anomaly, when present, is usually located along the anterior

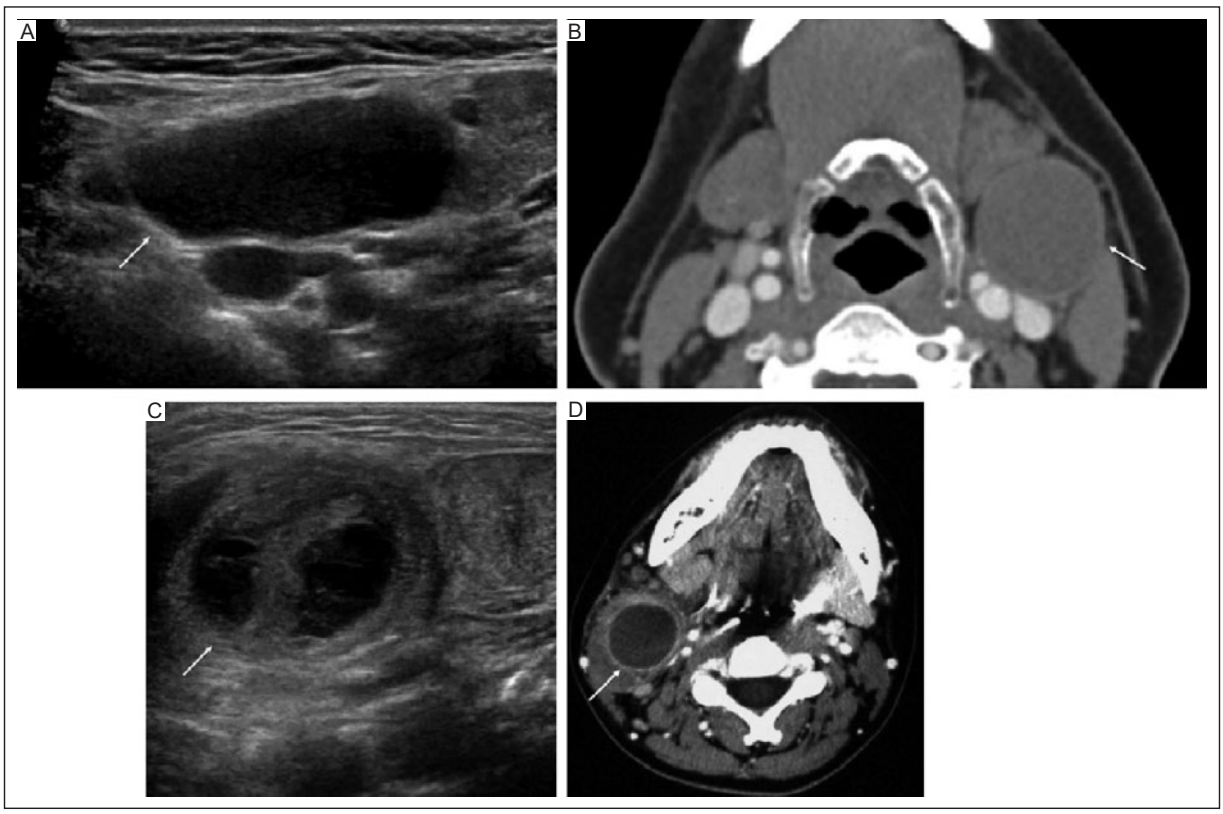

Figure 2. Second branchial cleft cyst. **A:** ultrasound, and **B:** contrast-enhanced CT of the neck show a thin-walled well-circumscribed non-enhancing hypoechoic/hypodense lesion between the left submandibular gland and sternocleidomastoid muscle, anterior/superficial to the carotid sheath, consistent with Bailey type II second branchial cleft cyst (arrows). **C:** ultrasound and **D:** contrast-enhanced CT of the neck show a more complex thick-walled hypoechoic/hypodense lesion deep to the right sternocleidomastoid muscle with internal septations, enhancement of the walls and peripheral fatty stranding, consistent with an infected Bailey type II second branchial cleft cyst (arrows).
CT: computed tomography.

border of the sternocleidomastoid muscle in the mid-to-lower third of the neck. A second branchial sinus or fistulous tract follows a course that involves the skin at that level (mid-to-lower third anterolateral neck), pierces the platysma, courses cranially along the carotid sheath to the level of the hyoid bone, turns medially under the posterior belly of the digastric muscle and over the hypoglossal nerve. It then courses between the internal and external carotid arteries, deep to the stylohyoid ligament, superficial to the glossopharyngeal nerve, and terminates at the tonsillar fossa[13-17]. A second branchial cleft cyst can be found anywhere along this tract from the anterior border of the sternocleidomastoid muscle to the tonsillar fossa. A classification system proposed by Bailey[20] in 1929 dividing the cysts into four types depending on their anatomic location from lateral to medial is still widely accepted.

Bailey Type I: The lesion is anterior to the sternocleidomastoid muscle and does not touch the carotid sheath.

Bailey Type II: The most common type of second branchial cleft cyst, the lesion is deep to the sternocleidomastoid muscle, posterior to the submandibular gland, and immediately lateral to the carotid sheath (Figure 2).

Bailey Type III: The lesion extends between the internal and external carotid arteries and is lateral to the pharynx.

Bailey Type IV: The lesion is medial to the carotid sheath close to the pharynx and tonsillar fossa.

Fistulae and sinuses are usually present in infancy or early childhood as chronic drainage from an opening in the anterolateral neck along the anterior border of the sternocleidomastoid muscle[3]. Cysts are more frequently diagnosed during the second to fourth decade of life as a progressive non-tender lump or swelling, usually noticed when they enlarge rapidly in the setting of a respiratory tract infection or infection within the cyst itself. An infected cyst may present with pain or mass effect, resulting in dyspnea or dysphagia. An infected cyst may develop into

Figure 3. Retropharyngeal suppurative lymphadenitis. Contrast-enhanced CT of the neck shows a peripherally enhancing hypodense lesion in the left retropharyngeal space with surrounding soft tissue edema and fat stranding, consistent with retropharyngeal suppurative lymphadenitis (arrow). Note the anterolateral displacement of the left parapharyngeal fat pad indicating the lesion location in the retropharyngeal space.

CT: computed tomography.

a frank abscess and may rupture to the skin, resulting in a "pseudo-sinus" tract or opening.

Ultrasound may be used as an initial assessment modality and can guide subsequent imaging. CT or MRI with contrast is helpful not only to assess the size, location, and contents of the cyst, but also to determine its relationship with surrounding structures and delineate potential associated sinus or fistulous tract. Especially in adults, a fine needle aspiration (FNA) biopsy of the cyst wall lining may be needed to rule out other possible etiologies, and this may be performed under ultrasound guidance[21].

Important differential diagnostic considerations for a Bailey type II second branchial cleft cyst include level II metastatic cystic/necrotic lymphadenopathy and suppurative lymphadenitis (if there is superimposed inflammatory change, Figure 3), and tuberculous granuloma or mycobacterial adenitis. A lymphatic malformation is possible in almost all locations in the neck, and is an especially pertinent differential diagnosis for a cystic cervical lesion in a child. A thyroglossal duct cyst is generally more anterior and midline or, when infrahyoid, in a paramedian location related to the strap muscles and/or close to the thyroid cartilage. A dermoid cyst is also usually found in the anterior midline neck superficially[21].

Third and fourth branchial cleft anomalies

Third branchial arch anomalies are rare with a reported incidence of 2-8%[13,16,21]. The external opening of third branchial arch anomalies is along the anterior border of the sternocleidomastoid muscle in the lower neck. The sinus or fistulous tract, if present, passes deep to the platysma, along the carotid sheath, deep to the glossopharyngeal nerve, superficial to the hypoglossal nerve, pierces the thyrohyoid membrane cranial to the superior laryngeal nerve to terminate into the pyriform sinus[21].

Fourth branchial arch anomalies are extremely rare with a reported incidence of 1-2%[13,16,21]. From the external opening along the anterior border of the sternocleidomastoid muscle in the lower neck, usually on the left side, the fistulous tract of the fourth branchial pouch extends down posterior to the internal carotid artery. On the right it loops under the subclavian artery whereas on the left it loops under the aortic arch and courses cranially lateral to the trachea and recurrent laryngeal nerve, passing inferior to the superior laryngeal nerve with internal opening in the pyriform sinus at the level of cricothyroid joint. Due to its convoluted course, a complete fourth branchial fistula has never been clinically described[21].

More commonly, both third and fourth branchial tracts do have an opening at the pyriform sinus, descending a short distance in the neck, but with the other side blind-ending within the soft tissues of the neck in the paratracheal or thyroid region. It is generally clinically difficult to distinguish between these two. On the skin side, there have been a few case reports describing tracts from the anterior border of the sternocleidomastoid muscle extending down below the clavicle into the mediastinum[22-24]. It is therefore of key importance to determine the relationship of the anomalous tract with the superior and recurrent laryngeal nerves during surgery. A course inferior to the superior laryngeal nerve and superior to the recurrent laryngeal nerve suggests a fourth pouch origin, while a course superior to the superior laryngeal nerve suggests a third pouch origin[25,26]. Termination or adherence of an anomalous sinus tract to the lateral aspect of the thyroid gland may suggest a fourth pouch origin, since the lateral thyroid primordia and superior parathyroid glands are derived from the fourth pouch[21,27].

Clinically, a third and fourth branchial anomaly may present as a pit or draining sinus along the anterior border of the sternocleidomastoid muscle in the lower neck. Third branchial anomalies can present

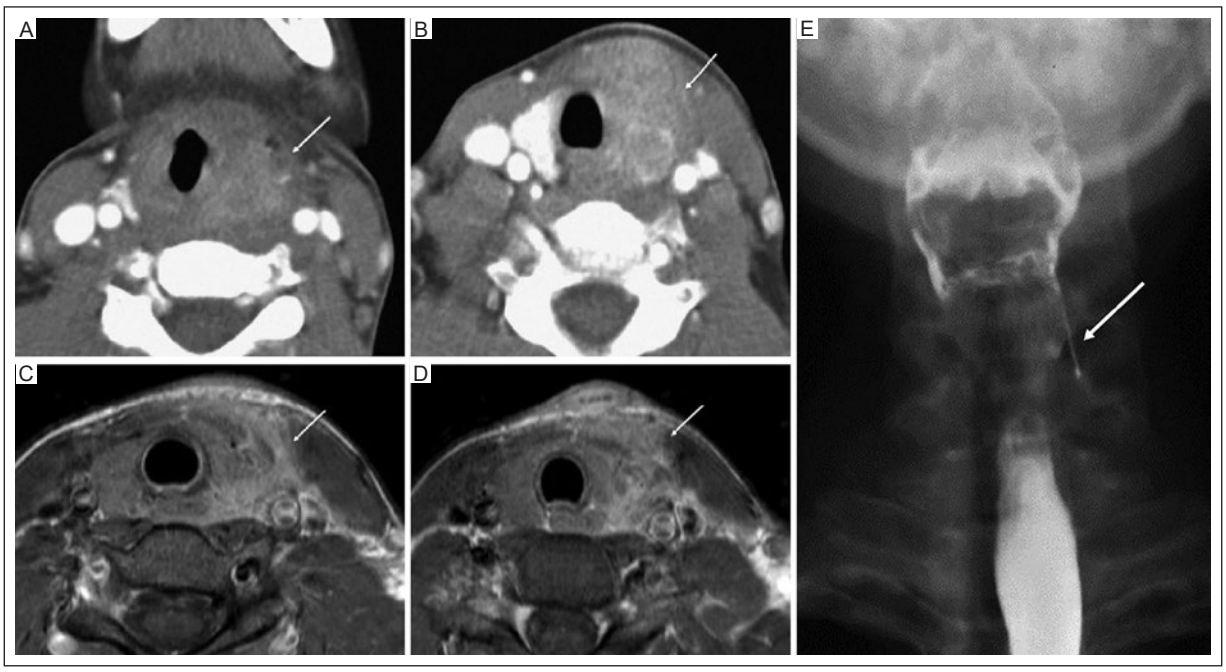

Figure 4. Fourth branchial cleft anomaly. **A-B:** axial contrast-enhanced CT, and **C-D:** axial T1-weighted post-contrast MRI show diffuse inflammatory changes with edema and contrast enhancement within and around the left thyroid lobe (arrows). There are also small multifocal foci of peripherally enhancing hypodense abscesses in the region. Findings are consistent with left-sided thyroiditis. **E:** coronal video fluoroscopic swallow study depicts a thick linear area of ingested contrast passing through the left pyriform sinus towards the left thyroid lobe (arrow), consistent with the fistulous/sinus tract. Findings are consistent with a left-sided fourth branchial cleft anomaly.

CT: computed tomography; MRI: magnetic resonance imaging.

with hypoglossal nerve palsy in the setting of infection. Fourth branchial anomalies can present with acute or recurrent suppurative thyroiditis, usually on the left (Figure 4)[28]. Occasionally the fourth branchial anomalies can also present as a "cold thyroid nodule" on scintigraphy or may be mistaken for a thyroglossal duct cyst[29]. Other presentations may include a rapidly enlarging lateral neck infection in neonates as they start to swallow with the potential to compromise the airway, recurrent upper respiratory tract infections, neck or thyroid pain, or recurrent cervical abscesses. A CT or MRI in conjunction with a fluoroscopic barium pharyngogram study may occasionally be able to demonstrate the tract connecting to the pyriform sinus (Figure 4). Direct pharyngoscopy may allow visualization of the tract opening in the pyriform sinus.

Branchial anomalies may be associated with or be a prominent feature in congenital syndromes, such as mandibulofacial dysostosis (Treacher Collins syndrome, bilaterally symmetrical first and second branchial arch anomalies), velocardiofacial syndrome (DiGeorge syndrome, anomalies of the third and fourth branchial pouches resulting in maldevelopment of thymus and parathyroid glands), Oculo-auriculo-vertebral spectrum (Goldenhar syndrome/hemifacial microsomia, maldevelopment of first and second arch structures, pre-auricular pit or sinus) and branchio-oto-renal (BOR) syndrome (pre-auricular pit and second branchial cleft cyst, sinus, or fistula).

Thyroglossal duct anomalies

During the third week of gestation, the endodermal lining in the midline of the primitive pharynx, at a level between the first and second branchial pouches, becomes thick, giving rise to the tuberculum impar[30]. From here, a diverticulum develops, from which thyroid primordia descend to its final location in the lower neck. This diverticulum remains as a pit at the junction of the anterior two-thirds and posterior one-third of the tongue, called the foramen cecum[30]. As the thyroid primordia descends, it retains an attachment to the foramen cecum by the means of a thin epithelial stalk. This stalk canalizes to become the thyroglossal duct by the beginning of the fifth week of gestation and passes anterior to the hyoid bone and laryngeal cartilages. Remodeling of the hyoid bone after the passage of the thyroglossal

duct creates the hooked appearance of the thyroglossal duct around the inferior and posterior border of the hyoid bone[30,31]. The Thyroid is hollow during early descent, but solidifies as follicular elements form during the descent[32]. The thyroid becomes bilobed by the end of the fifth week, descends to its final position by the seventh week, and the thyroglossal duct obliterates by the ninth or tenth week of gestation[2,30,32].

Thyroglossal duct (TGD) anomalies are the most common congenital head and neck malformation[4]. They may be related to incomplete descent of thyroid primordia resulting in remnants along the course of the thyroglossal duct, or related to incomplete involution of the thyroglossal duct itself resulting in a thyroglossal duct cyst or fluid-filled segment of the tract. When there is incomplete descent of thyroid primordia, ectopic thyroid tissue can be present anywhere along the TGD tract and can range from a small rest of cells to the entire gland. When thyroid tissue remains at the foramen cecum, it is termed lingual thyroid (Figure 5). Lingual thyroid may be the only functioning thyroid tissue in up to 70-80% of patients with this anomaly, and its removal may lead to hypothyroidism[4,33]. It is important to bear in mind that ectopic thyroid tissue can undergo the same disorders as ectopically located thyroid gland, such as hyperthyroidism, thyroiditis, and carcinoma[30,34].

When there is failure of TGD involution, a thyroglossal duct cyst (TGDC) or sinus results, and this may occur anywhere along the tract from the posterior tongue to the thyroid isthmus. A TGDC is lined by respiratory epithelium, which accounts for the viscous fluid found within the cyst secreted by the mucus glands. Occasionally, lymphoid tissue can also be seen along the walls of the TGDC, resulting in inflammation and enlargement in the setting of respiratory infection. A TGDC does not contain skin appendages or cholesterol crystals, contrary to branchial cleft cysts[30]. Two-thirds of thyroglossal duct anomalies present in the first to third decades of life, with more than half in the first decade. There is no gender predilection[35]. The majority of the cases are sporadic, but can rarely be familial[36]. Approximately 90% of TGDCs occur in the midline neck. A smaller proportion of the cysts can be found in a paramedian location, usually in the infrahyoid region (two-thirds of paramedian TGDCs). Very rarely, intralingual TGDCs can be seen[30,37].

Many TGD anomalies are asymptomatic and incidentally found. When symptomatic, the common presentation is a painless, mobile midline or near midline neck mass which often moves with swallowing or tongue protrusion. TGDCs are prone to infections due to their anatomic relation with the oral cavity and approximately one-third of the individuals with a TGD anomaly present when the lesion undergoes acute or recurrent infection, more commonly in adults[38]. The most common pathogens include *Haemophilus influenzae, Staphylococcus aureus, and Staphylococcus epidermidis.* The TGD does not communicate with the skin during embryogenesis but may present with a sinus tract in the midline neck due to abscess with spontaneous rupture or surgical drainage[30,38].

A minority of patients can also present with a foul taste in the mouth if drainage occurs through the foramen cecum. Rare presentations may include feeding difficulties, respiratory distress, and sudden infant death syndrome by the lesions at the tongue base[6,38-40]. TGDC may contain solid thyroid tissue. In approximately 1.5% of patients with TGDC, the only

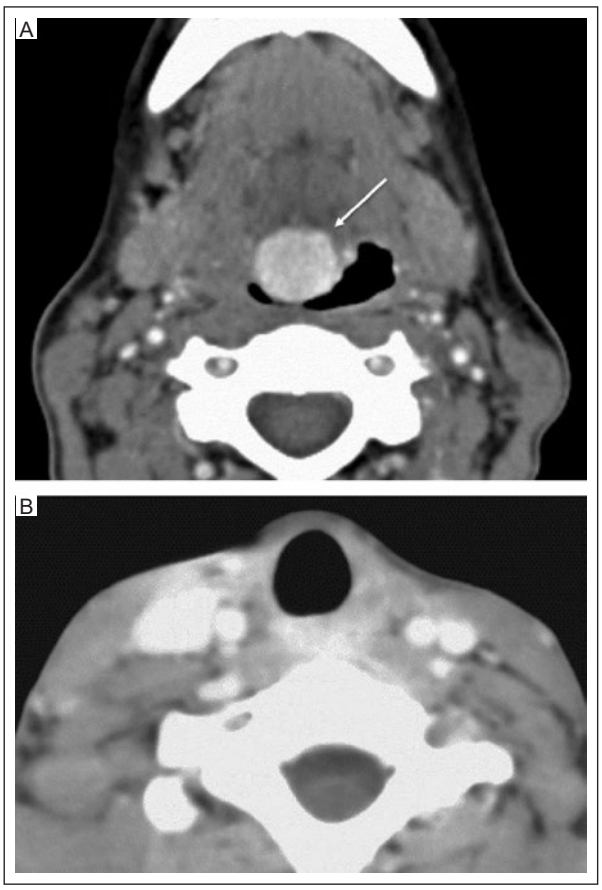

Figure 5. Ectopic thyroid. **A:** axial contrast-enhanced CT of the neck at the level of tongue base, and **B:** at the level of thyroid bed shows a well-circumscribed rounded hyperattenuating lesion in the midline tongue base at the expected location of the foramen cecum consistent with ectopic thyroid tissue (arrow). Also, note no appreciable thyroid tissue in the thyroid bed.

CT: computed tomography.

functional thyroid tissue is located within the TGD[35]. These patients often have hypothyroidism with elevated TSH and resultant hypertrophy of the ectopic thyroid. Rarely, patients may also present with a malignancy within the thyroid tissue of a TGD, with papillary carcinoma being the most common histological type[41].

Ultrasound is the modality of choice, especially in the pediatric population, not only to characterize the lesion but also to identify any orthotopic thyroid tissue within the neck. CT and MRI may be needed in cases of larger, recurrent, or complex lesions. On ultrasound, a TGDC is a well-circumscribed hypo- or anechoic structure in the midline or paramedian neck with posterior acoustic enhancement. On CT or MRI, the TGDC appears as a well-circumscribed thin-walled, fluid filled structure in the neck along the course of TGD with an intimate relation to the tongue base, hyoid bone, or strap muscles depending on the level it is found (Figure 6). Internal septations and debris may be seen due to proteinaceous material. Thickening of the cyst wall with increased peripheral vascularity may be noted in the setting of infection. Solid tissue associated with the cyst may represent ectopic thyroid rest, but rarely could represent a thyroid malignancy, especially when there are associated foci of calcification (Figure 6).

Papillary carcinoma is the histological subtype in more than 80% of the cases of thyroid malignancy in a TGDC[42,43]. Given the risk of recurrent infections and the potential for harboring malignancy in the presence of a mural nodule or calcifications, surgical resection is generally advisable. A normally positioned thyroid gland in the neck must be confirmed before surgery, as the ectopic thyroid may be the only functioning thyroid tissue, resection of which may lead to a hypothyroid crisis and/or render patients permanently hypothyroid.

There is generally not much of a differential diagnosis for a TGDC. At times, a midline cervical dermoid may have a CT or ultrasound appearance resembling a TGDC with internal complex debris, but the location is often slightly different, with a dermoid usually more superficial and remaining midline or near-midline even in the lower neck. A thymic cyst is more lateral. Third or fourth branchial anomalies most often present as recurrent perithyroidal inflammation or edema leading to the pyriform sinus.

Cervical thymus

The thymus originates from the endoderm of the third branchial pouch during the sixth week of gestation[2,44]. More specifically, the thymus arises from the ventral part of the third pouch, whereas the inferior parathyroid gland arises from the dorsal part. The thymic primordia migrate inferiorly along the thymopharyngeal ducts, one on each side, which fuse in the midline neck by the eighth week of gestation before reaching the superior mediastinum by the twelfth week. The lumen of the thymopharyngeal duct is obliterated by endothelial proliferation and transforms into a solid cord called a thymopharyngeal cord. By the tenth week of gestation, the thymopharyngeal cord is destroyed by adjacent mesenchymal cells. The remaining epithelium transforms into Hassall's corpuscles[45]. Failed or incomplete involution, migration, or sequestration of the thymopharyngeal duct or cord may result in remnant or ectopic thymic tissue along its path. A cervical thymic cyst is a result of cystic degeneration of remnant thymic tissue, thymic (Hassall's) corpuscles, or thymopharyngeal duct.

Cervical thymic cysts are uncommon with only around 150 cases reported in the literature, but probably occur much more frequently than reported as they are mostly asymptomatic and discovered incidentally[46]. They may become symptomatic due to rapid enlargement secondary to infection or hemorrhage[45,46]. Asymptomatic ectopic thymic tissue in the neck has been reported in 10% of adults and over 30% among the pediatric population on autopsy[47,48]. More than two-thirds of cervical thymic cysts are diagnosed in the first decade of life, usually after 2 years of age, with males being affected twice as often as females[2,45,49,50]. They can present as a cystic mass in the lateral or midline neck anywhere between the mandibular angle to the mediastinum, more commonly on the left side, and often in or near the anterior triangle of the lower neck, paralleling the sternocleidomastoid muscle, within or adjacent to the carotid sheath[45,46,50,51]. These cysts may be present at birth, or may develop after birth within ectopic thymic tissue. Those present at birth develop from the persistent remnants of the thymopharyngeal duct and are usually unilocular. They can be large, involving the almost entire duct spanning the length of the neck, in which case they are referred to as thymopharyngeal duct cysts[45,52]. The thymic cysts that develop after birth result from degeneration of thymic corpuscles within ectopic thymus along the thymopharyngeal duct, and are more often multilocular[45].

Cervical ectopic thymus demonstrates the same imaging characteristics as normally positioned thymus. On ultrasound, the thymic tissue demonstrates multiple linear hyperechoic septae and homogeneously distributed speckled hyperechoic foci (Figure 7)[11,53].

Figure 6. Thyroglossal duct cyst. **A-B:** axial, and **C:** sagittal contrast-enhanced CT of the neck show a thin-walled hypodense lesion in the midline neck, deep to the strap muscles, extending from the undersurface of the hyoid bone to the level of the thyroid cartilage (arrows), consistent with a thyroglossal duct cyst. **D:** axial contrast-enhanced CT shows a slightly lobulated hypodense lesion in the midline neck at the level of the thyroid cartilage, deep to the strap muscle, with mild peripheral enhancement and surrounding edema and fat stranding, consistent with an infected thyroglossal duct cyst (arrow). **E:** ultrasound, and **F:** sagittal contrast-enhanced CT of the neck show a hypoechoic lesion (arrow) with foci of calcification (arrowheads) in the midline infrahyoid neck on ultrasound and corresponding hyperattenuating lesion on CT (arrow). The lesion was confirmed to be a papillary thyroid carcinoma in the thyroglossal duct remnant.

CT: computed tomography.

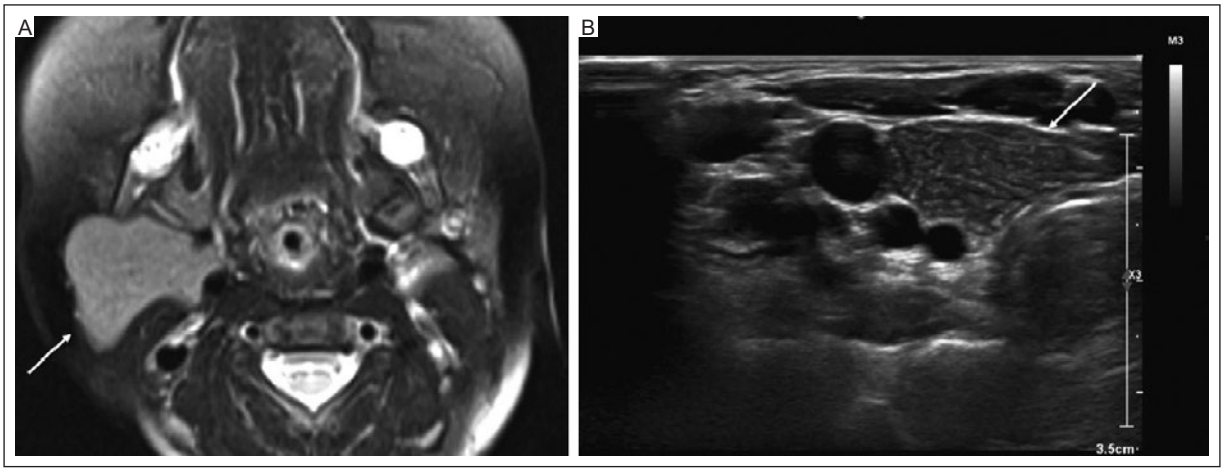

Figure 7. Ectopic/cervical thymus. **A:** axial T2-weighted fat-suppressed MRI, and **B:** ultrasound of the neck show a well-circumscribed lobulated T2 hyperintense mass in the right neck, anterior to the sternocleidomastoid and carotid sheath with homogeneously distributed speckled hyperechoic foci on ultrasound, consisted with ectopic thymus (arrows).
MRI: magnetic resonance imaging.

Thymic cysts are well-defined thin-walled uni- or multilocular cystic lesions without enhancement (Figure 8). Increased attenuation of the cystic components with peripheral enhancement can be seen in the setting of hemorrhage or infection. In half the cases, the cyst extends into the mediastinum. Continuity with the dominant thymus through the thymopharyngeal duct may aid in the diagnosis. Treatment of a cervical thymic cyst consists of surgical removal of the cyst with an excellent prognosis and no recurrence in children[54].

Congenital midline cervical cleft

Failure of fusion of the lateral branchial arches in the midline may result in a superficial vertical defect in the midline neck, known as congenital midline cervical cleft (CMCC). This lesion is rare with only around 200 cases reported in the literature[55]. It occurs sporadically without known hereditary form or gender predilection. The lesion appears as a midline skin defect with a focal skin protuberance at its superior aspect and may be located anywhere between the lower lip to the sternal notch. A blind-ending sinus tract may be present at the inferior aspect of the cleft, from where mucoid discharge may be expressed. The overlying epithelium is usually erythematous. Over time, the cleft epithelializes and a fibrous cord develops and thickens with age, which may lead to restriction of mandibular movements and neck extension in early childhood[4,55]. Ultrasound of the neck shows a hypoechoic blind ending sinus tract in the midline neck. On MRI the sinus tract is peripherally enhancing with central T1 hypo and T2 hyperintensity without disruption of the surrounding structures and with a normal thyroid gland. In advanced cases, bony spurring from the midline mandible can be seen due to traction from the underlying fibrous cord[56]. The cleft is treated with complete surgical excision.

Lymphatic malformation

Lymphatic malformations (LMs) are congenital endothelial-lined cystic lesions derived from lymphatics and vasculature that fail to undergo proper anastomosis, or portions of lymphatic sacs that group together during embryogenesis[57]. Previously, lymphatic malformations were categorized according to their size and depth of development, with the smaller, superficial lesions known as lymphangioma circumscriptum and the deeper lesions known as cavernous lymphangiomas and cystic hygromas. The new classification by the International Society for the Study of Vascular Anomalies (ISSVA) divides the “common (cystic) lymphatic malformations” into microcystic, macrocystic, and mixed cystic types[58].

LMs constitute approximately 5.6% of all benign lesions of childhood with no gender predilection[59]. They can occur anywhere in the body but around 80% are found in the neck[4,60]. LMs are most commonly sporadic but can also be associated with genetic syndromes such as congenital ovarian hypoplasia syndrome (Turner syndrome), Noonan syndrome, and trisomies 13, 18, and 21[11,61]. About half of the lesions are detected at birth and up to 90% are detected by 2 years of age[60].

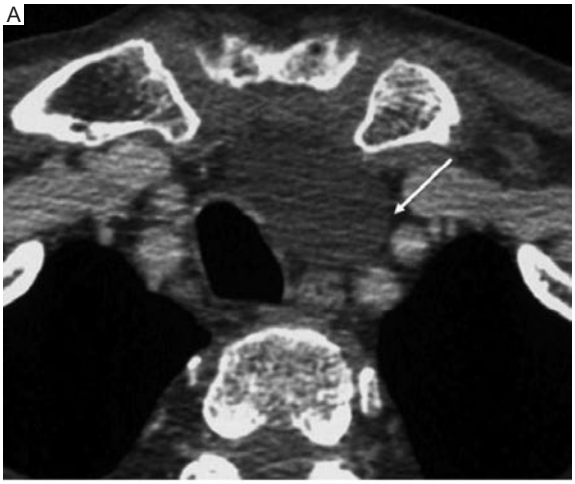

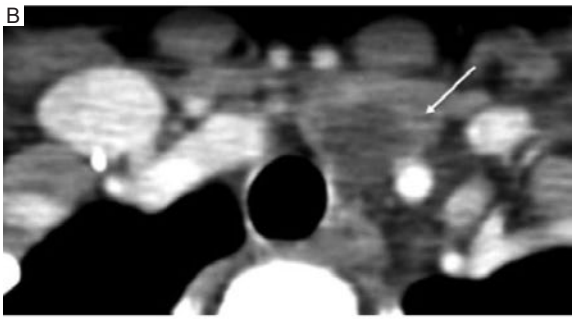

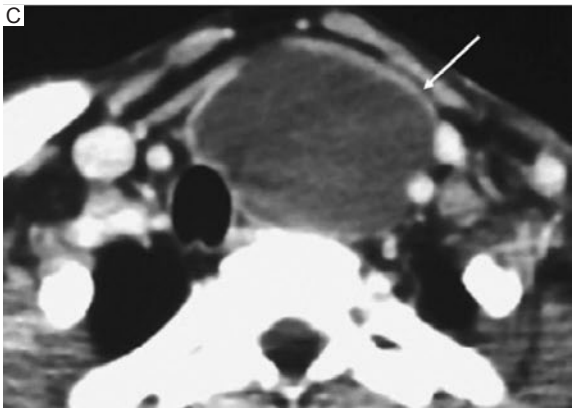

Figure 8. Thymic cyst. **A, B, C:** axial contrast-enhanced CTs of the neck in three different patients at the level of the thoracic inlet show hypodense non-enhancing cystic lesions in the left lower neck extension into the superior/anterior mediastinum consistent with thymic cysts (arrows).

CT: computed tomography.

LMs usually present as soft, non-tender masses and they often occur in the submandibular region and posterior cervical triangle, although they can be found anywhere in the head and neck. If the lesion is located centrally near the aerodigestive tract and is large, it may lead to respiratory and feeding difficulties. They can rapidly enlarge in the setting of infection or with intralesional hemorrhage. On ultrasound, macrocystic lesions appear as multilocular hypo- or anechoic lesions containing internal septae of varying thickness, with vascularity along the walls and septae. The cyst contents may be hyperechoic in cases of internal hemorrhage, infection, or elevated lipid contents. Microcystic forms may appear hyperechoic due to the prevalence of septations[11,62]. When lesions are large, they have the propensity to cross multiple anatomic spaces. Contrast-enhanced MRI is useful in determining the location, size, and extent of the malformation, ruling out a coexisting venous component, and assessing lesion relationship with adjacent neck structures, usually without surrounding aggressive changes. LMs follow fluid signals on MRI (T1 hypointense and T2 hyperintense), but T1 hyperintensity can be seen in cases of internal hemorrhage and proteinaceous contents.

A characteristic imaging feature of an LM is internal "fluid-fluid levels" related to heterogeneous fluid contents related to hemorrhagic and proteinaceous material settling out in layers due to their differential densities from simple cyst fluid (Figure 9). There is enhancement of the walls and septae on post-contrast sequences, and when there is a high concentration of septae in a microcystic LM, it may appear to enhance like and mimic a solid mass and is a pitfall to avoid. Asymptomatic LMs can be monitored. Large or symptomatic LMs can be treated surgically or with sclerotherapy or a combination of both. Microcystic LMs are generally more resistant to sclerotherapy and are usually surgically resected[63].

Hemangiomas

A wide range of terminologies has been used to describe hemangiomas and various vascular anomalies in the past. Historically, lesions of endothelial proliferation were described based on the size of vascular channels and internal contents. Lesions containing blood were termed hemangiomas and were subclassified into capillary, strawberry, and cavernous hemangiomas based on channel sizes, whereas lymph-containing lesions were termed lymphangiomas or cystic hygromas[64]. Many subsequent classifications used anatomic or descriptive terms to describe these lesions without taking into account the biological behavior of the lesions, which resulted in the misconception that most of these lesions spontaneously disappear[65]. A new biological classification adopted by the International Society for the Study of Vascular Anomalies (ISSVA) was influenced by the work of Mulliken and Glowacki[66]. This classification groups endothelial malformations

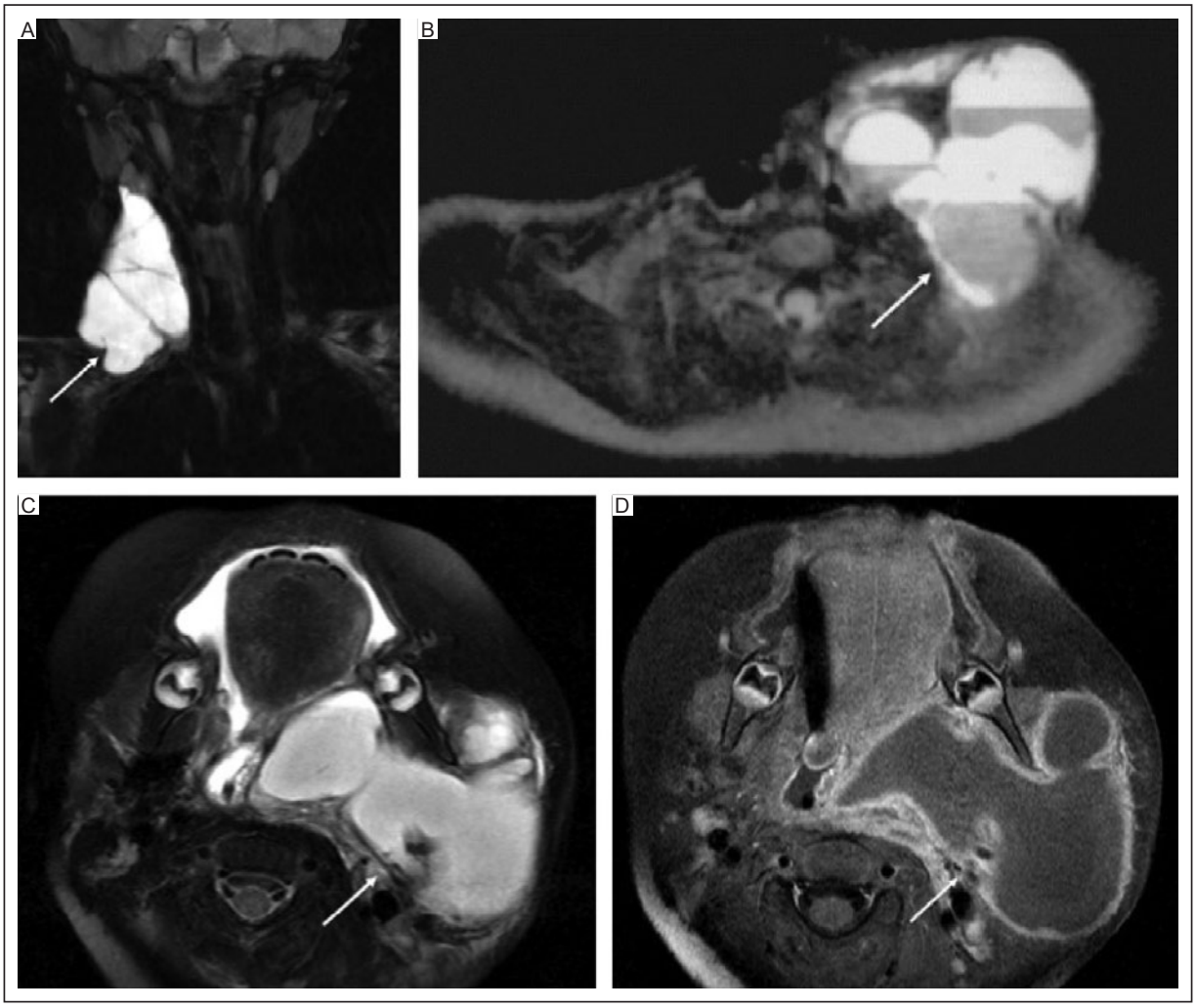

Figure 9. Lymphatic malformation. **A:** coronal T2-weighted fat-suppressed, and **B:** axial T2-weighted MRI of the neck in two different patients shows multilobulated T2 hyperintense lesions in the neck extending into multiple fascial planes with internal septations and fluid levels (arrows), consistent with macrocystic lymphatic malformations. **C:** axial T2-weighted fat-suppressed, and **D:** axial T1-weighted fat-suppressed post-contrast MRI of the neck in the same patient show a multi-lobulated but unilocular cystic lesion in the left neck extending into multiple fascial planes and thick peripheral enhancement consistent with an infected macrocystic lymphatic malformation (arrows).
MRI: magnetic resonance imaging.

into two groups, hemangioma and vascular malformation, based on physical findings, natural history, cellular turnover, and histology. Hemangiomas are true benign neoplasms of the endothelial cells and are further classified into infantile and congenital forms.

Infantile hemangiomas are the most common congenital malformation, present in 5-10% of infants[67]. They are 5 times more common in girls than boys, with higher incidence in Caucasians and preterm infants. The head and neck are the most commonly involved locations (60%)[68]. They are usually small or absent at birth, and often present between 2 weeks and 2 months of age. These lesions progressively enlarge during the first year of life (proliferative phase), followed by a stationary phase and gradual regression (involution phase) between ages 1 and 8 years with nearly all lesions resolved by puberty[69]. On histology, infantile hemangiomas are glucose transporter protein type 1 (GLUT-1) positive. In contrast to infantile hemangiomas, congenital hemangiomas are present at birth as they begin their proliferative phase in-utero and are GLUT-1 negative. Three types of congenital hemangiomas are included in ISSVA classification based on their clinical course. Rapidly involuting congenital hemangiomas (RICH) involute by 1-2 years of age. Non-involuting congenital hemangiomas (NICH) do not involute or may steadily grow. Partially involuting congenital hemangiomas (PICH) only partially involute.

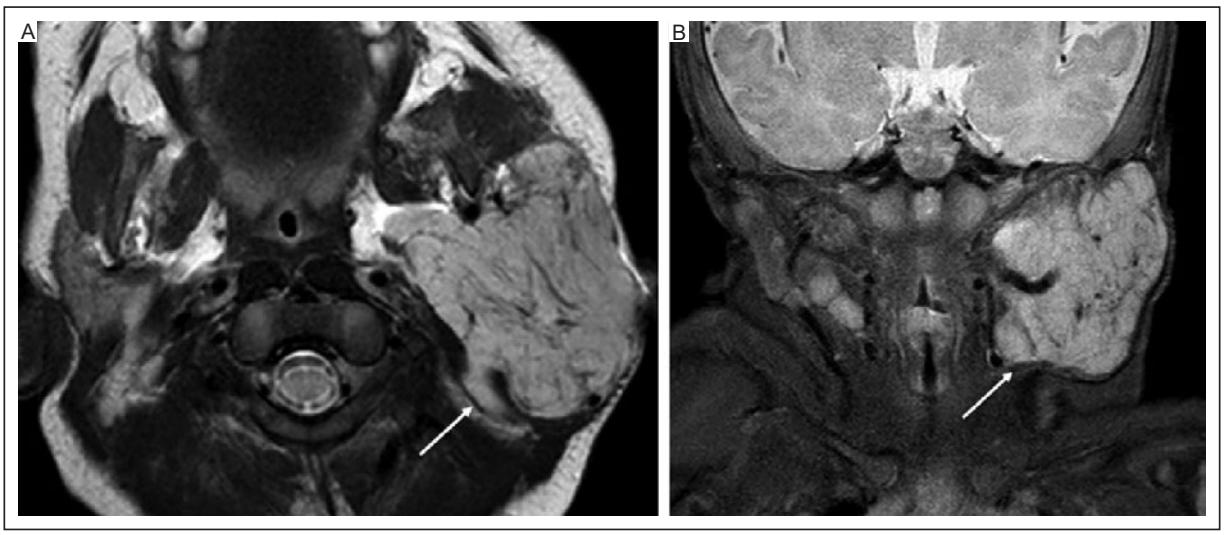

Figure 10. Infantile hemangioma. **A:** axial T2-weighted, and **B:** coronal T2-weighted fat-suppressed MRI of the neck of a 3-month-old boy shows a large T2 hyperintense lesion in the left anterior neck with multiple T2 hypointense internal flow voids consistent with an infantile hemangioma (arrows).

MRI: magnetic resonance imaging.

Hemangiomas may have superficial, deep, or mixed components. Superficial lesions have a "strawberry" appearance when there is skin involvement, and a blue appearance when there is deeper tissue involvement. During the proliferative phase, these lesions may become symptomatic due to rapid growth, resulting in ulceration and/or bleeding. Up to 10% of the patients with cutaneous hemangiomas also have airway lesions, typically in the subglottic region, mostly posteriorly on the left. Enlargement of the airway lesions may result in breathing difficulties, stridor, and airway compromise. Intra/perilesional bruit, pulsatility, or warmth can be appreciated during the proliferative phase[4,64,70].

Diagnosis is predominantly based on clinical examination. On ultrasound, the lesions appear as cutaneous or subcutaneous masses with prominent vascularity, demonstrating both arterial and venous waveforms on Doppler. On MRI, it appears as a mass with heterogeneous T1 signal, hyperintense T2 signal with prominent flow voids, high ADC values, and fairly homogeneous enhancement with gradual filling on post-contrast sequences, without surrounding aggressive changes (Figure 10)[71]. The presence of flow voids in a discrete enhancing mass helps to differentiate hemangiomas from arteriovenous malformations, which have much more aggressive behavior and require prompt treatment planning. In the absence of complications, hemangiomas may be observed as they regress spontaneously. In the setting of complications, medical therapy such as beta blockers or steroids and surgery may be needed. Hemangiomas should be differentiated from venous malformations which are low-flow vascular malformations related to abnormal development of venous channels, present at birth and grow proportionately to the body growth without spontaneous regression, and have heterogeneous enhancement and internal phleboliths that maybe seen on imaging[65].

Dermoid and epidermoid lesions

Dermoid and epidermoid lesions arise from entrapped elements of ectoderm within the substance of the neck, and are, therefore "inclusion cysts." As such, they may be found near the skin surface, at locations where folding and morphological changes occur (e.g., along the median and paramedian fusion plates at the junction of bones, soft tissues, and embryonic membranes)[72], or at locations where surface ectoderm fails to separate from the neural tube during embryologic development. Whether a dermoid or epidermoid results depends on the internal types of cells and elements. Both lesions are lined by ectodermal squamous epithelium. Dermoids contain, in addition, dermal adnexa and mesodermal components, such as hair, sebaceous glands, and rarely tooth or bone. Both may contain "cheesy" keratinous material[73]. Teratomas, on the other hand, are true neoplasms that arise from abnormally located embryologic germ cells, and usually contain elements of all three germ layers and a typical solid-cystic appearance with internal areas of fat well identified on

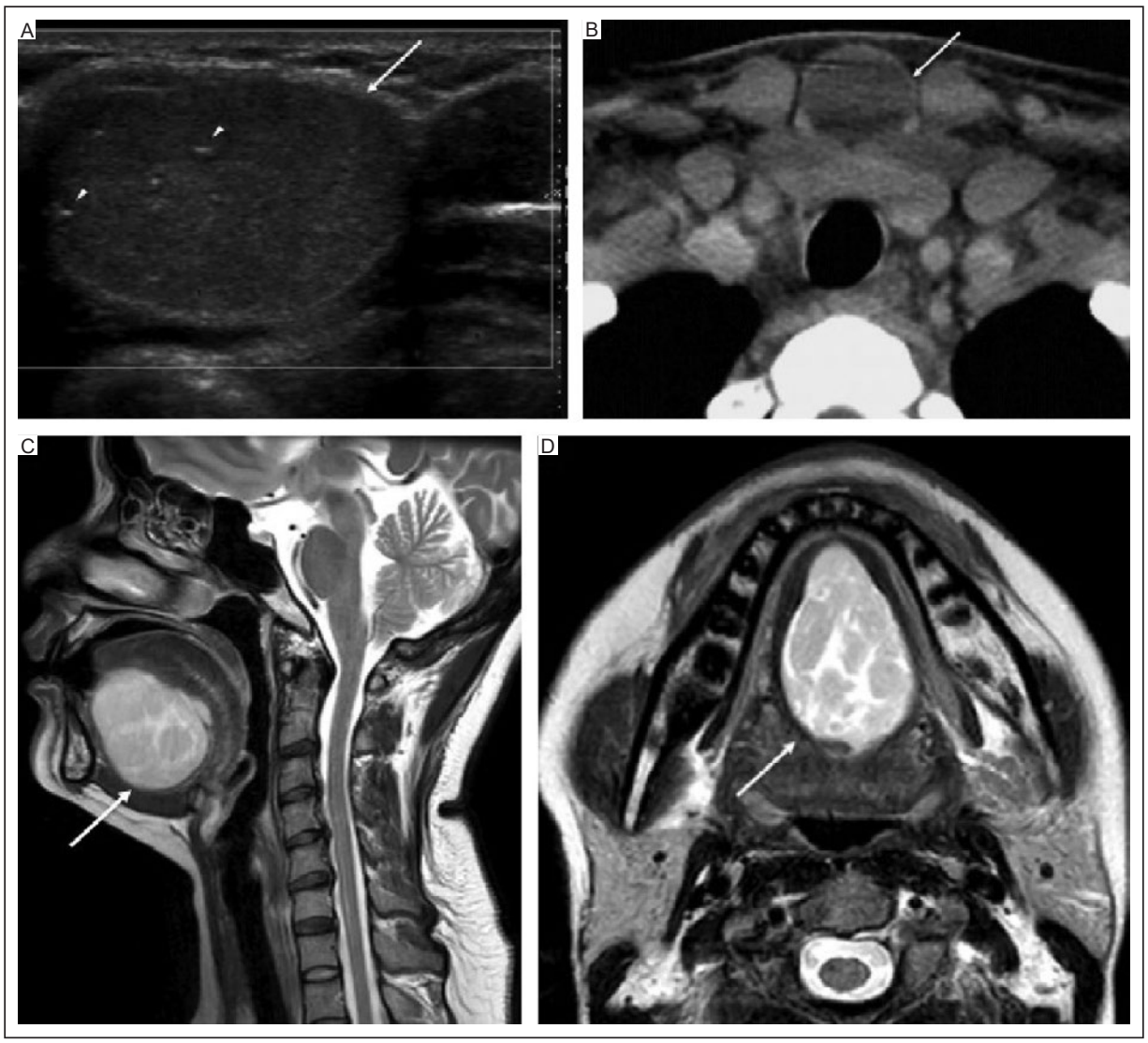

Figure 11. Dermoid cyst. **A:** ultrasound, and **B:** contrast-enhanced CT of the neck show a well-circumscribed thin-walled hypoechoic and hypodense lesion (arrows) in the lower midline neck with internal punctate echogenic foci (arrowheads) likely representing fat, complex debris, or calcification. **C:** sagittal, and **D:** axial T2-weighted MRI of the neck demonstrates a well-circumscribed T2 hyperintense lesion in the midline floor of the mouth with an internal "sack of marbles" appearance consistent with a dermoid cyst (arrows).

CT: computed tomography; MRI: magnetic resonance imaging.

MRI. One-third of dermoid cysts are found in the head and neck region[72,74]. Congenital dermoid cysts of the head and neck can be categorized into 4 groups[72,75]:

Group 1: Develops in the periorbital region - along the naso-optic groove or lateral brow. Most common location in the head and neck region.

Group 2: Develops along the nasal dorsum during ossification of the frontonasal plate. Mostly confined to the nasal dorsum but may have extension to the nasal cartilage, ethmoid sinus, sphenoid sinus, cribriform plate or intracranial compartment. When the embryologic tract extends to the anterior skull base and a small amount of ectopic brain tissue is entrapped in the tract, this is termed nasal glial heterotopia.

Group 3: Develops in the submental region, floor of mouth, and along the fusion line of first and second branchial arches in the midline.

Group 4: Develops along the mid-ventral and mid-dorsal fusion lines at the suprasternal, pre-thyroidal, and suboccipital regions.

More than half of dermoid cysts are detected before 6 years of age and approximately one-third are present at birth. There is no gender predilection[72]. They usually manifest as a mobile, non-tender, palpable mass. Lesions

arising from the skull (group 1 and group 2) may be immobile and hard on palpation. On ultrasound, dermoid and epidermoid cysts are well-circumscribed, hypoechoic lesions compared to subcutaneous fat. Echogenic foci may be seen in dermoids due to the presence of fat and calcifications. Hyperechoic areas may be seen when there is soft tissue or mucoid/purulent material. On CT, the lesions are unilocular and hypodense with varying degrees of internal inhomogeneous densities. In dermoids, calcifications appear as punctate hyperdensities, while fat globules appear as hypodense round areas giving the lesion a "sack of marbles" appearance, pathognomonic for dermoid cysts (Figure 11). Fat-fluid levels may be found. On MRI, the lesions are T2 hyperintense with varying degrees of T1 hyperintensity owing to the presence of fat in dermoids. There may be enhancement or calcification of the cyst walls. Treatment includes complete surgical excision.

CONCLUSION

A sound knowledge of embryology of the head and neck spaces is essential to aid in timely imaging diagnosis of congenital lesions of the neck in the pediatric population. A thorough clinical history and physical examination, age at presentation, evaluation of the anatomical site of origin, the clinical and radiological appearance of a lesion, and its relationship with nearby structures are important elements to consider, in order to generate an appropriate differential diagnosis, arrive at a most likely diagnosis, avoid non-essential testing, and to guide the type and urgency of appropriate intervention.

Funding

The authors declare that they did not receive any funding or support for this article.

Conflicts of interest

The authors declare no conflicts of interest.

Ethical disclosures

Protection of Individuals*:* This study was conducted in compliance with the Declaration of Helsinki (1964) and its subsequent amendments.

Confidentiality of Data. The authors declare they followed their center's protocol for sharing patient data.

Right to privacy and informed consent. The authors declare that there are no ethical responsibilities since humans' confidential information was not presented.

REFERENCES

1. Carlson BM. Human embryology and developmental biology. 2nd.ed. St. Louis: Mosby; 1999.
2. Luna MA, Pfaltz M. Cysts of the Neck, Unknown Primary Tumor, and Neck Dissection. In: Gnepp, DR. Diagnostic Surgical Pathology of the Head and Neck (Second Edition). Philadelphia: Saunders; 2009. p. 839–881.
3. Waldhausen JH. Branchial cleft and arch anomalies in children. Semin Pediatr Surg. 2006;15(2):64–69. doi: 10.1053/j.sempedsurg.2006.02.002.
4. MacLean JA, Sobol SE. Congenital Malformations of the Neck. Congenital Malformations of the Head and Neck. 2014:159–183. doi:10.1007/978-1-4419-1714-0_8.
5. Enepekides DJ. Management of congenital anomalies of the neck. Facial Plast Surg Clin North Am. 2001;9(1):131–145.
6. Acierno SP, Waldhausen JHT. Congenital cervical cysts, sinuses and fistulae. Otolaryngol Clin North Am. 2007;40(1):161–176, vii - viii. doi: 10.1016/j.otc.2006.10.009.
7. Park SW, Han MH, Sung MH, Kim IO, Kim KH, Chang KH, et al. Neck infection associated with pyriform sinus fistula: imaging findings. AJNR Am J Neuroradiol. 2000;21(5):817–822.
8. Arndal H, Bonding P. First branchial cleft anomaly. Clin Otolaryngol Allied Sci. 1996;21(3):203–207. doi: 10.1111/j.1365-2273.1996.tb01725.x.
9. Olsen KD, Maragos NE, Weiland LH. First branchial cleft anomalies. Laryngoscope.1980;90(3):423–436. doi: 10.1002/lary.5540900309.
10. Work WP. Newer concepts of first branchial cleft defects. Laryngoscope. 1972;82(9):1581–1593. doi:10.1288/00005537-197209000-00001.
11. Bansal AG, Oudsema R, Masseaux JA, Rosenberg HK. US of Pediatric Superficial Masses of the Head and Neck. RadioGraphics. 2018;38(4):1239–1263. doi: 10.1148/rg.2018170165.
12. Whetstone J, Branstetter BF 4th, Hirsch BE. Fluoroscopic and CT fistulography of the first branchial cleft. AJNR Am J Neuroradiol. 2006;27(9):1817–1819.
13. Ford GR, Balakrishnan A, Evans JN, Bailey CM. Branchial cleft and pouch anomalies. J Laryngol Otol. 1992;106(2):137–143. doi: 10.1017/s0022215100118900.
14. Doi O, Hutson JM, Myers NA, McKelvie PA. Branchial remnants: a review of 58 cases. J Pediatr Surg. 1988;23(9):789–792.doi:10.1016/s0022-3468(88)80223-9.
15. Agaton-Bonilla FC, Gay-Escoda C. Diagnosis and treatment of branchial cleft cysts and fistulae. A retrospective study of 183 patients. Int J Oral Maxillofac Surg. 1996;25(6):449–452. doi: 10.1016/s0901-5027(96)80081-6.
16. Choi SS, Zalzal GH. Branchial anomalies: a review of 52 cases. Laryngoscope.1995;105(9 Pt 1):909–913. doi: 10.1288/00005537-199509000-00007.
17. Proctor B, Proctor C. Congenital lesions of the head and neck. Otolaryngol Clin North Am. 1970;3(2):221–248.
18. Androulakis M, Johnson JT, Wagner RL. Thyroglossal duct and second branchial cleft anomalies in adults. Ear Nose Throat J. 1990;69(5):318–322.
19. Briggs RD, Pou AM, Schnadig VJ. Cystic metastasis versus branchial cleft carcinoma: a diagnostic challenge. Laryngoscope. 2002;112(6):1010–1014. doi:10.1097/00005537-200206000-00014.
20. Bailey H. Branchial cysts and other essays on surgical subjects in the facio-cervical region. London: Lewis & Company; 1929.
21. Mandell DL. Head and neck anomalies related to the branchial apparatus. Otolaryngol Clin North Am. 2000;33(6):1309–1332. doi:10.1016/s0030-6665(05)70283-8.
22. Godin MS, Kearns DB, Pransky SM, Seid AB, Wilson DB. Fourth Branchial Pouch Sinus. Laryngoscope. 1990;100(2):174–178. doi:10.1288/00005537-199002000-00012.
23. Takimoto T, Yoshizaki T, Ohoick H, Sakashita H. Fourth branchial pouch anomaly. J Laryngol Otol. 1990;104(11):905–907. doi:10.1017/s0022215100011432x.
24. Ohno M, Kanamori Y, Tomonaga K, Yamashita T, Migita M, Takezoe T, et al. Congenital cutaneous fistula at the sternoclavicular joint – Not a dermoid fistula but the remnant of the fourth branchial (pharyngeal) cleft? Int J Pediatr Otorhinolaryngol. 2015;79(12):2120–2123. doi:10.1016/j.ijporl.2015.09.025.
25. Burge D, Middleton A. Persistent pharyngeal pouch derivatives in the neonate. J Pediatr Surg. 1983;18(3):230–234. doi:10.1016/s0022-3468(83)80090-6.
26. Rosenfeld RM, Biller HF. Fourth branchial pouch sinus: diagnosis and treatment. Otolaryngol Head Neck Surg. 1991;105(1):44–50. doi: 10.1177/019459989110500107.

27. Burstin PP, Briggs RJ. Fourth branchial sinus causing recurrent cervical abscess. Aust N Z J Surg. 1997;67(2–3):119–122. doi: 10.1111/j.1445-2197.1997.tb01915.x.
28. Nicoucar K, Giger R, Jaecklin T, Pope HG Jr, Dulguerov P. Management of congenital third branchial arch anomalies: a systematic review. Otolaryngol Head Neck Surg. 2010;142(1):21–28.e2. doi: 10.1016/j.otohns.2009.09.001.
29. Liberman M, Kay S, Emil S, Flageole H, Nguyen LT, Tewfik TL, et al. Ten years of experience with third and fourth branchial remnants. J Pediatr Surg. 2002;37(5):685–690. doi:10.1053/jpsu.2002.32253.
30. Solomon JR, Rangecroft L. Thyroglossal-duct lesions in childhood. J Pediatr Surg. 1984;19(5):555–561. doi:10.1016/s0022-3468(84)80103-7.
31. Ellis PD, van Nostrand AW. The applied anatomy of thyroglossal tract remnants. Laryngoscope. 1977;87(5 Pt 1):765–770. doi: 10.1002/lary.5540870512.
32. Rosen RD, Sapra A. Embryology, Thyroid. In: StatPearls. Treasure Island (FL): StatPearls Publishing; 2022.
33. Rahbar R, Yoon MJ, Connolly LP, Robson CD, Vargas SO, McGill TJ, et al. Lingual thyroid in children: a rare clinical entity. Laryngoscope. 2008;118(7):1174–1179. doi: 10.1097/MLG.0b013e31816f6922.
34. Shepard GH, Rosenfeld L. Carcinoma of thyroglossal duct remnants. Review of the literature and addition of two cases. Am J Surg. 1968;116(1):125–129. doi:10.1016/0002-9610(68)90434-0.
35. Allard RH. The thyroglossal cyst. Head Neck Surg.1982;5(2):134–146. doi:10.1002/hed.2890050209.
36. Greinwald JH Jr, Leichtman LG, Simko EJ. Hereditary thyroglossal duct cysts. Arch Otolaryngol Head Neck Surg. 1996;122(10):1094–1096. doi: 10.1001/archotol.1996.01890220060010.
37. Ewing CA, Kornblut A, Greeley C, Manz H. Presentations of thyroglossal duct cysts in adults. Eur Arch Otorhinolaryngol. 1999;256(3):136–138. doi: 10.1007/s004050050126.
38. Foley DS, Fallat ME. Thyroglossal duct and other congenital midline cervical anomalies. Semin Pediatr Surg. 2006;15(2):70–75. doi: 10.1053/j.sempedsurg.2006.02.003.
39. Diaz MCG, Stormorken A, Christopher NC. A Thyroglossal Duct Cyst Causing Apnea and Cyanosis in a Neonate. Pediatr Emerg Care. 2005;21(1):35–37. doi:10.1097/01.pec.0000150987.19228.c8.
40. Samuel M, Freeman NV, Sajwany MJ. Lingual thyroglossal duct cyst presenting in infancy. J Pediatr Surg. 1993;28(7):891–893. doi: 10.1016/0022-3468(93)90689-i.
41. Peretz A, Leiberman E, Kapelushnik J, Hershkovitz E. Thyroglossal duct carcinoma in children: case presentation and review of the literature. Thyroid. 2004;14(9):777–785. doi:10.1089/thy.2004.14.777.
42. Koeller KK, Alamo L, Adair CF, Smirniotopoulos JG. Congenital cystic masses of the neck: radiologic-pathologic correlation. RadioGraphics. 1999;19(1):121–146; quiz 152–153. doi: 10.1148/radiographics.19.1.g99ja06121.
43. Branstetter BF, Weissman JL, Kennedy TL, Whitaker M. The CT appearance of thyroglossal duct carcinoma. AJNR Am J Neuroradiol. 2000;21(8):1547–1550.
44. Palumbo, C. Embryology and anatomy of the thymus gland. In: Lavini C, Moran CA, Morandi U, Schoenhuber R. Thymus gland pathology: clinical, diagnostic and therapeutic features, Milan, Springer, 2008, 13–18.
45. Berenos-riley L, Manni JJ, Coronel C, De Wilde PCM. Thymic cyst in the neck. Acta Otolaryngol. 2005;125(1):108-112. doi: 10.1080/00016480310016046.
46. Cigliano B, Baltogiannis N, De Marco M, Faviou E, Antoniou D, De Luca U, et al. Cervical thymic cysts. Pediatr Surg Int. 2007;23(12):1219–1225. doi:10.1007/s00383–006-1822-5.
47. Wenglowski R. Ueber de Halsfirtern and cysten. Arch Klein Chir. 1912–1913:100:789.
48. Wagner CW, Vinocur CD, Weintraub WH, Golladay ES. Respiratory complications in cervical thymic cysts. J Pediatr Surg. 1988;23(7):657–660. doi: 10.1016/s0022-3468(88)80640-7.
49. Joshua BZ, Raveh E, Saute M, Schwarz M, Tobar A, Feinmesser R. Familial thymic cyst. Int J Pediatr Otorhinolaryngol. 2004;68(5):573–579. doi: 10.1016/j.ijporl.2003.11.024.
50. De Caluwé D, Ahmed M, Puri P. Cervical thymic cysts. Pediatr Surg Int. 2002;18(5-6):477–479. doi:10.1007/s00383-002-0803-6.
51. Sturm-O'Brien AK, Salazar JD, Byrd RH, Popek EJ, Giannoni CM, Friedman EM, et al. Cervical thymic anomalies--the Texas Children's Hospital experience. Laryngoscope. 2009;119(10):1988–1993. doi: 10.1002/lary.20625.
52. Kaufman MR, Smith S, Rothschild MA, Som P. Thymopharyngeal duct cyst: an unusual variant of cervical thymic anomalies. Arch Otolaryngol Head Neck Surg. 2001;127(11):1357–1360. doi: 10.1001/archotol.127.11.1357.
53. Han BK, Yoon HK, Suh YL. Thymic ultrasound. II. Diagnosis of aberrant cervical thymus. Pediatr Radiol. 2001;31(7):480–487. doi: 10.1007/s002470100468.
54. Tovi F, Mares AJ. The aberrant cervical thymus. Embryology, Pathology, and clinical implications. Am J Surg. 1978;136(5):631–637. doi: 10.1016/0002-9610(78)90324-0.
55. Puscas L. Midline cervical cleft: review of an uncommon entity. Int J Pediatr. 2015;2015:209418. doi: 10.1155/2015/209418.
56. Villanueva-Meyer J, Glastonbury C, Marcovici P. Congenital midline cervical cleft. J Radiol Case Rep. 2015;9(3):7–11. doi: 10.3941/jrcr.v9i3.2202.
57. Rockson SG. Embryology of the Lymphatic System and Lymphangiogenesis. Lymphedema. 2011:43–48. doi:10.1007/978-0-85729-567-5_4.
58. Wassef M, Blei F, Adams D, Alomari A, Baselga E, Berenstein A, et al. Vascular Anomalies Classification: Recommendations From the International Society for the Study of Vascular Anomalies. Pediatrics. 2015;136(1):e203-e214. doi:10.1542/peds.2014-3673.
59. Zadvinskis DP, Benson MT, Kerr HH, Mancuso AA, Cacciarelli AA, Madrazo B, et al. Congenital malformations of the cervicothoracic lymphatic system: embryology and pathogenesis. RadioGraphics. 1992;12(6):1175–1189. doi: 10.1148/radiographics.12.6.1439020.
60. Acevedo JL, Shah RK, Brietzke SE. Nonsurgical therapies for lymphangiomas: a systematic review. Otolaryngol Head Neck Surg. 2008;138(4):418–424. doi: 10.1016/j.otohns.2007.11.018.
61. Friedman ER, John SD. Imaging of pediatric neck masses. Radiol Clin North Am. 2011;49(4):617–632, v. doi: 10.1016/j.rcl.2011.05.005.
62. Sajedi P, Shet N. Imaging of Pediatric Neck Masses. Int J Head Neck Surg. 2016;7(2):89–96. doi:10.5005/jp-journals-10001-1271.
63. Perkins JA, Manning SC, Tempero RM, Cunningham MJ, Edmonds JL Jr, Hoffer FA, et al. Lymphatic malformations: review of current treatment. Otolaryngol Head Neck Surg. 2010;142(6):795–803, 803.e1. doi: 10.1016/j.otohns.2010.02.026.
64. Donnelly LF, Adams DM, Bisset GS 3rd. Vascular malformations and hemangiomas: a practical approach in a multidisciplinary clinic. AJR Am J Roentgenol. 2000;174(3):597–608. doi:10.2214/ajr.174.3.1740597.
65. Tucci FM, De Vincentiis GC, Sitzia E, Giuzio L, Trozzi M, Bottero S. Head and neck vascular anomalies in children. Int J Pediatr Otorhinolaryngol. 2009;73 Suppl 1:S71-S76. doi: 10.1016/S0165-5876(09)70014-X.
66. Mulliken JB, Glowacki J. Hemangiomas and vascular malformations in infants and children: a classification based on endothelial characteristics. Plast Reconstr Surg. 1982;69(3):412–422. doi:10.1097/00006534-198203000-00002.
67. Kilcline C, Frieden IJ. Infantile hemangiomas: how common are they? A systematic review of the medical literature. Pediatr Dermatol. 2008;25(2):168–173. doi: 10.1111/j.1525-1470.2008.00626.x.
68. Baer AH, Parmar HA, DiPietro MA, Kasten SJ, Mukherji SK. Hemangiomas and vascular malformations of the head and neck: a simplified approach. Neuroimaging Clin N Am. 2011;21(3):641–658, viii. doi: 10.1016/j.nic.2011.05.007.
69. Kollipara R, Dinneen L, Rentas KE, Saettele MR, Patel SA, Rivard DC, et al. Current Classification and Terminology of Pediatric Vascular Anomalies. AJR Am J Roentgenol. 2013;201(5):1124–1135. doi:10.2214/AJR.12.10517.
70. O-Lee TJ, Messner A. Subglottic Hemangioma. Otolaryngol Clin North Am. 2008;41(5):903-911. doi:10.1016/j.otc.2008.04.009.
71. D'Arco F, Ugga L. Pearls, Pitfalls, and Mimics in Pediatric Head and Neck Imaging. Neuroimaging Clin N Am. 2022;32(2):433–445. doi: 10.1016/j.nic.2022.02.003.
72. Pryor SG, Lewis JE, Weaver AL, Orvidas LJ. Pediatric dermoid cysts of the head and neck. Otolaryngol Head Neck Surg. 2005;132(6):938–942. doi: 10.1016/j.otohns.2005.03.005.
73. Meyer I. Dermoid cysts (dermoids) of the floor of the mouth. Oral Surg Oral Med Oral Pathol. 1955;8(11):1149–1164. doi:10.1016/0030-4220(55)90380-7.
74. Görür K, Talas DU, Ozcan C. An unusual presentation of neck dermoid cyst. Eur Arch Otorhinolaryngol. 2005;262(4):353–355. doi: 10.1007/s00405-004-0813-1.
75. McAvoy JM, Zuckerbraun L. Dermoid cysts of the head and neck in children. Arch Otolaryngol. 1976;102(9):529–531. doi: 10.1001/archotol.1976.00780140061004.

JMeXFRI

Journal of the Mexican Federation of Radiology and Imaging

Check for updates

FULL RESEARCH ARTICLE

Knowledge of bioethical principles and elements of responsibility in radiology

Gerardo E. Ornelas-Cortinas[1,2,a], Adriana C. Cantu-Salinas[3,4] and Ana K. Luna-Marroquin[2]*

[1]Radiology and Imaging Department, Doctors Hospital AUNA; [2]Centro Universitario de Imagen Diagnostica, Hospital Universitario "Dr. Jose Eleuterio Gonzalez," Facultad de Medicina, Universidad Autonoma de Nuevo Leon, [3]Servicio de Neurologia Pediatrica, Hospital Universitario "Dr. Jose Eleuterio Gonzalez", Facultad de Medicina, Universidad Autonoma de Nuevo Leon; [4]Instituto de Investigaciones en Bioetica. Monterrey, Nuevo Leon, Mexico

ORCID: [a]0000-0003-2927-7700

ABSTRACT

Introduction: *Radiologists' participation in diagnosis and interventional therapeutic procedures has bioethical implications and professional responsibilities. We determined the level of knowledge of bioethical principles and elements of responsibility of radiologists and residents in public and private institutions in Mexico.* **Material and Methods:** *We conducted a digital survey to assess the level of knowledge of bioethical principles (beneficence, nonmaleficence, autonomy, and justice), and elements of responsibility. A low-level score was 0 to 9 points; a medium level, 10 to 13 points; and a high level, 14 to 22 points. Responsibility elements included appropriate imaging examination, informed consent, patient protection, radiologic reporting, patient and attending physician communication, continuous education, and continuous quality improvement. A low level of knowledge was 6 to 13 points; a medium level, 14 to 16 points, and a high level, 17 to 29 points.* **Results:** *We included a total of 228 participants,104 (45.6%) radiologists and 124 (54.4%) residents. A medium level of knowledge of bioethical principles was the most frequent in 55 (52.9%) radiologists and 75 (60.5%) residents. There was no statistically significant difference between levels. Residents had higher levels of knowledge of responsibility (n = 49, 39.5%) than radiologists (n = 26, 25.0%). Radiologists had low and medium (n = 39, 37.5%) in each level; in contrast to low (n = 36, 29.0%) and medium levels (n = 39, 31.5%) in residents. There was no statistically significant difference between groups.* **Conclusion:** *A medium level of knowledge of bioethical principles and elements of responsibility in radiologists and residents of public and private institutions was found. This study is the first in Mexico that presents information about radiology specialists.*

Keywords: *Principlism. Principle-Based. Ethics. Bioethics. Elements of responsibility. Radiology.*

INTRODUCTION

Like other health professionals, radiologists focus primarily on scientific knowledge and rarely consider bioethical aspects of the physician-patient relationship[1]. The four bioethical principles of principlism in relation to patient vulnerability are autonomy, beneficence, non-maleficence, and justice[2]. Technological and scientific advances in radiology have led to a dissociation between the benefits of imaging and patients´ human rights. Bioethical dilemmas may arise when performing and interpreting images, such as placing an image over clinical information, overlooking the target, who are patients, subjecting them to various imaging examinations, often without having interviewed or examined them[3], and ethical dilemmas that are thought to arise

***Corresponding author:**
Gerardo E. Ornelas-Cortinas
E-mail: ornelasge@yahoo.com.mx

Received for publication: 01-03-2023
Accepted for publication: 30-03-2023
DOI: 10.24875/JMEXFRI.M23000047

Available online: 13-07-2023
J Mex Fed Radiol Imaging. 2023;2(2):98-105
www.JMeXFRI.com

when the right choice is not clear[4]. As technological development increases, so does the risk of inappropriate use[5]. According to the World Health Organization, about 80% of medical decisions are made with imaging studies[6]. The credibility and popularity of imaging have reached a point where it is felt that no treatment can be initiated, or a patient discharged, without an imaging modality[7].

Berlin[8] points out that due to the nature of the procedures in their workplace, the radiologist has become distanced from the patient and is dedicated only to viewing images[9] leaving aside the responsibility associated with thinking over behavior in the face of bioethical dilemmas and decision-making based on technological advances[3,10,11]. Armstrong[3] described the seven basic elements of radiologists' responsibility: appropriate imaging examination, informed consent, patient protection, radiologic reporting, communication with the patient and attending physician, continuous education, and continuous quality improvement. Failure to comply with these elements of responsibility can lead to errors that affect patients[3,12].

Published studies have assessed the knowledge of bioethical principles and elements of responsibility in different medical specialties[13-15], but these have not been assessed in radiology. The radiologist has gradually and imperceptibly lost contact and communication with the patient, with a depersonalized attitude that is more scientific than focused on medical care. This study determined the level of knowledge of the bioethical principles and elements of responsibility of radiologists and residents in public and private institutions in Mexico. The theoretical basis of this study is related to the four bioethical principles that apply to radiology,[2,16] and the seven elements of radiologists´ responsibility[3].

MATERIAL AND METHODS

This cross-sectional, analytical study was conducted from April to September, 2022, in Monterrey, Nuevo Leon, Mexico. Mexican radiologists and residents of either sex, with no age limit, working in public or private institutions who agreed to participate were included. Incomplete questionnaires and physicians or residents from other specialties were not included. Informed consent was obtained. The study was approved by the Bioethics and Research Committees of the Instituto de Investigaciones in Bioetica of Monterrey, Nuevo Leon, Mexico.

Study development and variables

Radiology department heads and colleagues from hospitals were contacted electronically or by telephone in the following cities and states of Mexico: Aguascalientes, Aguascalientes; Mexicali, Baja California; Chihuahua, Chihuahua; Torreon and Saltillo, Coahuila; Guadalajara, Jalisco; Mexico City; Morelia, Michoacan; Monterrey, Nuevo Leon; Oaxaca, Oaxaca; Puebla, Puebla; Matamoros, Nuevo Laredo, and Ciudad Victoria, Tamaulipas. The aim of the study was explained, and the radiologists were invited to participate in the electronic digital survey. A digital consent form was provided, and the survey had a one-week deadline. It took approximately 20 minutes to complete.

The variables recorded were age, sex, public or private institutional affiliation (the affiliation of the radiologists who worked in both institutions was recorded in relation to the institution with the highest number of hours per day), the years of professional practice of the radiologists and the year of education of the residents. In addition, the following questions were asked: Have you ever taken a bioethics course? Would you be interested in taking a bioethics course? Do you think that updating your knowledge of bioethics would be useful in your daily practice?

Instrument to measure knowledge of bioethical principles

The instrument described by Casanova,[17] and Porra[18] was used (Supplementary material, Appendix 1). Knowledge of the bioethical principles, autonomy, beneficence, nonmaleficence, and justice was assessed. The survey included 22 multiple-choice questions that were scored by the author (GOC) as low knowledge, 0 to 9 points; medium knowledge, 10 to 13 points, and high knowledge, 14 to 22 points.

Instrument to measure knowledge of the elements of responsibility

The instrument was based on the seven elements of radiologists' responsibility previously published[3]. The author (GOC) designed a Likert-type questionnaire with 29 items (Supplementary material, Appendix 2). The author (GOC) scored a low level of knowledge of the elements of responsibility as 6 to 13 points, a medium level as 14 to 16 points, and a high level as 17 to 29 points.

Table 1. Characteristics of radiologists and residents

Description	Radiologists (n = 104)	Residents (n = 124)	Total (n = 228)
Public institutions, n (%)	52 (50.0)	119 (96.0)	171 (75.0)
Private institutions, n (%)	52 (50.0)	5 (4.0)	57 (25.0)
Age (years), mean SD ±	47.6 ± 12.97	29.1 ± 2.94	
Age groups, years, n (%)			
< 30	1 (1.0)	80 (64.5)	81 (35.5)
30 to 39	36 (34.6)	42 (33.9)	78 (34.2)
40 to 49	26 (25.0)	2 (1.6)	28 (12.3)
50 to 59	13 (12.5)	0	13 (5.7)
> 60	28 (26.9)	0	28 (12.3)
Year of Residency			
R1	NA	39 (31.5)	39 (31.5)
R2		31 (25.0)	31 (25.0)
R3		31 (25.0)	31 (25.0)
R4		23 (18.5)	23 (18.5)
Years of professional practice of radiologists, n (%)			
1 to 10	46 (44.2)	NA	46 (44.3)
11 to 20	21 (20.2)		21 (20.2)
21 to 30	20 (19.2)		20 (19.2)
31 to 40	12 (11.5)		12 (11.5)
41 to 50	4 (3.9)		4 (3.8)
> 50	1 (1.0)		1 (1.0)
Have you taken a bioethics course? Yes, n (%)	66 (63.5)	90 (72.6)	156 (68.4)
Would you be interested in taking a bioethics course? Yes, n (%)	95 (91.3)	106 (85.5)	201 (88.2)
Do you think that updating bioethics knowledge is useful in daily practice? Yes, n (%)	101 (97.1)	114 (91.9)	215 (94.3)

NA: not aplicable.

Statistical analysis

The sample size was calculated non-probabilistically using simple random sampling. Inference of proportions and comparison of two independent samples were used with a power of 80%. The calculated sample size was 96 radiologists and 96 residents. Categorical variables were described as absolute frequencies and percentages, and continuous variables as means and standard deviations. Knowledge of bioethical principles and elements of responsibility of radiologists and residents was assessed with the chi^2 test for categorical variables and Student's t-test for continuous variables. IBM-SPSS software version 25 (IBM Corp., Armonk, NY, USA) was used for data analysis.

RESULTS

Two hundred twenty-eight questionnaires from 228 participants were completed; 88 (38.6%) were women, and 140 (61.4%) were men. There were 104 (45.6%) radiologists and 124 (54.4%) residents (Table 1). Public institution participation (n = 171, 75.0%) was higher, mainly among residents (n = 119, 96.0%). The mean age of the radiologists was 47.6 ± 12.97 years and 29.1 ± 2.94 years for residents. Participation by age group was lower among radiologists under age 30 (n = 1, 1.0%), in contrast to residents where most participants were under age 30 (n = 80, 64.5%). No significant differences were found in the number of residents per school year. Radiologists between 1 and 10 years

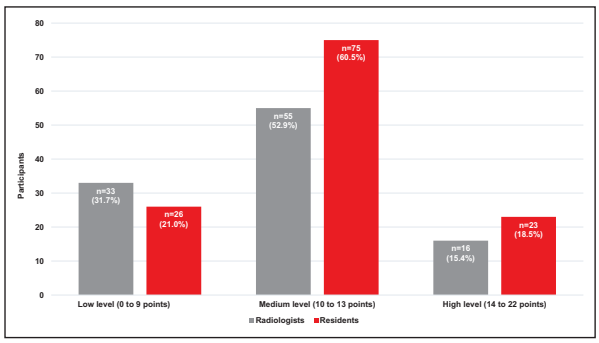

Figure 1. Level of knowledge of radiologists and residents regarding the bioethical principles. A medium level (10 to 13 points) was most common in both groups. Differences were not statistically significant.

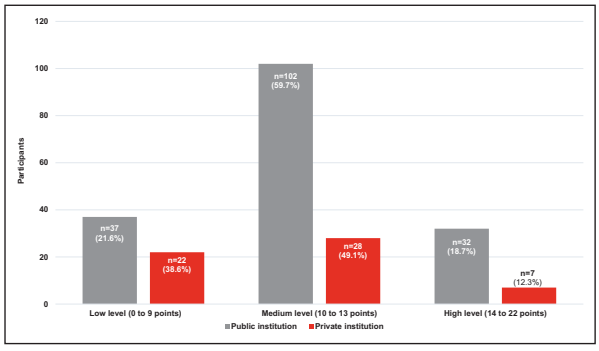

Figure 2. Level of knowledge of bioethical principles according to the type of institution. A medium level was more common among participants from public institutions. A low level was significantly more common in private institutions and a high level in public institutions ($p < 0.05$).

of professional practice after graduation from the specialty had higher participation (n = 46, 44.2%). One hundred fifty-six (68.4%) participants reported having taken a bioethics course; 201 (88.2%) would be interested in taking a bioethics course, and 215 (94.0%) of 228 felt that knowledge of bioethics would be useful in their daily practice. Participation in bioethics courses was higher among radiologists and residents of public institutions; 120 (76.5%) of 156; of these, 66 (42.3%) were radiologists, and 90 (57.7%) were residents.

Level of knowledge of bioethical principles

Figure 1 shows the level of knowledge of radiologists and residents regarding bioethical principles. A medium level (10 to 13 points) was most common in 55 (52.9%) of 104 radiologists and 75 (60.5%) of 124 residents. A high level was more common among residents (n = 23, 18.5%) than radiologists (n = 16, 15.4%). In contrast, fewer residents showed a low level (n = 26, 21.0%) than radiologists (n = 33, 31.7%). These differences were not statistically significant.

The level of knowledge of bioethical principles by type of institution is shown in Figure 2. A medium level was more common, with 102 (59.7%) of 171 participants from public institutions and 28 (49.1%) of 57 participants from private institutions. The low level was significantly more common in private institutions (n = 22, 38.6%) and the high level in public institutions (n = 32, 18.7%) ($p < 0.05$).

The level of radiologists´ knowledge of bioethical principles regarding to the number of years of professional practice was comparable among the different groups (Table 2). Regardless of the years of professional practice, a higher number of radiologists had a medium level. The differences were not statistically significant. The level of knowledge of bioethical principles among residents did not show significant differences in relation to the year of residency (Table 3). Regardless of the year of residency, a medium level of knowledge was most common. A higher proportion of residents with a high level of knowledge was observed in residency year 4 (R4) (n = 7, 30.4%), but the difference was not significant compared with the other years of residency. Figure 3 shows the relationship between the level of knowledge of bioethical principles and whether a bioethics course was taken. There were no statistically significant differences between knowledge levels.

Level of knowledge of the elements of responsibility

Figure 4 shows the level of knowledge of the elements of responsibility of radiologists and residents. A greater number of residents had a high level of knowledge (n = 49, 39.5%) compared to radiologists (n = 26, 25%). On the other hand, more radiologists had a low and medium level (n = 39, 37.5% in each level), in contrast to residents with a low (n = 36, 29.0%) and medium level (n = 39, 31.5%). The differences were not statistically significant.

No statistically significant difference was found with respect to knowledge of the elements of responsibility by type of institution, as the frequency of the different levels of knowledge by institution was very similar (Figure 5). Among radiologists, a medium level of knowledge was found to be predominant in the group with 1 to 10 years of professional practice, whereas a low level of knowledge was higher among radiologists with more than 30 years of professional practice;

Table 2. Level of radiologists' knowledge of bioethical principles regarding number of years of professional practice

Description	Years of professional practice				Total (n = 104)
	1 to 10 (n = 46)	11 to 20 (n = 21)	21 to 30 (n = 20)	> 30 (n = 17)	
Low level, n (%)	13 (28.3)	7 (33.3)	7 (35.0)	6 (35.3)	33 (31.7)
Medium level, n (%)	24 (52.1)	11 (52.4)	10 (50.0)	10 (58.8)	55 (52.9)
High level, n (%)	9 (19.6)	3 (14.3)	3 (15.0)	1 (5.9)	16 (15.4)

Table 3. Level of knowledge of bioethical principles among residents regarding year of residency

Description	Year of residency				Total (n = 124)
	R1 (n = 39)	R2 (n = 31)	R3 (n = 31)	R4 (n = 23)	
Low level, n (%)	4 (10.2)	8 (25.8)	8 (25.8)	6 (26.1)	26 (21.0)
Medium level, n (%)	29 (74.4)	16 (51.6)	20 (64.5)	10 (43.5)	75 (60.5)
High level, n (%)	6 (15.4)	7 (22.6)	3 (9.7)	7 (30.4)	23 (18.5)

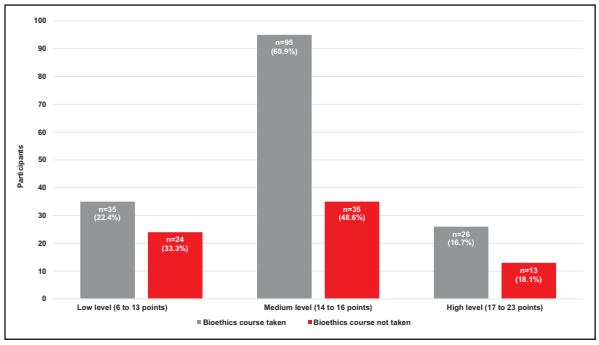

Figure 3. Relationship between the level of knowledge of bioethical principles and whether a bioethics course was taken. There were no statistically significant differences.

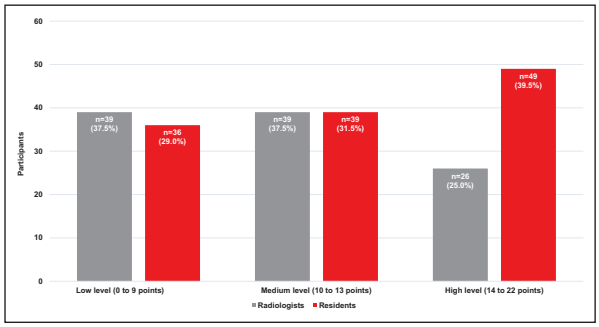

Figure 4. Level of knowledge of elements of responsibility of radiologists and residents. A greater number of residents with a high level of knowledge was observed compared with radiologists. Differences were not statistically significant.

however, the number of radiologists older than 30 was low (n = 17); therefore, this group cannot be considered a representative sample (Table 4).

Regarding the level of knowledge of the elements of responsibility among residents, participants in their first and second years (R1 and R2) achieved the highest level of knowledge of the elements of responsibility (43.6% and 45.2%, respectively) (Table 5). There was no statistically significant difference between the different years of residency and the level of knowledge about the elements of responsibility. Figure 6 shows the relationship between the level of knowledge about the elements of responsibility and whether a bioethics course was taken. No statistically significant differences were found between knowledge levels.

DISCUSSION

We found that a medium level of knowledge of bioethical principles and elements of responsibility prevails among radiologists and residents in public and private institutions in Mexico. It is recommended to support training in residency programs and continuing education courses, to achieve an optimal level of knowledge to provide dignified, fair, and respectful care for patients and to keep in mind that *"Behind an image is a person who deserves personalized care with high scientific quality"* (Figure 7).

The bioethical profile of radiology professionals requires knowledge and application of bioethical and deontological principles. Velázquez et al.[14] conducted a study to measure the bioethical knowledge of 15 general surgeons and 37 residents of the General Hospital of Mexico City. An instrument from the College of Toronto was used based on 4 clinical cases with ethical

Table 4. Level of knowledge of the elements of responsibility by years of professional practice among radiologists

Description	Years of professional practice				Total (n = 104)
	1 to 10 (n = 46)	11 to 20 (n = 21)	21 to 30 (n = 20)	>30 (n = 17)	
Low level, n (%)	14 (30.4)	7 (33.3)	9 (45.0)	9 (52.9)	39 (37.5)
Medium level, n (%)	22 (47.9)	8 (38.1)	7 (35.0)	2 (11.8)	39 (37.5)
High level, n (%)	10 (21.7)	6 (28.6)	4 (20.0)	6 (35.3)	26 (25.0)

Table 5. Level of knowledge of responsibility elements in residents by year of residency

Description	Year of residency				Total (n = 124)
	R1 (n = 39)	R2 (n = 31)	R3 (n = 31)	R4 (n = 23)	
Low level, n (%)	12 (30.8)	4 (12.9)	11 (35.5)	9 (39.2)	36 (29.0)
Medium level, n (%)	10 (25.6)	13 (41.9)	9 (29.0)	7 (30.4)	39 (31.5)
High level, n (%)	17 (43.6)	14 (45.2)	11 (35.5)	7 (30.4)	49 (39.5)

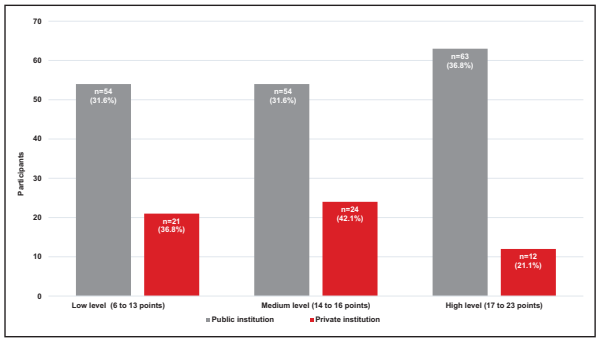

Figure 5. The elements of responsibility show a comparable frequency of the different levels of knowledge by type of institution.

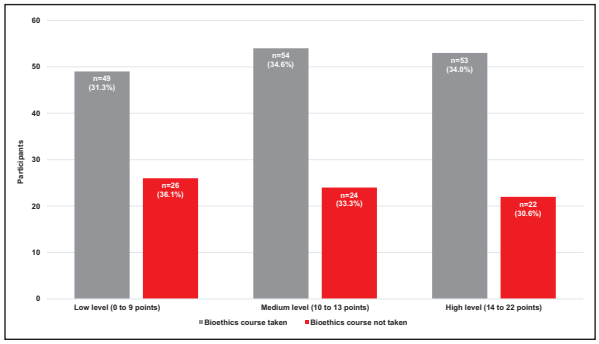

Figure 6. Relationship between the level of knowledge regarding the elements of responsibility and whether a bioethics course was taken. No statistically significant differences were found.

dilemmas related to autonomy, beneficence, and justice[15]. General surgeons performed better than residents in identifying bioethical dilemmas based on bioethical principles. Casanova et al.[17] conducted a study with 20 general surgeons, 20 internists, 16 pediatricians, and 16 obstetrician-gynecologists to determine the level of knowledge of bioethical principles. The survey included 13 questions. The level of knowledge was unsatisfactory, with a mean of 46% correct answers. Pediatricians performed better with 9 (59%) correct responses. No significant differences were found between participants regarding sex, master's or doctoral degree, or history of bioethics training. The authors believed that the better performance of the pediatricians was related to the fact that they had undergraduate studies in bioethics, unlike the other participants who had not received bioethics education during their professional training. Our study found that knowledge of bioethical principles was at a medium level among radiologists and residents. We believe that a medium level of knowledge of bioethical principles is not optimal for providing high-quality care based on bioethical principles.

Radiologists must have relevant knowledge of the elements of tasks and responsibilities to achieve optimal professional performance quality. Tachiquin Sandoval et al.[19] conducted a study in community, general, and specialty hospitals of the health services of Zacatecas, Mexico, to determine the knowledge of responsibility among 861 health professionals, including general practitioners and specialists, interns, general nurses, auxiliary nurses, and nurses from other areas; 267 were physicians. Knowledge of professional responsibility was poor (0.4%). López-Almejo et al.[13] assessed the knowledge of professional responsibility of 130 physicians specializing in orthopedics and

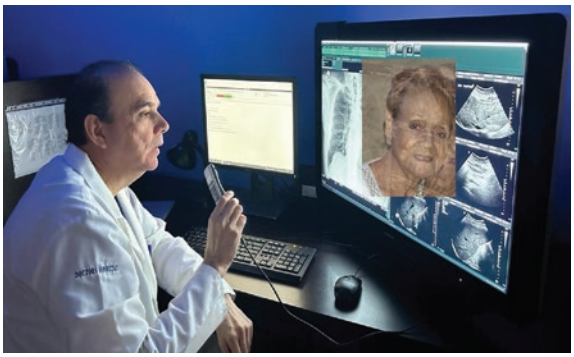

Figure 7. Behind an image, there is a person who deserves personalized care with high scientific quality.

traumatology in hospitals in Mexico City. The instrument included 15 questions on professional responsibility and the legal framework. The mean score was 5.7 (poor). Our study found a predominant medium level of knowledge of the elements of responsibility. There were no significant differences among participants who attended bioethics courses or by type of institution, years of professional practice, and year of residency. Reinforcement of responsibility elements in radiology beyond the medical-legal aspects and recognizing the patient's human rights are necessary[20].

In addition to the cognitive processes for efficient performance, radiologists need knowledge of bioethical principles and elements of responsibility to avoid errors due to ethical misconduct or irresponsibility. Hebert et al.[15] conducted a study to measure ethical sensitivity in 498 medical students in their first four years of undergraduate study at the University of Toronto, Canada. Participants evaluated four clinical cases to identify the bioethical principles of autonomy, beneficence, and justice. The authors found that ethical sensitivity decreases as they progress through the specialty. They suggested that this may result from socialization in 4th-year residency students. In our study, radiologists with fewer years of practice (1-10 years) and first- and second-year residents demonstrated better knowledge levels (medium and high) of bioethical principles and elements of responsibility. The differences were not statistically significant. It is likely that due to the increasing interest in new technologies, radiologists with more years of practice and residents of higher education levels (R3/R4) focus their attention on cognitive aspects with disinterest in patient contact.

The strengths of our study relate to the sample size and the study population, which included radiologists with different years of professional practice and residents with four years of education. The weaknesses relate to the fact that the participants were mostly from public institutions. Some radiologists may practice in public and private institutions, but this was not recorded in the survey.

CONCLUSION

Our study showed that radiologists and residents have a medium level of knowledge about bioethical principles and elements of responsibility. This research arose from an interest in promoting bioethics and deontology courses in radiologists' residency and fellowship programs to increase their knowledge level of bioethics and elements of responsibility and to provide more humane, dignified, responsible, and beneficial care for their patients.

Supplementary data

Supplementary data are available online in the Journal online (DOI: 10.24875/JMEXFRI.M23000047). These data are provided by the corresponding author and published online for the reader's benefit. The contents of supplementary data are the sole responsibility of the authors.

Acknowledgments

The authors thank Professor Ana M. Contreras-Navarro for her guidance in preparing and writing this scientific paper.

Funding

This research received no external funding.

Conflicts of interest

The authors declare that they have no conflicts of interest.

Ethical disclosures

Protection of Individuals. This study complied with the Declaration of Helsinki (1964) and subsequent amendments.

Confidentiality of Data. The authors declare they followed their center's protocol for sharing patient data.

Right to privacy and informed consent. Informed consent was obtained from all participants.

REFERENCES

1. Beauchamp TL, Childress JF. Principios de Ética Biomédica. Bioetica & Debat. 2011; 17(64) [accessed 2023 February 09]. Available from: http://www.ucv.ve/fileadmin/user_upload/facultad_agronomia/Producion_Animal/ProducciOn_Animal/Bioetica.pdf
2. Black WC, Welch HG. Advances in diagnostic imaging and overestimations of disease prevalence and the benefits of therapy. N Engl J Med. 1993; 328(17):1237–1243. doi: 10.1056/NEJM199304293281706.
3. Armstrong JD 2nd. Morality, ethics, and radiologists' responsibilities. AJR Am J Roentgenol. 1999; 173(2): 279-284. doi: 10.2214/ajr.173.2.10430119.
4. Ahmad K, Ethics in Radiology. Global Bioethics Enquiry. 2019; 7(3):160–164. doi:10.38020/GBE.7.3.2019.160-164.
5. Perojo Páez VM, Matanzas García N, Azcuy González Y. El principio de Responsabilidad, una necesidad de estos tiempos. INFODIR. 2014; 18: 54–61.
6. SERAM. Una guía para considerar una especialización en radiodiagnóstico. [Internet]. 2015. [Accessed 2023 February 09]. Available from: https://seram.es/images/site/documentosSeram/ser_radiologo.pdf
7. Raymond J, Trop I. The practice of ethics in the era of evidence-based radiology. Radiology. 2007; 244(3): 643–649. doi: 10.1148/radiol.2443052026.
8. Berlin L. The radiologist: doctor's doctor or patient's doctor. AJR Am J Roentgenol. 1977; 128(4): 702. doi: 10.2214/ajr.128.4.702.
9. Moënne, K. Profesionalismo en el ejercicio de la Radiología. Rev Chil Radiol. 2017; 23(4): 180-181.
10. Jonas, H. El principio de responsabilidad. Ensayo de una ética para la civilización tecnológica. [Internet]. Barcelona. 1995. [Accessed 2023 February 09]. Available from: https://doctoradohumanidades.files.wordpress.com/2015/04/jonas-el-principio-de-responsabilidad.pdf
11. Escobar Triana J. Bioética: Orígenes y Tendencias. Rev Facultad Med. 2000; 48 (4): 219–223.
12. Barron BJ, Banja J. Radiologic reporting: the ethical obligation of the interpreting physician to provide an accurate report. AJR Am J Roentgenol. 2013; 201(2): 356-360. doi: 10.2214/AJR.12.9746.
13. López Almejo AL, Palapa García LR, Bueno Olmos ME, Méndez Gómez MA. Conocimiento de la responsabilidad profesional en la práctica médica. Acta Ortop Mex. 2006; 20(3): 132–138.
14. Velázquez Aviña J, Pulido Cejudo A, Ruiz Suárez M, Hurtado López M. Medición del conocimiento en bioética en residentes y médicos de base de cirugía general del Hospital General de México. Cir Gen. 2011; 33(4): 248-254.
15. Hébert PC, Meslin EM, Dunn EV. Measuring the ethical sensitivity of medical students: a study at the University of Toronto. J Med Ethics. 1992; 18: 142–147.
16. Peralta Cornielle A. Código de *ética* y deontología médica. [Internet]. Colegio Interamericano de Radiología. 2013. [Accessed 2023 February 09]. Available from: https://www.webcir.org/docs/bioetica_codigo_eticacir.pdf
17. Casanova Saldarriaga JF. Conocimiento de los principios fundamentales de la bioética en los médicos de Hospital IV [dissertation]. Universidad Nacional Mayor de San Marcos; 2007.
18. Porra Casals JM, Díaz Valladares I, Cordero López G. Conocimientos y aplicación de los principios éticos y bioéticos en el proceso de atención de enfermería. Rev Cubana Enferm. 2001; 17(2): 132–138.
19. Tachiquin Sandoval R, Romero Escobedo AC, Padilla Villalobos LA. Conocimiento sobre responsabilidad profesional en la atención médica: ¿falta de actitud, interés o educación?. Rev Conamed. 2014; 19(1): 23–31.
20. Ramírez Vicente RM, Del Barrio Fernández JL, Rodríguez Caravaca G. Radiología médico-legal. Un dilema ético para el técnico en radiología. Acta bioeth. 2017; 23(2): 245–251.

JMeXFRI

Journal of the Mexican Federation of Radiology and Imaging

Check for updates

FULL RESEARCH ARTICLE

Tomographic assessment of pulmonary abnormalities of Long COVID: a cohort study

*Cinthia Diaz-Salas[1,a], Mariana Amaya-Tellez[1], Vania Hinojos-Armendariz[2], Sofia Valencia-Pacheco[1], Arturo Reyes-Esparza[1], Dizan Mendoza-Pedroza[2], Yamile Lopez-Hernandez[3] and Joel Monarrez-Espino[1,4,b]**

[1]Medical Specialties Program, Universidad de Monterrey, Sede Chihuahua;[2]Department of Radiology, Christus Muguerza del Parque Hospital, Chihuahua, Chihuahua, Mexico; [3]Academic Unit of Biological Sciences, Universidad Autonoma de Zacatecas, Zacatecas, Mexico; [4]Department of Health Research, Christus Muguerza del Parque Hospital, Chihuahua, Chihuahua, Mexico.

ORCID: [a]0009-0004-7078-3837; [b]0000-0002-0695-5356

ABSTRACT

Introduction: *SARS-CoV-2 infection primarily affects the lungs leading to a range of tomographic findings, from ground-glass opacity to emphysema. However, studies on the long-term effects of the infection, known as Long COVID, are still limited. Therefore, this cohort aimed to identify pulmonary abnormalities in adult patients with Long COVID, assessed by chest computed tomography (CT) 6 to 30 months after the initial infection.* **Material and Methods:** *A cohort of patients from northern Mexico, diagnosed with COVID-19 in 2020-2021 using RT-PCR and undergoing a simple chest CT examination, was followed up for 6 to 30 months. Logistic regression was used to determine predictors of Long COVID.* **Results:** *A total of 67 patients were included. Pulmonary tomographic abnormalities at 6 to 30 months were interstitial thickening (n = 41, 61.2%), subpleural bands (n = 41, 61.2%), ground-glass opacity (n = 30, 44.8%), pleural thickening (n = 18, 26.9%), bronchiectasis (n = 13, 19.4%), lymphadenomegaly (n = 11, 16.4%), emphysema (n = 6, 9.0%), and consolidation (n = 2, 3.0%). Ground-glass opacity and fibrotic abnormalities decreased with increasing follow-up time: e.g., interstitial thickening from 6 to 11 months (84.6%), 12 to 18 (65.0%), and 19 to 30 months (50.0%). Hypertension was the most significant predictor of Long COVID.* **Conclusion:** *Our study showed a high prevalence of persistent pulmonary abnormal tomographic findings in patients with Long COVID, probably due to the high prevalence of hypertension and diabetes. Ground-glass opacity and fibrotic abnormalities were the most commonly observed findings, which showed a decreasing trend over time.*

Keywords: *Long COVID. Pulmonary sequelae. COVID-19. Chest Computer tomography. Chest CT.*

INTRODUCTION

COVID-19 became a major global health challenge since of the pandemic. Initially, up to one-third of patients experienced severe pulmonary complications, including acute respiratory distress syndrome (ARDS)[1]. The clinical and radiological features of COVID-19 have been extensively studied. Chest computed tomography (CT) has played a crucial role in assessing the pulmonary condition of COVID-19 patients. Typical manifestations during the acute phase include peripherally distributed ground-glass opacity, consolidation, and interlobular interstitial thickening[2]. While most infected patients have recovered and resumed their normal lives after being infected, a significant number still experience persistent symptoms such as fatigue, shortness of breath, and cognitive impairment, adversely affecting their quality of life[3]. This clinical condition is now known as post COVID-19 syndrome or Long COVID[4]. Risk factors associated with the development of Long COVID are

***Corresponding author:**
Joel Monarrez-Espino
E-mail: joel.monarrez@christus.mx

Received for publication: 20-02-2023
Accepted for publication: 27-03-2023
DOI: 10.24875/JMEXFRI.M23000048

Available online: 13-07-2023
J Mex Fed Radiol Imaging. 2023;2(2):106-114
www.JMeXFRI.com

inconsistent, but mainly include sex, age, obesity and severity of infection[5-8].

Initial studies showed that severe and critical ARDS caused by COVID-19 pneumonia was associated with significant radiological abnormalities (i.e., mosaic hypoattenuation on chest CT) at four months of follow-up[1]. Six months after recovering from severe COVID-19 pneumonia, follow-up chest CT scan showed residual fibrosis-like changes, including traction bronchiectasis, honeycomb pattern, interlobular pleural traction, and pleural thickening[9]. Approximately one-third of patients with moderate-to-severe pneumonia, particularly those who required mechanical ventilation in the intensive care unit (ICU), exhibited persistent abnormalities on chest CT scans one year after the initial diagnosis, consistent with the spectrum of COVID -19 syndrome, ranging from parenchymal bands, bronchial dilatation, and fibrosis, or with other findings such as unilobar and multilobar areas of hypoattenuation, ground-glass opacities with mosaic attenuation pattern, linear and curvilinear densities, reticulations, honeycomb pattern, distortion of lung architecture at various sites, and pneumatoceles[10].

One of the longest follow-up series with 83 patients who survived severe COVID -19 pneumonia showed a high prevalence of residual findings on the chest CT scans at hospital discharge, with sustained improvement observed 12 months after discharge. The proportion of patients with residual CT findings progressively decreased from 78% at three months post-discharge to 48% at six months, 27% at nine months, and 24% at one-year later[11]. While radiological features have been extensively studied at different stages of COVID-19 pneumonia, there are still insufficient data on the tomographic features of Long COVID[12-14]. Although most changes following COVID-19 pneumonia resolve within the first year of recovery, persistent or progressive fibrosis appears to be a significant concern[13,15]. Hence, the primary aim of this study was to identify the chest CT features of Long COVID in adult patients evaluated 6 to 30 months after the initial infection.

MATERIAL AND METHODS

A cohort study was conducted on patients diagnosed with COVID-19 in 2020 and 2021 at the Department of Radiology in Christus Muguerza del Parque Hospital, located in the city of Chihuahua in northern Mexico. This private institution, with 80 beds, admits nearly ten thousand patients annually. Participants who provided primary data signed written informed consent, and approval from hospital authorities was obtained to retrieve secondary data from the radiology department's electronic archives. The study protocol was approved by institutional ethics and research committees.

Study population and definitions

Participants were patients diagnosed with COVID-19 using reverse transcription-polymerase chain reaction (RT-PCR) from a nasopharyngeal specimen using standard methods[16], and who had a simple chest CT scan positive for COVID-19 at the initial diagnosis (COVID-19 Reporting and Data System/CO-RADS 5 and 6)[17], and underwent a follow-up chest CT at least six months after the baseline chest CT. Follow-up period ranged from 6 to 30 months. Patients treated at ICU were excluded from the study.

According to WHO[4], Long COVID-19 is a new medical condition that *"occurs in individuals with a history of probable or confirmed SARS-CoV-2 infection, usually three months from the onset of COVID-19, with symptoms that last for at least two months and cannot be explained by an alternative diagnosis."*

Three groups of participants were sampled, corresponding to prospective, retrospective, and ambispective cohorts of patients. Figure 1 shows a flowchart depicting the sampling strategy used to select study participants.

Prospective cohort: this group consisted of a sample of COVID-19 patients involved in the baseline study between August and December 2020[18]. Individuals were treated at home or hospitalized with or without oxygen support depending on the clinical severity of the infection.

Retrospective cohort: this group included patients diagnosed with COVID-19 who were hospitalized in 2020 and 2021 and had both a baseline and a follow-up chest CT examination separated by at least six months. Both the chest CT scans and the patients baseline data were available in the hospital's radiology archive (secondary data).

Ambispective cohort: this group consisted of hospitalized COVID-19 patients diagnosed in 2020 and 2021 who had a baseline chest CT available in the hospital's radiology archive. From the 369 eligible, a stratified by age random sample of 35 was taken of which 26 were followed under informed consent.

Study development and variables

Patients from the prospective and ambispective cohorts were interviewed and physically examined by trained medical residents, and various clinical,

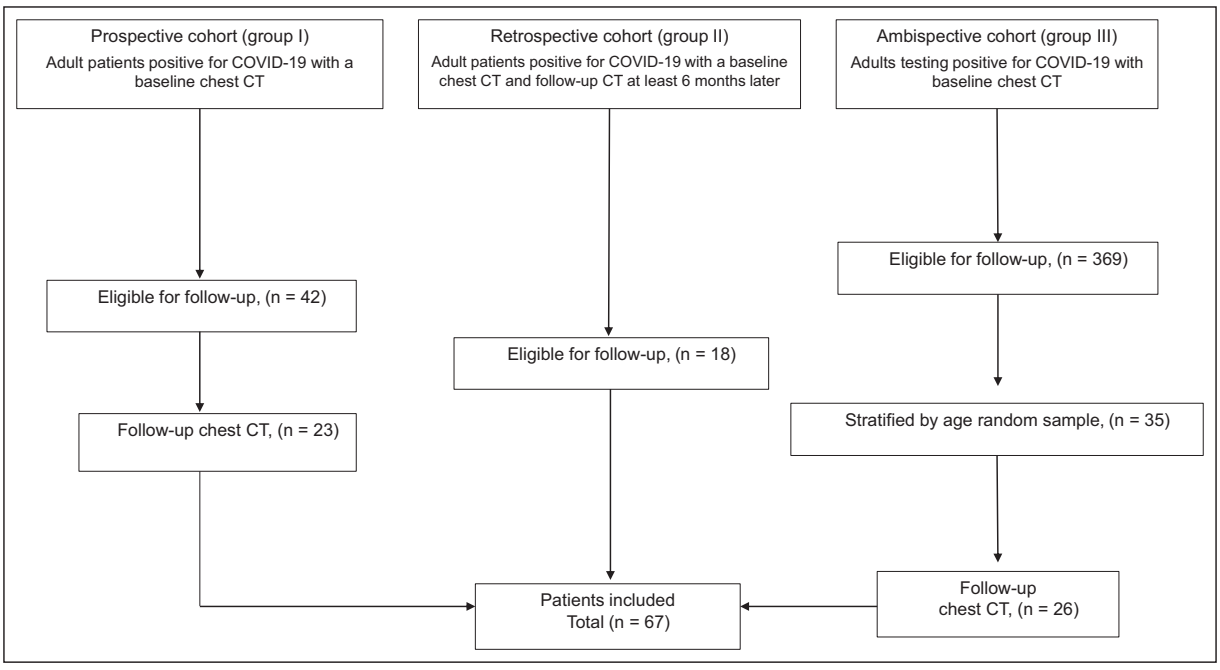

Figure 1. Flowchart of a cohort study on persistent pulmonary tomography abnormalities in COVID-19 patients and their follow-up.
CT: computed tomography; COVID: coronavirus disease.

neuropsychological, and laboratory assessments were performed. Presentation of clinical and metabolomic results is ongoing[19]. Subsequently, the patients were transferred to the radiology department for a simple chest CT scan. The total duration of the hospital visit lasted around 60-75 minutes (10-15 minutes for follow-up chest CT).

Basic sociodemographic and clinical data were collected, including sex, age, smoking and alcohol use, main comorbidities, and weight and height for calculating body mass index (BMI).

Image acquisition and analysis

A *Somatom Definition AS*® tomograph (Siemens Corp., Munich, Germany) was used to obtain the chest CT scans. The tomographic findings of the baseline and follow-up chest CTs were assessed by two fourth-year radiology residents and two senior radiologists (VHA) (DMP) with 10 and 7 years of experience, respectively. Consensus was reached in case of disagreement. A dichotomous checklist was used to document the following tomographic features: ground-glass opacity, consolidation, interstitial thickening, pleural thickening, subpleural bands, bronchiectasis, emphysema and lymphadenomegaly.

A modified semiquantitative severity scale[20] was also used to evaluate pulmonary damage. This scale scored the extent of damage for each pulmonary lobe (three in the right lung and two in the left lung) as follows: 0: 0%; 1: < 5%; 2: 5-25%; 3: 26-49%; 4: 50-75%, and 5: > 75% for a maximum of 25 points. The scores for each lobe were summed, and the total score was classified as mild (1-5 points), moderate (6-15 points), and severe (> 15 points). This scale has demonstrated good diagnostic performance, with an area under the curve of 0.87; sensitivity of 80.0%, specificity of 82.8% for assessing clinical severity and interobserver agreement (intraclass correlation coefficient > 0.90; $p < 0.001$)[21].

Statistical analysis

The prevalence of pulmonary damage according to the semiquantitative assessment was presented by age group (< 40, 40-59, and ≥ 60 years). The prevalence of pulmonary tomographic findings at baseline was stratified by cohort group (I: prospective, II: retrospective, and III: ambispective), and by follow-up time (6-11, 12-18, and 19-30 months). The tomographic relationship between baseline chest CT and 6- to 30-month follow-up was presented separately for each dichotomous feature,

resulting in four possible alternatives: (1) If both chest CTs were negative, this meant that there was no abnormal finding in either CT; (2) If the finding was negative at baseline but positive at follow-up, this meant that the finding may have been missed at the baseline CT or that the feature had occurred after baseline CT (i.e., later during hospitalization); (3) if the finding was positive at baseline CT and remained positive at follow-up, it meant that the feature persisted (i.e., sequelae); and (4) if the finding was positive at baseline CT and became negative at follow-up, it meant that the finding had completely disappeared. McNemar tests were used to determine statistically significant differences ($p < 0.05$). Crude and adjusted odds ratios (OR) with 95% confidence intervals (CI) were calculated using binary logistic regression to identify predictors of at least one, two, and three persistent tomographic features (i.e., positive CT at follow-up). In the crude models only predictors with $p \leq 0.10$ were included, while in the adjusted models, only predictors with $p \leq 0.05$ were considered. The predictors tested included sex, age, smoking, alcohol use, diabetes, hypertension, and obesity. Data were entered and analyzed using SPSS v.24.0 (IBM Corp. Armonk, NY, USA).

RESULTS

A cohort of 67 patients with a baseline and follow-up chest CT scans was included (Figure 1). At baseline, the mean ± SD age of patients was 53 ± 14.8 years, with 46 (68.7%) being women and 21 (31.3%) being men. Hypertension (n = 27, 55.2%), diabetes (n = 18, 26.9%), and asthma (n = 3, 4.5%) were the most common comorbidities. Tobacco and alcohol use were by 13 (19.4%) and 28 (41.8%) patients, respectively. Only 8 (12.9%) patients had normal BMI, 17 (27.4%) were overweight, 21 (33.9%) had obesity grade I, 9 (14.5%) had obesity grade II, and 7 (11.3%) had obesity grade III.

Most patients had moderate (n = 38, 56.7%) or severe (n = 25, 37.3%) pulmonary damage according to tomographic findings. Among patients aged 40-59 years, severe damage was more prevalent (n = 16, 47.1%) followed by those aged ≥ 60 years (n = 7, 33.3%) (Table 1).

In total, 62 (92.5%) patients had a CO-RADS 5 tomographic assessment, while 5 (7.5%) had a CO-RADS 6 assessment (Table 2). Ground-glass opacity was present in nearly all patients (n = 66, 98.5%), and a large proportion showed interstitial thickening (n = 60, 89.6%). Consolidation (n = 46, 68.7%), subpleural bands (n = 39, 58.2%), and lymphadenomegaly (n = 32, 47.8%) were also commonly observed. These findings were more frequently reported in patients who underwent chest CT scans under informed consent (group I) compared to those obtained from the tomographic database (groups II and III).

The most persistent tomographic findings (positive at baseline and positive at follow-up CT) were interstitial thickening (n = 36, 53.7%), followed by ground-glass opacity (n = 30, 44.7%), and subpleural bands (n = 28, 41.8%) ($p < 0.05$) (Table 3). The finding most likely to completely disappear (positive at baseline and negative at follow-up) was consolidation (n = 45, 67.0%), followed by ground-glass opacity (n = 36, 53.7%), interstitial thickening (n = 24, 35.8%), and lymphadenomegaly (n = 22, 32.8%). Some of the negative findings in the baseline examination that turned positive on follow-up

Table 1. Severity of pulmonary damage was semiquantitatively[a] measured at the baseline chest CT in patients diagnosed with COVID-19 in 2020-2021

Age, years	Tomographic severity, n (%)			
	Mild	Moderate	Severe	Total
< 40	2 (16.7)	8 (66.7)	2 (16.7)	12 (17.9)
40-59	1 (2.9)	17 (50.0)	16 (47.1)	34 (50.7)
≥ 60	1 (4.8)	13 (61.9)	7 (33.3)	21 (31.3)
Total	4 (6.0)	38 (56.7)	25 (37.3)	67 (100)

[a]Semiquantitative scale for COVID-19 patients: mild 1-5, moderate 6-15, severe > 15 points from Li K, Fang Y, et al.[20]

Table 2. Baseline chest CT findings in patients diagnosed with COVID-19 in 2020-2021

Description	Group[a]			Total, (n = 67)
	I, (n = 23)	II, (n = 18)	III, (n = 26)	
CO-RADS 5, n (%)	23 (100)	15 (83.3)	24 (92.3)	62 (92.5)
CO-RADS 6, n (%)	0 (0)	3 (16.6)	2 (7.6)	5 (7.5)
Ground-glass opacity, n (%)	22 (95.6)	18 (100)	26 (100)	66 (98.5)
Interstitial thickening, n (%)	22 (95.6)	16 (88.8)	22 (84.6)	60 (89.6)
Consolidation, n (%)	19 (82.6)	10 (55.5)	17 (65.3)	46 (68.7)
Subpleural bands, (%)	19 (82.6)	5 (27.7)	15 (57.0)	39 (58.2)
Lymphadenomegaly, (%)	15 (65.2)	4 (22.2)	13 (50.0)	32 (47.8)
Bronchiectasis, n (%)	8 (34.7)	1 (5.55)	2 (7.6)	11 (16.4)
Emphysema, (%)	2 (8.6)	0 (0)	1 (3.84)	3 (4.5)

[a]Group I (prospective) patients who underwent chest CT under informed consent (primary data); Groups II (retrospective), and III (ambispective) patients whose baseline chest CT was obtained from the tomographic electronic database (secondary data) and the follow-up chest CT under informed consent (primary data).

Table 3. Chest CT findings of patients diagnosed with COVID-19 in 2020-21 and followed-up 6-30 months after the initial infection

Description	Baseline chest CT	Follow-up chest CT	
		Negative	Positive
Interstitial thickening, n (%)	Negative	2 (3.0)	5 (7.5)
	Positive	24 (35.8)	36 (53.7)[a]
Ground-glass opacity, n (%)	Negative	1 (1.4)	0 (0)
	Positive	36 (53.7)	30 (44.7)[a]
Subpleural bands, n (%)	Negative	15 (22.4)	13 (13.4)
	Positive	11 (16.4)	28 (41.8)[a]
Lymphadenomegaly, n (%)	Negative	34 (50.7)	1 (1.5)
	Positive	22 (32.8)	10 (14.9)[a]
Pleural thickening, n (%)	Negative	37 (55.2)	9 (13.4)
	Positive	12 (17.9)	9 (13.4)
Bronchiectasis, n (%)	Negative	52 (77.6)	4 (6.0)
	Positive	2 (3.0)	9 (13.4)
Emphysema, n (%)	Negative	61 (91.0)	3 (4.5)
	Positive	0 (0)	3 (4.5)
Consolidation, n (%)	Negative	20 (29.8)	0 (0)
	Positive	45 (67.0)	2 (3.0)

[a]Statistically significant McNemar test ($p < 0.05$).

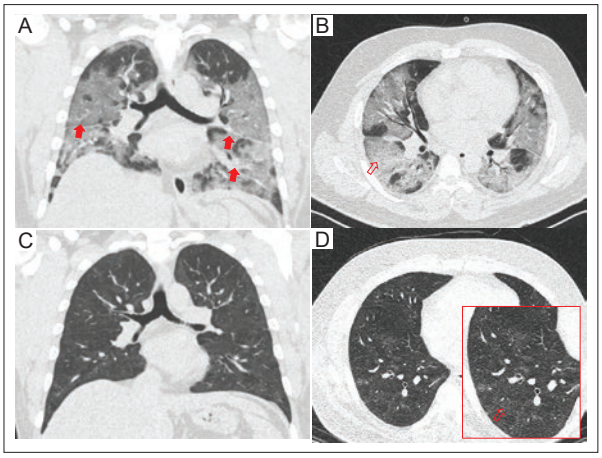

Figure 2. Chest CT of a 41-year-old male diagnosed with Long COVID. **A:** coronal and **B:** axial baseline images show pleural thickening in the fissures (solid arrows) and areas of interstitial impairment with ground-glass opacity in the lobules, predominantly in the peripheral and inferior segments with tendency for consolidation (open arrow). **C:** coronal and **D:** axial follow-up images taken 17 months after the initial infection, show focal and peripheral impairment with diffuse ground-glass areas, mainly in the periphery (zoomed image with open arrow).

CT: computed tomography; COVID: coronavirus disease.

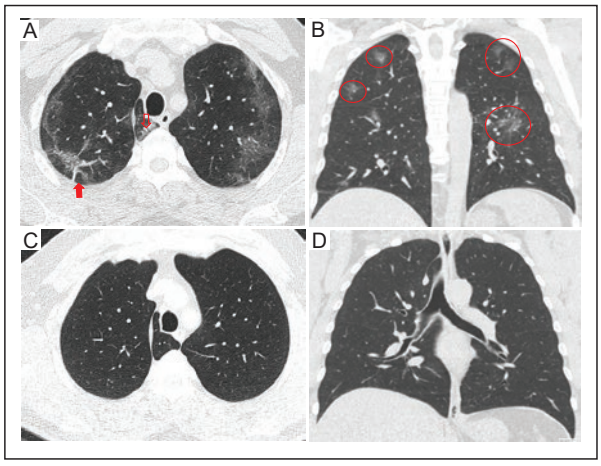

Figure 3. Chest CT of a 51-year-old male diagnosed with COVID-19. **A:** coronal and **B:** axial baseline images showing an azygos lobe with interstitial impairment (open arrow) and subpleural atelectasis in the right lung (solid arrow), along with pleural thickening in the fissures (solid arrows) and patches of ground-glass opacity with peripheral and bilateral distribution (circles). **C:** coronal and **D:** axial follow-up images obtained 19 months after the initial infection, demonstrate complete remission of the findings.

CT: computed tomography; COVID: coronavirus disease.

chest CT included pleural thickening (n = 9, 13.4%), subpleural bands (n = 13, 13.4%), and interstitial thickening (n = 5, 7.5%) (Table 3). Examples of coronal and axial chest CT scans from Long COVID patients are shown in Figures 2 through 8.

The proportion of patients with persistent tomographic pulmonary abnormalities tended to decrease with increasing follow-up time, except for lymphadenomegaly and emphysema (Table 4). This trend was particularly evident in interstitial thickening (6-11 months: 84.6%,12-18 months: 65.0%, and 19-30 months: 50.0%), pleural thickening (6-11 months: 46.2%, 12-18 months: 30.0%, and 19-30 months: 17.6%), and for ground-glass opacity (6-11 months: 84.6%,12-18 months: 30%, and 19-30 months: 38.2%).

In crude analyses, diabetes, hypertension, and obesity were associated with persistent tomographic abnormal findings 6 to 30 months after the initial COVID-19 diagnosis (Table 5). Hypertension was the only statistically significant predictor of at least one (adjusted OR 3.90; 95% CI 1.05-14.4) and at least two (adjusted OR 3.11; 95% CI 1.13-8.8) persistent tomographic abnormalities in adjusted analyses. Hypertension was also a risk factor for at least three features (adjusted OR 3.03; 95% CI 1.13-8.8). Obesity appeared to have a protective effect (adjusted OR 0.34; 95% CI 0.11-1.01).

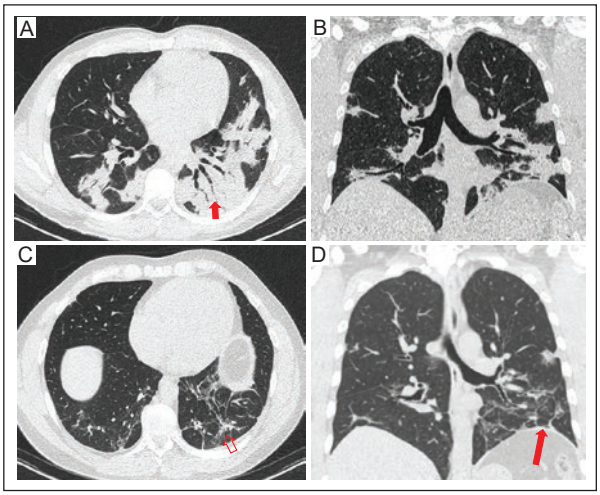

Figure 4. Chest CT of a 42-year-old male diagnosed with Long COVID. **A:** coronal and **B:** axial baseline images showing consolidation areas with bilateral distribution, predominantly in the lower lobules and peripheral segments, along with an air bronchogram (solid arrow). **C:** coronal and **D:** axial follow-up images taken 25 months after the initial infection, show septal thickening and distortion of the pulmonary architecture (open arrow) in the areas of initial consolidation, as well as retraction bands and subsegmental laminar atelectasis (solid arrow).

CT: computed tomography; COVID: coronavirus disease.

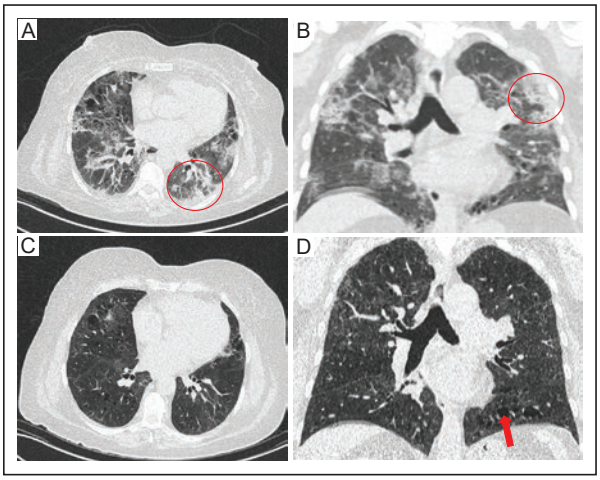

Figure 6. Chest CT of a 73-year-old female diagnosed with Long COVID. **A:** coronal and **B:** axial baseline images showing areas of ground-glass opacity and alveolar occupation with bilateral distribution, predominantly subpleural in the upper lobes (circle), along with areas of centrilobular emphysema in the left lower lobe. **C:** coronal and **D:** axial follow-up images, taken 19 months after the initial infection, show persistent residual ground-glass opacity with less density and centrilobular emphysema (solid arrow) without changes compared to the baseline findings.

CT: computed tomography; COVID: coronavirus disease.

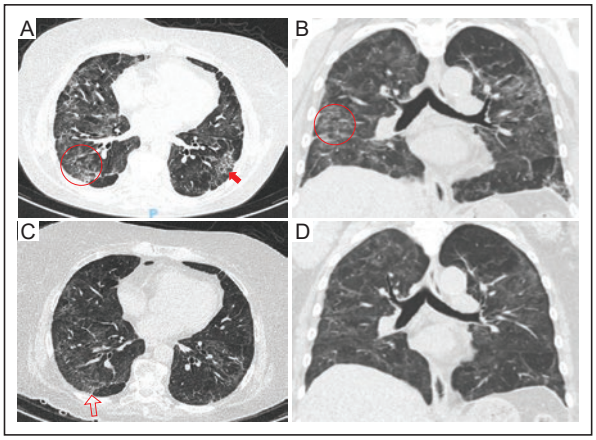

Figure 5. Chest CT of a 68-year-old female diagnosed with Long COVID. **A:** coronal and **B:** axial baseline images showing septal thickening and multiple areas of ground-glass opacity (circle) associated with subpleural reticular bands (solid arrow). **C:** coronal and **D:** axial follow-up images, obtained 14 months after the initial infection, show decreased density and extension of the ground-glass opacity, but persistence of interstitial centrilobular thickening and subpleural reticular opacities (open arrow).

CT: computed tomography; COVID: coronavirus disease.

Table 4. Chest CT persistent abnormal findings by follow-up time in patients diagnosed with COVID-19

Description	Follow-up in months			Total
	6-11	12-18	19-30	
Interstitial thickening[a], n (%)	11 (84.6)	13 (65.0)	17 (50.0)	41 (61.2)
Subpleural bands, n (%)	7 (53.8)	14 (70.0)	20 (58.8)	41 (61.2)
Ground glass[a], n (%)	11 (84.6)	6 (30.0)	13 (38.2)	30 (44.8)
Pleural thickening, n (%)	6 (46.2)	6 (30.0)	6 (17.6)	18 (26.9)
Bronchiectasis, n (%)	2 (15.4)	6 (30.0)	5 (14.7)	13 (19.4)
Lymphadenomegaly, n (%)	1 (7.7)	2 (10.0)	8 (23.5)	11 (16.4)
Emphysema, n (%)	1 (7.7)	2 (10.0)	3 (8.8)	6 (9.0)
Consolidation, n (%)	1 (7.7)	1 (5.0)	0 (0)	2 (3.0)
Total, n	13	20	34	67

[a]Statistically significant ($p < 0.05$), Pearson chi^2 test was used.

DISCUSSION

This study has one of the longest published follow-up period evaluating persistent abnormal pulmonary tomographic findings 6-30 months after the initial COVID-19 infection. The most common findings included ground-glass opacity, interstitial thickening, and subpleural bands, with nearly half or more of the patients having these abnormalities throughout the follow-up period.

One study with a follow-up period of 18.5 months is a longitudinal cohort of 208 COVID-19 convalescents patients from Wuhan, China, in which approximately 30% of patients still had abnormal chest CT patterns.

Table 5. Crude and adjusted odds ratios from binary logistic regression to identify predictors of persistent pulmonary tomographic findings at 6 to 30 months in Long COVID patients

Tomographic findings[a]	Odds Ratio (95% confidence interval)			
	Crude[b]	p-value	Adjusted[c]	p-value
At least one finding				
Diabetes	5.82 (0.69-48.5)	0.10	–	–
Hypertension	3.90 (1.05-14.4)	0.04	3.90 (1.05-14.4)	0.04
At least two findings				
Hypertension	3.11 (1.13-8.80)	0.02	3.11 (1.13-8.8)	0.02
At least three findings				
Diabetes	3.04 (0.99-9.36)	0.05	–	–
Hypertension	2.63 (0.93-7.48)	0.06	3.03 (0.99-9.32)	0.05
Obesity[d]	0.36 (0.12-1.03)	0.06	0.34 (0.11-1.01)	0.05

[a]It includes ground-glass opacity, consolidation, interstitial thickening, bronchiectasis, emphysema, pleural thickening, subpleural bands, and lymphadenomegaly; [b]Includes only predictors with p-values ≤ 0.10 in bivariate analyses; diabetes, arterial hypertension, sex, age, body mass index, smoking, alcohol use, and clinical severity at baseline were tested; [c]The final model included only predictors with p-values ≤ 0.05; [d]BMI ≥ 30 kg/m^2.

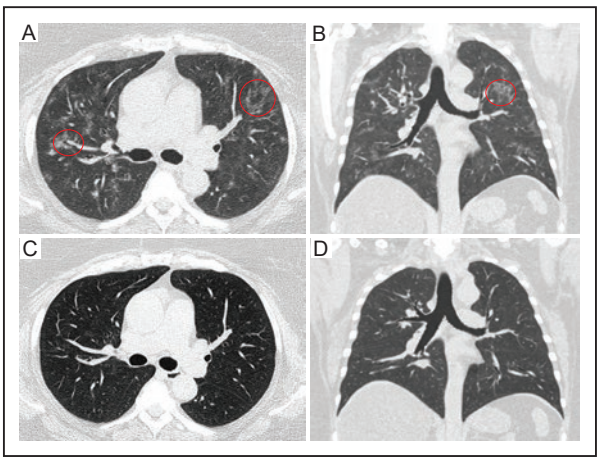

Figure 8. Chest CT of a 75-year-old female diagnosed with COVID-19. **A:** coronal and **B:** axial baseline images showing multifocal areas with ground-glass opacity with bilateral diffuse distribution (circles). **C:** coronal, and **D:** axial images of follow-up, taken 6 months after the initial infection showing complete resolution of the baseline pulmonary tomographic findings.

CT: computed tomography; COVID: coronavirus disease.

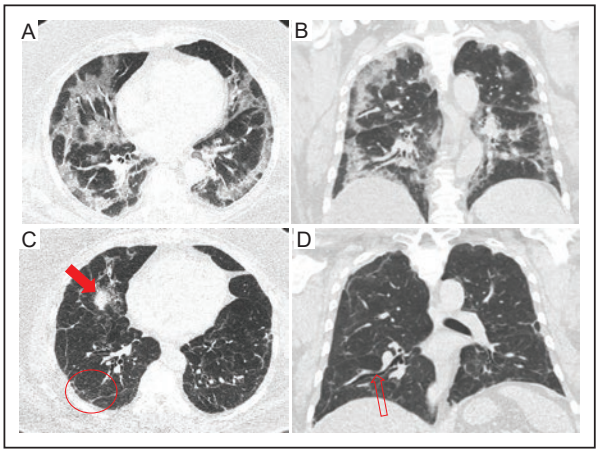

Figure 7. Chest CT of a 59-year-old male diagnosed with Long COVID. **A:** coronal and **B:** axial baseline images showing multifocal areas of ground-glass opacity with predominantly peripheral distribution (solid arrows). **C:** coronal and **D:** axial images of follow-up, obtained 18 months after the initial infection, show atelectasis (solid arrow), peripheral septal thickening (circle), and residual cylindrical bronchiectasis (open arrow).

CT: computed tomography; COVID: coronavirus disease.

The higher prevalence of persistent tomographic abnormalities in our cohort may be related to the high prevalence of comorbidities such as hypertension (55.2%) and diabetes (26.9%). Notably, ground-glass opacity and features associated with fibrosis, such as interstitial and pleural thickening, tended to diminish as the follow-up time increased, as reported in the systematic review and meta-analysis recently published on this topic[13]. In our cohort, ground-glass opacity was present in almost all patients at baseline (98.5%), but its prevalence progressively decreased to 53.8% at 6-11 months and continued to decline to nearly one-third thereafter. This decrease was also observed in abnormalities associated with fibrotic changes, such as interstitial thickening (from 84.6% at 6-11 months to 65% at 12-18 months to 50% at 19-30 months) and pleural thickening (from 46.2% to 30% to 17.6%). In the meta-analysis of CT findings of Long COVID-19 patients one year after initial infection, which included 15 studies, reported that one-third of patients had residual chest CT abnormalities. Ground-glass opacity (21.2%) and fibrotic changes (20.6%) were the most commonly observed, showing gradual recovery as the follow-up period increased (CT abnormalities at 6 months: 52.9% and at 12 months: 32.6%)[13].

A secondary objective was to identify potential risk factors for the persistence of pulmonary abnormal findings in Long COVID. Hypertension was the only consistent risk factor that increased the likelihood of persistent pulmonary abnormalities, particularly interstitial thickening. Although no specific study has addressed hypertension and the persistence of tomographic sequelae, evidence suggests that severe cases in convalescent COVID-19 patients have a higher prevalence of comorbidities, particularly hypertension and diabetes[23]. On the other hand, we found no association

between tomographic severity at baseline chest CT and the occurrence of follow-up abnormalities, as others have found among severe and critical cases[12,13]. Further studies are needed to better understand the persistence of tomographic pulmonary abnormalities in Long COVID patients in relation to the clinical characteristics of the infected population.

This study has several strengths. The most significant strength is the duration of follow-up period, which is one of the longest reported to date and provides relevant data on long-term pulmonary tomography findings in Long COVID. The presentation of tomographic abnormalities in a group with a high prevalence of comorbidities, such as hypertension and diabetes, suggests that persistent abnormalities may also depend on population characteristics. On the other hand, this cohort study has three major methodologic limitations that should be mentioned. First, the small sample size leads to unstable estimates, especially when the data are stratified. Second, there is a potential for selection bias, because Long COVID patients may not representative of those who attended the hospital. Third, the results have limited generalizability due to the differences in characteristics and treatment received by private patients compared to the general population.

CONCLUSION

In our study, the prevalence of persistent pulmonary tomographic abnormalities was high in Long COVID patients. This may be partly attributed to the high frequency of hypertension and diabetes in our patient population. Ground-glass opacity and fibrotic abnormalities (e.g., interstitial thickening) were the most frequently observed findings, which tended to decrease over time. Longer follow-up periods are needed to confirm the occurrence of long-lasting pulmonary tomographic abnormalities in Long COVID patients.

Acknowledgements

We are grateful the hospital authorities, particularly the staff of the Department of Radiology, for their valuable assistance. The authors also thank Professor Ana María Contreras-Navarro for her kind guidance in preparing the manuscript. This thesis in the field of Radiology Specialty was awarded at the Primera Convocatoria Nacional 2023 “Las Mejores Tesis para Publicar en el JMeXFRI”.

Conflicts of interest

The authors declare no conflicts of interest.

Funding

This study was funded by Christus Muguerza del Parque Hospital, Chihuahua, Mexico.

Ethical disclosures

Protection of individuals. This study was conducted in compliance with the Declaration of Helsinki (1964) and its subsequent amendments.

Confidentiality of data. The authors declare they followed their center’s protocol for sharing patient data.

Right to privacy and informed consent. Participants who provided primary data signed a written informed consent. Approval was obtained from the hospital authorities to retrieve secondary data from the radiology department’s electronic archives.

REFERENCES

1. Guler SA, Ebner L, Aubry-Beigelman C, Bridevaux PO, Brutsche M, Clarenbach C, et al. Pulmonary function and radiological features 4 months after COVID-19: first results from the national prospective observational Swiss COVID-19 lung study. Eur Respir J. 2021;57(4):2003690. doi: 10.1183/13993003.03690-2020.
2. Islam N, Salameh JP, Leeflang MM, Hooft L, McGrath TA, van der Pol CB, et al. Thoracic imaging tests for the diagnosis of COVID-19. Cochrane Database Syst Rev. 2020;11:CD013639. doi: 10.1002/14651858.CD013639.pub3
3. Malik P, Patel K, Pinto C, Jaiswal R, Tirupathi R, Pillai S, et al. Post-acute COVID-19 syndrome (PCS) and health-related quality of life (HR-QoL)-A systematic review and meta-analysis. J Med Virol. 2022;94(1):253-262. doi: 10.1002/jmv.27309.
4. World Health Organization. A clinical case definition of post COVID-19 condition by a Delphi consensus. WHO, October 6, 2021.
5. Boscolo-Rizzo P, Guida F, Polesel J, Marcuzzo AV, Capriotti V, D’Alessandro A, et al. Sequelae in adults at 12 months after mild-to-moderate coronavirus disease 2019 (COVID-19). Int Forum Allergy Rhinol. 2021;11(12):1685-1688. doi: 10.1002/alr.22832.
6. Premraj L, Kannapadi NV, Briggs J, Seal SM, Battaglini D, Fanning J, et al. Mid and long-term neurological and neuropsychiatric manifestations of post-COVID-19 syndrome: A meta-analysis. J Neurol Sci. 2022;434:120162. doi: 10.1016/j.jns.2022.120162.
7. Ceban F, Ling S, Lui LMW, Lee Y, Gill H, Teopiz KM, et al. Fatigue and cognitive impairment in post-COVID-19 Syndrome: A systematic review and meta-analysis. Brain Behav Immun. 2022; 101:93-135. doi: 10.1016/j.bbi.2021.12.020.
8. Zeng N, Zhao YM, Yan W, Li C, Lu QD, Liu L, et al. A systematic review and meta-analysis of long term physical and mental sequelae of COVID-19 pandemic: call for research priority and action. Mol Psychiatry. 2023;28(1):423-433. doi: 10.1038/s41380-022-01614-7.
9. Han X, Fan Y, Alwalid O, Li N, Jia X, Yuan M, et al. Six-month Follow-up Chest CT Findings after Severe COVID-19 Pneumonia. Radiology. 2021;299(1): E177-E186. doi: 10.1148/radiol.2021203153.
10. Bernheim A, Mei X, Huang M, Yang Y, Fayad ZA, Zhang N, et al. Chest CT Findings in Coronavirus Disease-19 (COVID-19): Relationship to Duration of Infection. Radiology. 2020;295(3):200463. doi: 10.1148/radiol.2020200463.
11. Wu X, Liu X, Zhou Y, Yu H, Li R, Zhan Q, et al. 3-month, 6-month, 9-month, and 12-month respiratory outcomes in patients following COVID-19-related hospitalization: a prospective study. Lancet Respir Med. 2021;9(7):747-754. doi: 10.1016/S2213-2600(21)00174-0.

12. Lee JH, Yim JJ, Park J. Pulmonary function and chest computed tomography abnormalities 6-12 months after recovery from COVID-19: a systematic review and meta-analysis. Respir Res. 2022;23(1):233. doi: 10.1186/s12931-022-02163-x.
13. Watanabe A, So M, Iwagami M, Fukunaga K, Takagi H, Kabata K, et al. One-year follow-up CT findings in COVID-19 patients: A systematic review and meta-analysis. Respirology. 2022;27(8):605-616. doi: 10.1111/resp.14311.
14. Wen R, Zhang M, Xu R, Gao Y, Liu L, Chen H, et al. COVID-19 imaging, where do we go from here? Bibliometric analysis of medical imaging in COVID-19. Eur Radiol. 2023;33(5):3133-3143. doi: 10.1007/s00330-023-09498-z.
15. Martini K, Larici AR, Revel MP, Ghaye B, Sverzellati N, Parkar AP, et al. COVID-19 pneumonia imaging follow-up: when and how? A proposition from ESTI and ESR. Eur Radiol. 2022;32(4):2639-2649. doi: 10.1007/s00330-021-08317-7.
16. Ward S, Lindsley A, Courter J, Assa'ad A. Clinical testing for COVID-19. J Allergy Clin Immunol. 2020;146(1):23-34. doi: 10.1016/j.jaci.2020.05.012.
17. Penha D, Pinto EG, Matos F, Hochhegger B, Monaghan C, Taborda-Barata L, et al. CO-RADS: Coronavirus Classification Review. J Clin Imaging Sci. 2021;11:9. doi: 10.25259/JCIS_192_2020.
18. Monárrez-Espino J, Zubía-Nevárez CI, Reyes-Silva L, Castillo-Palencia JP, Castañeda-Delgado JE, Herrera van-Oostdam AS, et al. Clinical Factors Associated with COVID-19 Severity in Mexican Patients: Cross-Sectional Analysis from a Multicentric Hospital Study. Healthcare (Basel). 2021;9(7):895. doi: 10.3390/healthcare9070895.
19. López-Hernández Y, Oropeza-Valdez JJ, García Lopez DA, Borrego JC, Murgu M, Valdez J, et al. Untargeted analysis in post-COVID-19 patients reveals dysregulated lipid pathways two years after recovery. Front Mol Biosci. 2023; 10:1100486. doi: 10.3389/fmolb.2023.1100486.
20. Li K, Fang Y, Li W, Pan C, Qin P, Zhong Y, et al. CT image visual quantitative evaluation and clinical classification of coronavirus disease (COVID-19). Eur Radiol. 2020;30(8):4407-4416. doi: 10.1007/s00330-020-06817-6.
21. Inoue A, Takahashi H, Ibe T, Ishii H, Kurata Y, Ishizuka Y, et al. Comparison of semiquantitative chest CT scoring systems to estimate severity in coronavirus disease 2019 (COVID-19) pneumonia. Eur Radiol. 2022;32(5):3513-3524. doi: 10.1007/s00330-021-08435-2.
22. Guo Y, Wang H, Xiao M, Guan X, Lei Y, Diao T, et al. Long-term outcomes of COVID-19 convalescents: An 18.5-month longitudinal study in Wuhan. Int J Infect Dis. 2023;127:85-92. doi: 10.1016/j.ijid.2022.12.008.
23. Zhang S, Liu L, Yang B, Li R, Luo J, Huang J, et al. Clinical characteristics of 134 convalescent patients with COVID-19 in Guizhou, China. Respir Res. 2020;21(1):314. doi: 10.1186/s12931-020-01580-0.

JMeXFRI

Journal of the Mexican Federation of Radiology and Imaging

Check for updates

FULL RESEARCH ARTICLE

Ultrasound features of breast nonmass using a standardized lexicon: prediction of malignancy

*Adriana Parada-Gallardo[1,2,a] and Jacqueline Preciado-Vargas[1,b]**

[1]Department of Breast Imaging, San Javier Hospital; [2]University Center of Health Sciences, Universidad of Guadalajara. Guadalajara, Jalisco, Mexico

ORCID: [a]0000-0002-0868-3198; [b]0000-0002-6303-684X

ABSTRACT

Introduction: *A breast nonmass (NM) on ultrasound (US) is associated with a wide spectrum of breast pathologies. The aims of this study were to (1) re-evaluate the ultrasonographic features of breast NM using a standardized lexicon and (2) identify the ultrasonographic features that predict malignancy in NM and its histopathologic confirmation.* **Material and Methods:** *Women with ultrasonographic report of breast NM with BI-RADS category 3, 4, or 5 and diagnosis by biopsy or ultrasonographic follow-up over 24 months were included. The following features of breast NM were assessed by ultrasound: echogenicity, distribution, orientation, and associated findings according to the standardized lexicon of the fifth-edition update of the ACR BI-RADS. Univariate and multivariate analyses were performed.* **Results:** *Seventy-two women with breast NM were included; 53 (73.6%) had confirmed benign NM, 3 (4.2%) had benign with upgrade potential (BWUP) NM, and 16 (22.2%) had malignant NM. Significant ultrasonographic findings predictive of malignant NM were echogenic rind (OR 12.66, 95% CI 2.08 - 76.83), hypervascularity (OR 7.96, 95% CI 1.71 - 37.02), and calcifications (OR 18.61, 95% CI 2.71-127.65) with sensitivity of 75.0% (95% CI, 50.5 - 89.8%), specificity of 96.1% (95% CI, 86.8-98.9), PPV of 85.7% (95% CI, 60.1-96.0), and NPV of 92.5% (95% CI, 82.1-97.0). The accuracy for diagnosing malignant breast NM was 91.0% (95% CI, 81.8-95.8%).* **Conclusion:** *The ultrasonographic features of breast NM were defined using a standardized lexicon. Malignant breast NM was diagnosed in one out of four women. The predictive ultrasound findings were echogenic rind, hypervascularity, and calcifications. In breast NMs, a biopsy is recommended to confirm the diagnosis.*

Keywords: *Ultrasound. BI-RADS. Breast nonmass. Nonmass lesion. Standardized lexicon. Breast carcinoma.*

INTRODUCTION

A breast nonmass (NM) includes a wide spectrum of benign, benign with upgrade potential (BWUP), or malignant pathologies[1,2]. NM ultrasound findings associated with breast malignancy include architectural distortion, hypervascularity, and calcifications[1,3-6]. Ductal carcinoma in situ and invasive lobular carcinoma can present as breast NM,[4,7,8] and are the most frequent diagnoses associated with malignant etiology[1,9,10].

The ultrasonographic features of breast NM vary. They are often as hypoechoic area, architectural distortion, asymmetry, or focal asymmetry[1,4-8,11,12]. Breast NM lacks the 3-dimensionality of a mass: is identifiable in at least 2 planes but may be primarily visualized in 1 plane only. Lacks definable shape and margin for assessment[13]. The American College of Radiology Breast Imaging Reporting and Data System (ACR BI-RADS) proposed standardized terminology to describe NMs detected on breast ultrasound (US)[13].

***Corresponding author:**
Jacqueline Preciado-Vargas
E-mail: drajackie@gmail.com

Received for publication: 13-02-2023
Accepted for publication: 27-03-2023
DOI: 10.24875/JMEXFRI.M23000049

Available online: 13-07-2023
J Mex Fed Radiol Imaging. 2023;2(2):115-125
www.JMeXFRI.com

It includes ultrasonographic features of echogenicity, distribution, orientation, and associated findings (echogenic rind, architectural distortion, posterior shadowing, hypervascularity, ductal extension or abnormal ductal changes, and calcifications)[13]. The aims of this study were to (1) re-evaluate the ultrasonographic features of breast NM using a standardized lexicon proposed in the fifth-edition update of the ACR BI-RADS, and (2) identify ultrasonographic features that predict malignant NM.

MATERIAL AND METHODS

This cross-sectional study was conducted from January 2016 to December 2022 in the Breast Imaging Department of Hospital San Javier in Guadalajara, Jalisco, Mexico. Women with ultrasonographic report of breast NM and diagnosis by histopathologic examination or 24-month follow-up with breast US were included. Women with BI-RADS 6 were excluded. Informed consent was not required for the use of data collected during routine clinical care. This study was approved by institutional ethics and research committees.

Study development and variables

Ultrasound examinations of breast NM cases with a report based on findings such as hypoechoic, architectural distortion, asymmetry, and/or focal asymmetry

Table 1. Etiologic diagnosis of breast NMs with histopathologic confirmation or stability by US examination at 24-month follow-up

Benign breast NM	n (%)
Fibrocystic changes	11 (20.7)
Fibroadenomatoid changes	6 (11.3)
Fibroadenoma	5 (9.4)
Sclerosing adenosis	4 (7.5)
Adenosis	2 (3.8)
Radial scar	2 (3.8)
Chronic granulomatous mastitis	1 (1.9)
Tuberculosis	1 (1.9)
Pseudoangiomatous stromal hyperplasia	1 (1.9)
Stromal fibrosis	1 (1.9)
Benign for stability	19[a] (35.9)
Total	53 (100)
BWUP breast NM	**n (%)**
Atypical ductal hyperplasia	2 (66.6)
Focal papillomatosis	1 (33.4)
Total	3 (100)
Malignant breast NM	**n (%)**
Invasive ductal carcinoma	10 (62.4)
Ductal carcinoma in situ	4 (25.0)
Invasive lobular carcinoma	1 (6.3)
Paget's disease associated with invasive ductal carcinoma	1 (6.3)
Total	16 (100)

[a]In 19 patients the lesion was stable by breast US examination at 24-month follow-up, and no biopsy was performed; BI-RADS: Breast Imaging- Reporting and Data System; NM: nonmass; BWUP: benign with upgrade potential.

Table 2. Comparison of breast NM diagnosis by age, purpose of US examination, and BI-RADS categories

Description	Benign breast NM n = 53 (73.6%)	BWUP breast NM n = 3 (4.2%)	Malignant breast NM n = 16 (22.2%)	Total n = 72 (100%)	p-value
Age, years, mean ± SD	44.7 ± 11.08	53.2 ± 16.34	51.1 ± 11.04	46.7 ± 11.73	0.068
min, med, max	(21, 44, 69)	(40, 49, 81)	(34, 51, 70)	(21, 45, 81)	
Age groups					0.295
< 52 years	40 (75.4)	1 (33.3)	9 (56.3)	50 (69.4)	
≥ 52 years	13 (24.6)	2 (66.7)	7 (43.7)	22 (30.6)	
Purpose of the US examination					0.563
Screening	32 (60.4)	2 (66.7)	9 (56.3)	43 (59.7)	
Diagnostic	21 (39.6)	1 (33.3)	7 (43.7)	29 (40.3)	
BI-RADS Category					< 0.001
BI-RADS 3	9 (17.3)	0	0	9 (12.5)	
BI-RADS 4A	13 (25.5)	1 (33.3)	0	14 (19.4)	
BI-RADS 4B	22 (41.5)	2 (66.7)	2 (12.5)	26 (36.1)	
BI-RADS 4C	7 (13.7)	0	6 (37.5)	13 (18.1)	
BI-RADS 5	2 (2.0)	0	8 (50.0)	10 (13.9)	

US: ultrasound; BI-RADS: Breast Imaging- Reporting and Data System; min: minimum; med: medium; max: maximum; NM: nonmass; BWUP: benign with upgrade potential.

Table 3. Comparison of breast US features between benign, BWUP and malignant breast NMs based on a standardized lexicon[a]

Description	Benign breast NM n = 53 (73.6%)	BWUP breast NM n = 3 (4.2%)	Malignant breast NM n = 16 (22.2%)	Total n = 72 (100%)	p-value
Echogenicity					0.117
Hypoechoic	33 (62.3)	2 (66.7)	8 (50.0)	43 (59.7)	
Isoechoic	1 (1.9)	1 (20.0)	0	2 (2.8)	
Hyperechoic	1 (1.9)	0	2 (12.5)	3 (4.2)	
Mixed echogenicity	18 (33.9)	0	6 (37.5)	24 (33.3)	
Distribution					0.210
Regional	12 (22.6)	0	5 (31.3)	17 (23.6)	
Focal	38 (71.6)	3 (100)	8 (50.0)	49 (68.1)	
Linear	2 (3.8)	0	0	2 (2.7)	
Segmental	1 (2.0)	0	3 (18.7)	4 (5.6)	
Orientation					0.372
Parallel	22 (41.6)	1 (33.3)	9 (56.3)	32 (44.4)	
Antiparallel	31 (58.4)	2 (66.7)	7 (43.7)	40 (55.6)	
Echogenic rind					0.015
Yes	11 (20.8)	0	9 (56.0)	20 (27.8)	
No	42 (79.2)	3 (100)	7 (44.0)	52 (72.2)	
Architectural distortion					0.280
Yes	27 (50.9)	3 (100)	12 (75.0)	42 (58.3)	
No	26 (49.1)	0	4 (25.0)	30 (41.7)	
Posterior shadowing					0.439
Yes	34 (64.1)	1 (33.3)	13 (81.3)	48 (66.7)	
No	19 (35.9)	2 (66.7)	3 (18.7)	24 (33.3)	
Hypervascularity					< 0.001
Yes	11 (20.8)	1 (33.3)	11 (68.7)	23 (31.9)	
No	42 (79.2)	2 (66.7)	5 (31.3)	49 (68.1)	
Ductal extension or abnormal ductal change					0.169
Yes	3 (5.7)	0	3 (18.7)	6 (8.3)	
No	50 (94.3)	3 (100)	13 (81.3)	66 (91.7)	
Calcifications					0.002*
Yes	5 (9.5)	0	8 (50.0)	13 (18.1)	
No	48 (90.5)	3 (100)	8 (50.0)	59 (81.9)	

US: ultrasound; NM: nonmass; BWUP: benign with upgrade potential. [a] Newell MS, Destounis S, Leung J, DeMartini W, Eby P. BI-RADS update: The edition formerly known as the 5th. Reston VA. USA. American College of Radiology (ACR); 2021.

classified as BI-RADS 3, 4A, 4B, 4C, and 5 were retrospectively reviewed. Histopathologic confirmation by breast biopsy or follow-up with breast US at 24 months was used to define stability. Images were obtained from PACS (Picture Archiving and Communication System) (Carestream TM, Health Inc, version 12.1.5, Rochester, NY, USA). Age and reason for the US examination (screening or diagnosis) were recorded.

Ultrasound acquisition and analysis

Ultrasound examinations were performed with an Aloka ultrasound system (Hitachi Co. Metzingen, Germany) with a 10-16 MHz multifrequency linear transducer in gray-scale, color Doppler, and power Doppler imaging. The evaluation was performed by a specialized radiologist (JPV) with 10 years of experience in breast imaging.

Table 4. Univariate analysis of significant ultrasonographic features comparing benign and malignant breast NM

Description	Benign breast NM (n = 53)	Malignant breast NM (n = 16)	p-value	OR (95% CI)
Echogenic rind, n (%)	11 (20.8)	9 (56.0)	0.009	5.27 (1.58-17.60)
Hypervascularity, n (%)	11 (20.8)	11 (68.7)	< 0.001	9.02 (2.55-31.90)
Calcifications, n (%)	5 (9.5)	8 (50.0)	0.001	9.20 (2.39-35.35)

NM: nonmass; OR: odds ratio; CI: confidence interval.

Table 5. Multivariate analysis of significant ultrasonographic features predicting malignant breast NM

Description	p-value	OR (95% CI)
Echogenic rind	0.006	12.66 (2.08-76.83)
Hypervascularity	0.008	7.96 (1.71-37.02)
Calcifications	0.003	18.61 (2.71-127.65)

NM: nonmass; OR: odds ratio; CI: confidence interval.

Table 6. Diagnostic performance of the three significant ultrasonographic features[a] predicting malignant breast NM

Parameter	%	95% CI
Sensitivity	75.0	50.5-89.8
Specificity	96.1	86.8-98.9
PPV	85.7	60.1-96.0
NPV	92.5	82.1-97.0
Accuracy	91.0	81.8-95.8

[a]Echogenic rind, hypervascularity and calcifications; CI: confidence interval; NPV: negative predictive value; PPV: positive predictive value; NM: nonmass.

The ultrasonographic features of breast NM included in the standardized lexicon of the updated ACR-BI-RADS fifth-edition[13] were echogenicity (hypoechoic, isoechoic, hyperechoic, or mixed), distribution (regional, focal, linear, or segmental), orientation (parallel or antiparallel), and associated findings (echogenic rind, architectural distortion, posterior shadowing, hypervascularity, ductal extension or abnormal ductal changes and calcifications).

Statistical analysis

The mean, standard deviation, minimum, median, and maximum of age was reported and ANOVA was calculated to compare the mean age between pathologic diagnoses of breast NM. Fisher's exact test was used to compare the frequency of ultrasonographic features suspicious for malignancy and histopathologic confirmation. Univariate odds ratio (crude OR) with a 95% confidence interval and a multivariate binary logistic regression were calculated to identify significant independent variables predictive of malignant breast NM. Sensitivity, specificity, positive predictive value, negative predictive value, false positive rate, false negative rate, and accuracy for predicting malignant breast NM were determined using significant ultrasonographic features in the logistic regression analysis. A p-value < 0.05 was considered significant. IBM-SPSS Version 25 (IBM Co. Armonk, NY, USA) was used for data analysis.

RESULTS

Seventy-two women with breast NM were included. Table 1 describes the diagnoses and histopathologic confirmation. The most common diagnoses of benignity were fibrocystic changes in 11 (20.7%), fibroadenomatoid changes in 6 (11.3%), fibroadenoma in 5 (9.4%), and sclerosing adenosis in 4 (7.5%). In 19 (35.9 %) cases benign breast NM was defined based on the 24-month follow-up US. Other less common benign histopathologic diagnoses are shown in Table 1. BWUP histopathologic diagnosis was made in three NM cases; two with atypical ductal hyperplasia, and one with focal papillomatosis. The most common diagnosis in the malignant NM group was invasive ductal carcinoma (n = 10, 62.4%) and ductal carcinoma in situ (n = 4, 25.0%). Other less common diagnoses were invasive lobular carcinoma (n = 1, 6.3%) and Paget's disease (n = 1, 6.3%).

Table 2 compares the age, reason for breast US, and BI-RADS category of the 72 women. There were 53 (73.6%) women with benign breast NM, 3 (4.2%) with BWUP breast NM, and 16 (22.2%) with malignant breast NM. Malignant etiology was found in approximately in 1 of 4 women with a breast NM. There were no significant differences in age for malignant NM in women younger, equal, or older than 52. Breast US screening was performed in 32 (60.4%) of 72 women. Malignant NMs were significantly associated with higher BI-RADS categories: BI-RADS 4B (n = 2, 12.5%),

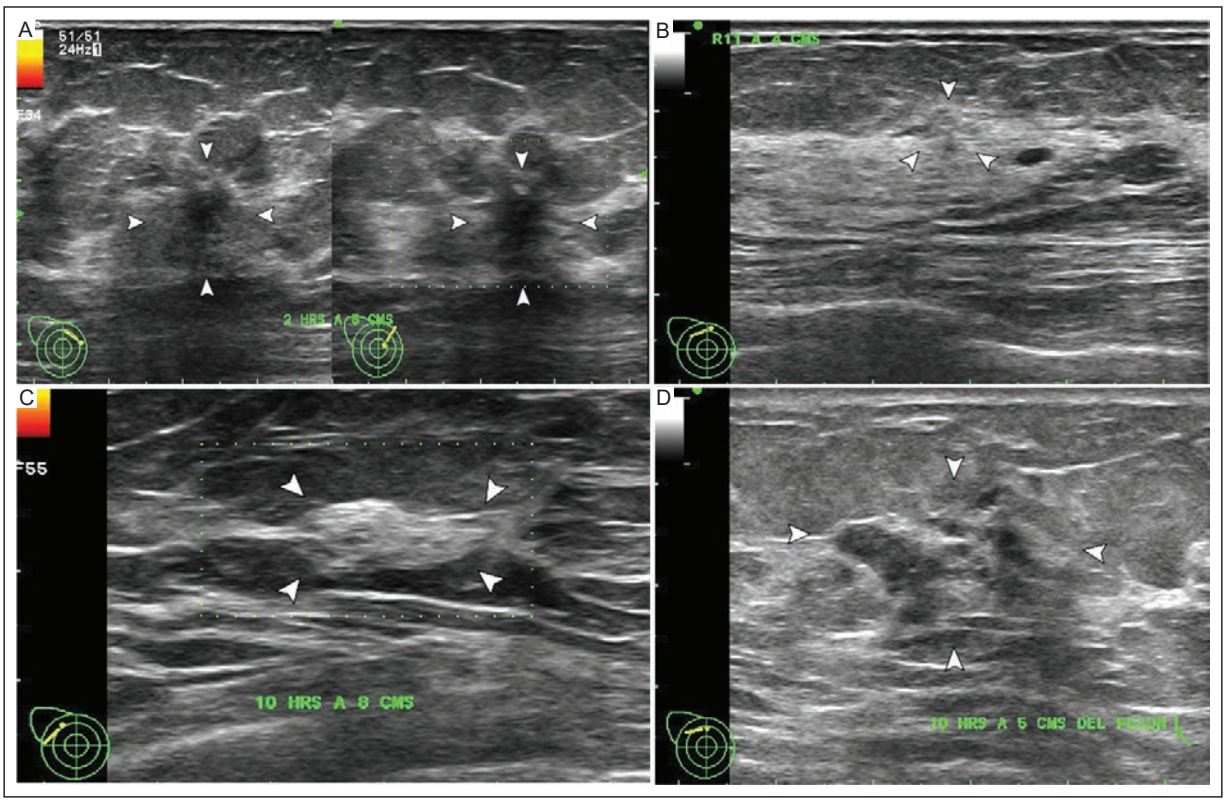

Figure 1. US in grayscale and power Doppler showing the **echogenicity** of breast NM. **A:** hypoechoic (arrowheads). **B:** isoechoic (arrowheads). **C:** hyperechoic (arrowheads). **D:** mixed echogenicity (arrowheads).

NM: nonmass; US: ultrasound.

BI-RADS 4C (n = 6, 37.5%), and BI-RADS 5 (n = 8, 50.0%), in contrast to benign NMs in categories 4B (n = 22, 41.5%), BI-RADS 4C (n = 7, 13.7%), and BI-RADS 5 (n = 2, 2.0%) (p < 0.001).

The ultrasonographic features of benign, BWUP, and malignant breast NMs are compared in Table 3. Echogenic rind (p = 0.015), hypervascularity (p < 0.001), and calcifications (p = 0.002) were more frequent in malignant breast NMs. There were no significant differences in echogenicity, distribution, orientation, posterior shadowing, or ductal changes between the three groups. Figure 1 shows the echogenicity features of the breast NM (hypoechoic, isoechoic, hyperechoic, and mixed echogenicity), Figure 2 the distribution features (regional, focal, linear, and segmental), and Figure 3 the orientation features (parallel and antiparallel). The associated findings (echogenic rind, architectural distortion, posterior shadowing, hypervascularity, ductal extension or abnormal ductal change, and calcifications) are shown in Figure 4. Figure 5 shows two cases of benign breast NM with histopathologic diagnosis of simple and sclerosing adenosis. Figure 6 shows one case of BWUP breast NM with histopathologic diagnosis of atypical ductal hyperplasia. Figure 7 shows two cases of malignant breast NM with histopathologic diagnosis of invasive ductal carcinoma and ductal carcinoma in situ.

In the univariate analysis (Table 4) and multivariate binary logistic regression (Table 5), we compared breast NM with benign and malignant diagnosis. Echogenic rind (OR 12.66, 95% CI 2.08-76.83), hypervascularity (OR 7.96, 95% CI 1.71-37.02), and calcifications (OR 18.61, 95% CI 2.71-127.65) were significantly associated with the risk of malignant breast NMs.

Regarding the diagnostic performance of the three significant ultrasonographic features predicting malignant breast NMs (echogenic rind, hypervascularity, and calcifications) (Table 6), sensitivity was 75% (95% CI, 50.5-89.8%), specificity 96.1% (95% CI, 86.8-98.9), positive predictive value 85.7% (95% CI, 60.1-96.0), negative predictive value 92.5% (95% CI, 82.1-97.0), and accuracy 91.0% (95% CI, 81.8-95.8%). There were false-positive results in 2 (3.8%, 95% CI, 1.1-13.2) of 53 cases with benign breast NM and false-negative results in 4 (25.0%, 95% CI, 10.2-49.5) of 16 cases with malignant breast NM.

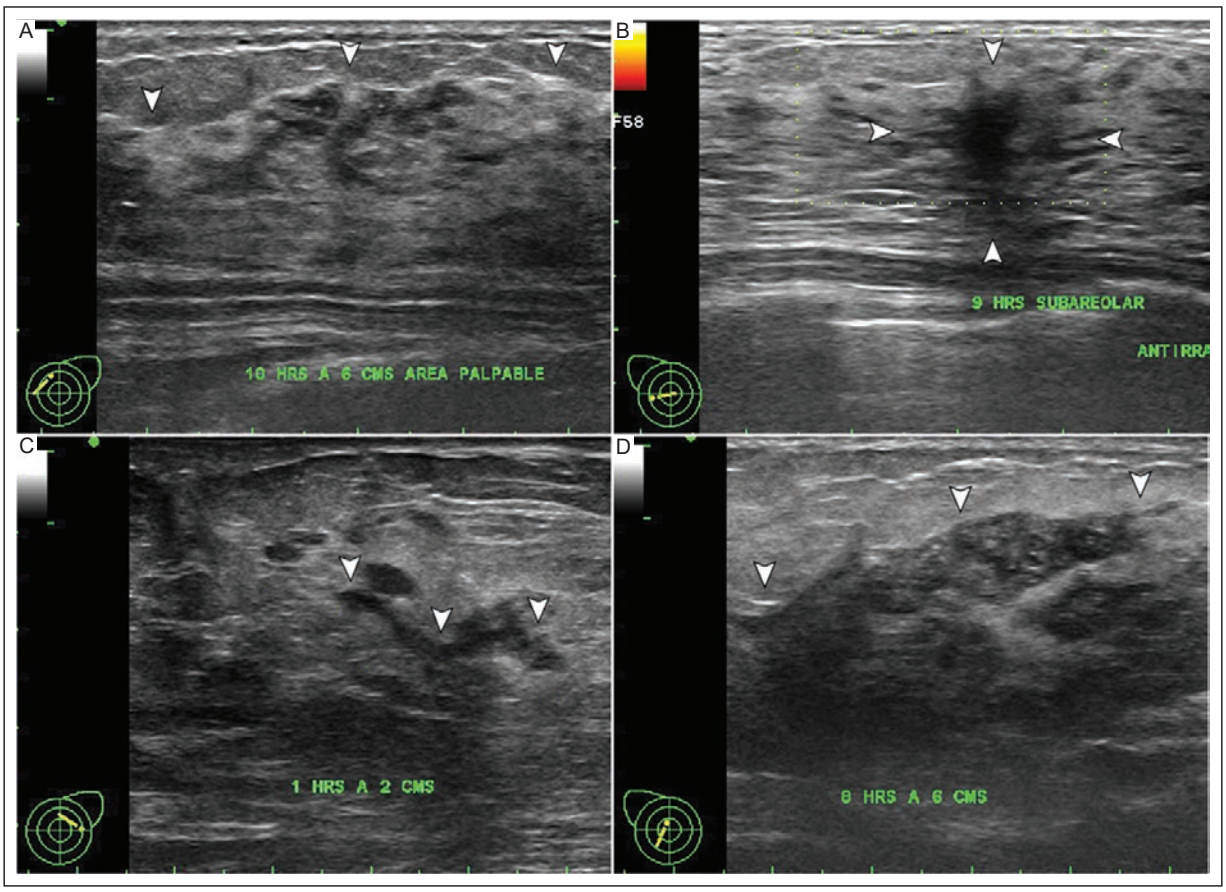

Figure 2. US in grayscale and power Doppler showing the **distribution** of breast NM **A:** regional (arrowheads). **B:** focal (arrowheads). **C:** linear (arrowheads). **D:** segmental (arrowheads).

NM: nonmass; US: ultrasound.

DISCUSSION

In our study, we found that the presence of echogenic rind, hypervascularity, and calcifications were ultrasonographic features that predicted malignancy in breast NM. These three features have high diagnostic accuracy; however, their absence may be a false-negative result. Therefore, we recommend breast biopsy in all patients with a breast NM. The use of the standardized breast US lexicon provided by the ACR BI-RADS fifth-edition update is useful for accurately describing breast NM and may allow systematizing management and follow-up.

Breast carcinoma can present as breast NM with different features on US. Lin et al.[14] reported an incidence of malignant NM of 4.59% (47/1024). Park et al.[6] found 88 (72.7%) cases of benign NM and 33 (27.3%) malignant NM cases in a retrospective study of 121 patients. Ductal carcinoma in situ (17/33, 51.5%) and invasive ductal cancer with or without ductal carcinoma in situ (13/33, 39.4%) were the main malignancies. These results are comparable to our study, in which malignant breast NM was detected in 16 (22.2%) of 72 women. In contrast, invasive ductal cancer was more frequent in our cases (n = 10, 62.4%). Ultrasonographic findings that predict malignant breast NMs were echogenic rind (OR 12.66, 95% CI 2.08-76.83), hypervascularity (OR 7.96, CI 1.71-37.02), and calcifications (OR 18.61, CI 2.71-127.65). On the other hand, in a retrospective study of 715 women[15] the significant US features associated with malignancy were segmental distribution (OR 3.03, 95% CI 1.50-6.15), calcifications (OR 4.26, 95% CI, 1.62-11.18), abnormal ductal changes (OR 4.91, 95% CI, 2.07-11.68), and posterior shadowing (OR 20.20, 95% CI, 6.46-63.23). Lin et al.[14] reported that microcalcifications and posterior shadowing were associated with malignant breast NM in 59 women. The ultrasonographic features that were significant for malignancy in our study may support the suspicion of malignant breast NM.

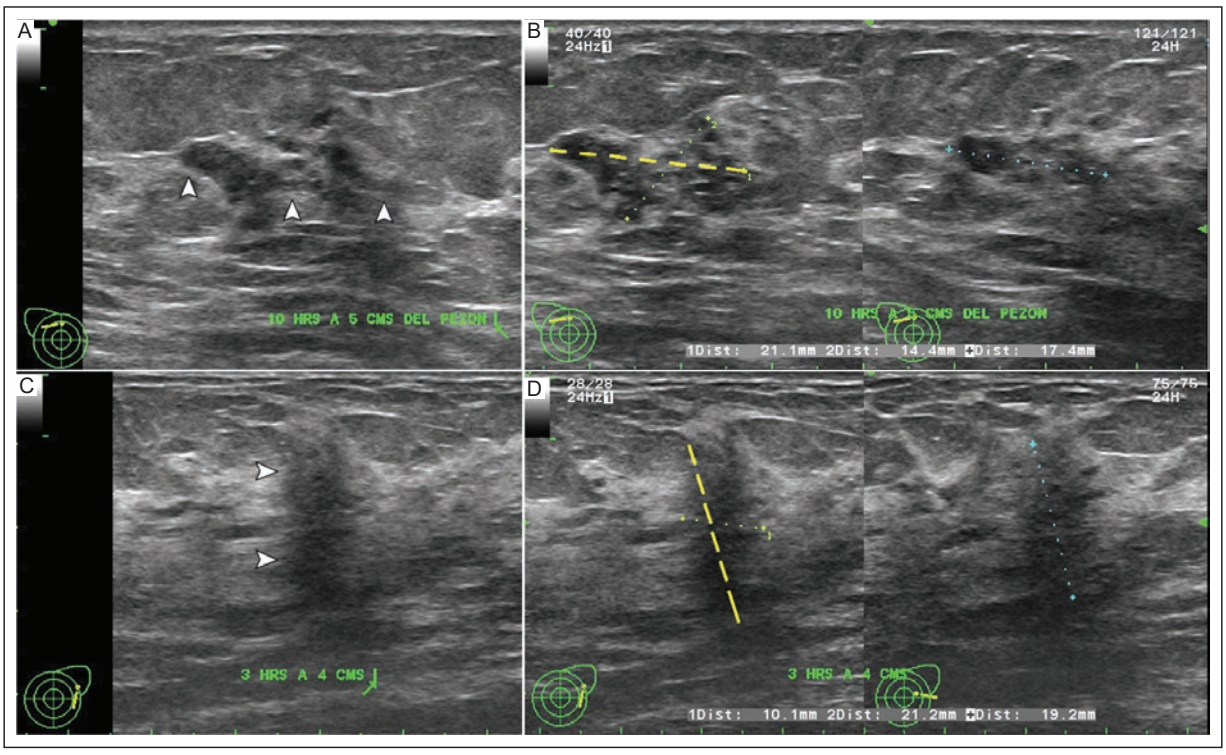

Figure 3. US in grayscale shows the **orientation** of breast NM. **A:** parallel (arrowheads), **B:** the 21-mm maximum axis (yellow line) of the lesion is shown parallel to the skin plane, **C:** antiparallel (arrowheads), and **D:** the 21.2-mm long maximal axis is in the anteroposterior plane (yellow line).

NM: nonmass; US: ultrasound.

The likelihood of malignancy in some breast NMs is underestimated[14]. The diagnostic accuracy of ultrasound findings in predicting malignant breast NMs has been evaluated. Zhang et al.[16] found a correlation between microcalcifications and malignant breast NMs in a retrospective study of 71 NMs assessed with US. The sensitivity was 100%, specificity was 29%, and accuracy was 69.0%. In our study, echogenic rind, hypervascularity, and calcifications had a sensitivity of 75%, specificity of 96.1%, and accuracy of 91%. The proportion of false negative results in our study population was high (25%); therefore, we cannot rule out malignancy based on breast US features alone. Biopsy of breast NM is recommended to confirm the diagnosis.

BWUP breast lesions are pathologies that increase the risk of subsequent breast malignancy over time[17]. In a systematic review and meta-analysis that included 129 studies, 11423 BWUP breast lesions were evaluated, and 2160 (17%) were found to have malignancy. BWUP breast lesions have different ultrasound features and may present as NM[18]. In our study, 3 (4.2%) of the 72 cases with breast NMs were BWUP cases. The US features of these BWUP breast NMs were predominantly hypoechoic, focal with antiparallel orientation, and architectural distortion. BWUP lesions presenting as breast NM have ultrasonographic features suspicious for malignancy, and biopsy is recommended for histopathologic confirmation.

Benign breast NM occurs in a variable proportion of cases, according to the literature[10,14,18]. Lee et al.[10] reported 95 (1.0%) NM in a retrospective study of 8856 asymptomatic women screened with breast US. Of the 93 lesions that were followed or confirmed histopathologically, 89 (95.6%) were benign, 2 (2.2%) were BWUP, and 2 (2.2%) were malignant breast NMs. Forester et al.[18] studied 166 patients with breast NM and found 104 (62.6%) benign NMs, 33 (19.9%) BWUP lesions, and 29 (17.5%) malignant breast NMs. These results are comparable to our study, in which 53 (73.6%) of 72 cases had benign breast NM. Fibrocystic changes were the most common benign diagnoses (11, 20.7%), similar as reported by other authors[4,8,10]. US features of benign breast NMs were variable, with hypoechoic (n = 33, 62.3%), focal (n = 38, 71.6%), avascular (n = 42, 79.2%), and noncalcified (n = 48, 90.5%) most frequently observed. Radiologists should be familiar with the ultrasonographic findings of

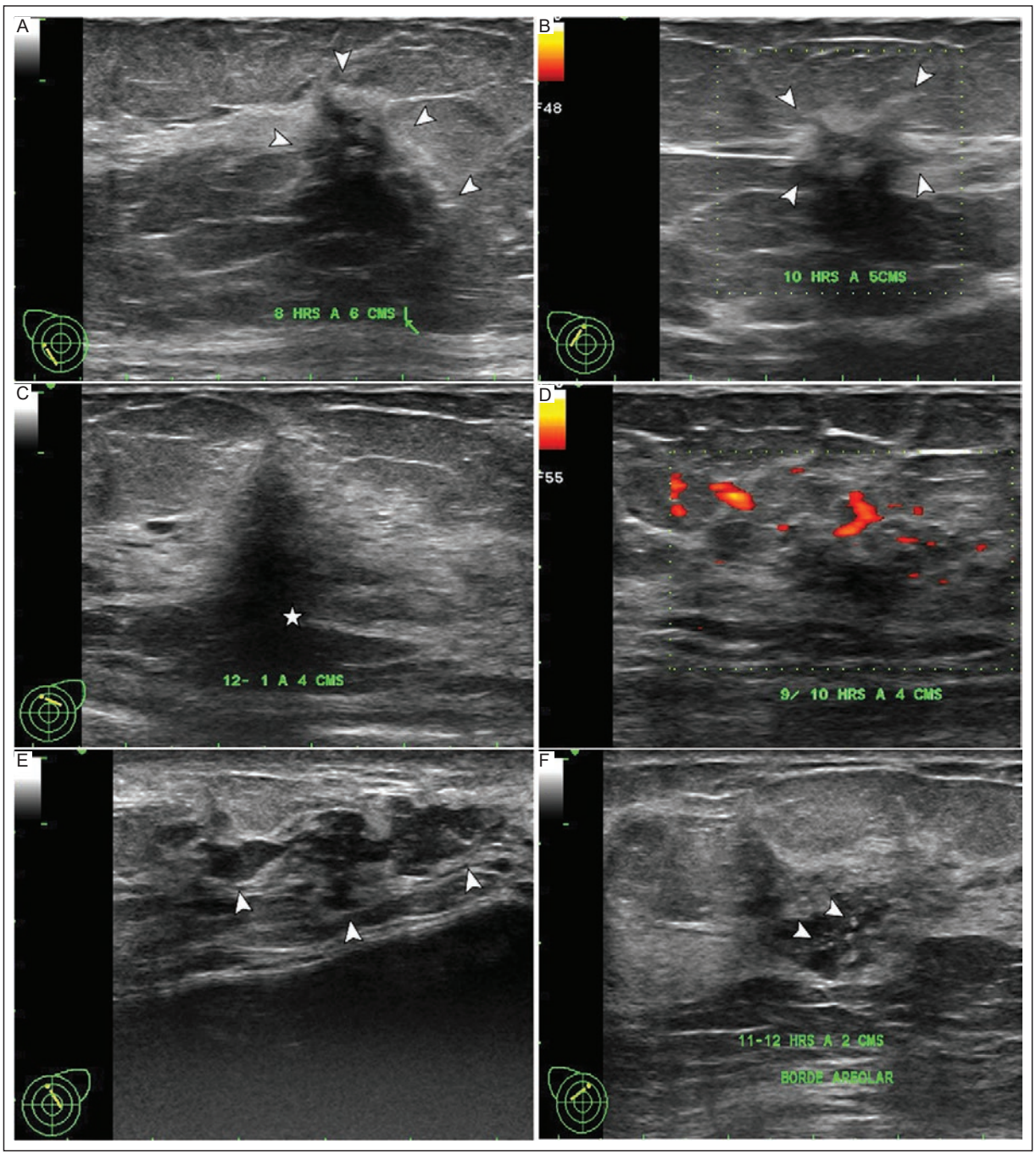

Figure 4. US in grayscale and power Doppler showing **the associated findings** of breast NM. **A:** echogenic rind (arrowheads). **B:** architectural distortion (arrowheads). **C:** posterior shadowing (star). **D:** Breast US power Doppler showing NM with hypervascularity. **E:** ductal extension (arrowheads). **F:** calcifications (arrowheads).

NM: nonmass; US: ultrasound.

benign breast NM to avoid upgrading their category in overestimated malignancy[14].

This study has several strengths. The diagnosis was confirmed in all included cases. The ultrasonographic features of breast NM were defined using a standardized lexicon that provides consistency and systematization to achieve the reproducibility. Some limitations are related to the small sample size and the retrospective design. On the other hand, the breast US was evaluated by only one observer, which may introduce bias due to the subjectivity of a single evaluator. Inter- and intraobserver agreement with the

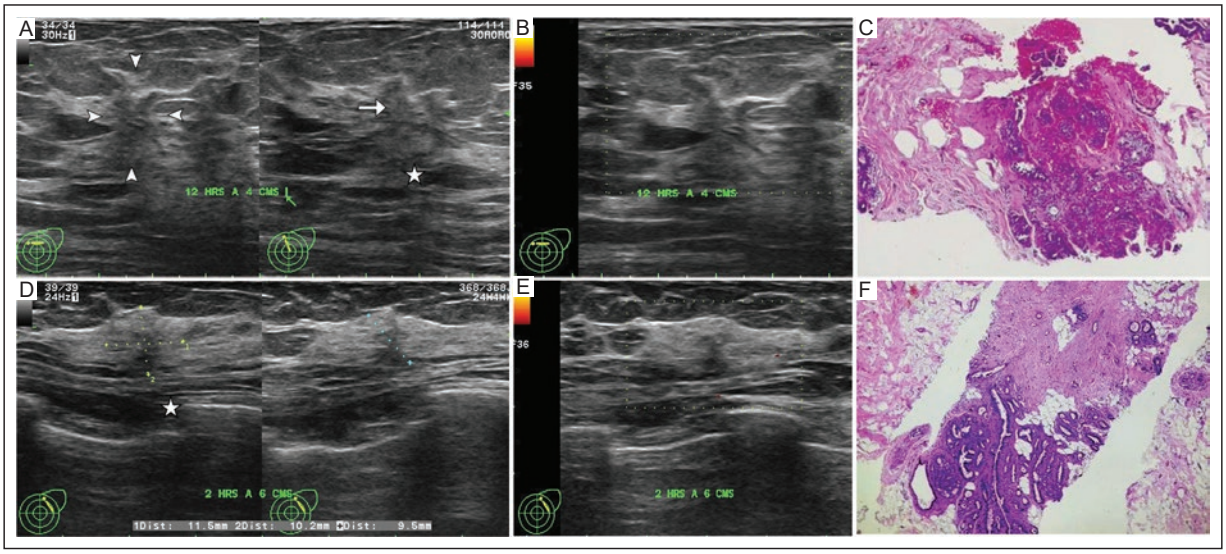

Figure 5. A 55-year-old woman with screening examination. **A:** grayscale US with focal breast NM (arrowheads), mixed echogenicity (arrow), antiparallel with architectural distortion and posterior shadowing (star). **B:** US Doppler power showing avascular breast NM. **C:** CNB. Mild focal proliferation of the small ducts with granular luminal secretion and lining by double row of polygonal, uniform cells without atypia, H&E 100×. Histopathologic diagnosis of simple adenosis. A 43-year-old woman with screening examination. **D:** US in grayscale with focal, hypoechoic, parallel breast NM with architectural distortion and posterior shadowing (star). **E:** US Doppler power showed avascular breast NM. **F:** CNB. Dense fibroelastic stroma with trapped and distorted ducts in an angulated shape with a layer of cubic to flat luminal cells, H&E 100×. Histopathologic diagnosis of sclerosing adenosis.

NM: nonmass; US: ultrasound; CNB: core needle biopsy; H&E: hematoxylin and eosin.

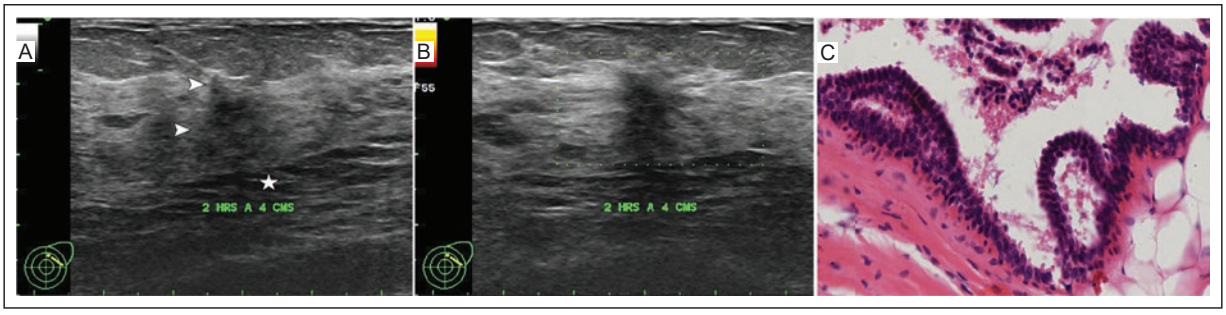

Figure 6. A 78-year-old woman with a routine study. **A:** US in grayscale with breast NM, hypoechoic (arrowheads), and posterior shadowing (star). **B:** US Doppler power showed avascular breast NM. **C:** CNB. Breast tissue with dilated ducts, hyperplasia of luminal cells forming roman bridges and broad-headed papillae. The cells are cylindrical with moderate eosinophilic cytoplasm, the nuclei are monomorphous, round, hyperchromatic, basal and myoepithelial cells are evident H&E, 200×. The histopathologic diagnosis was atypical ductal hyperplasia.

NM: nonmass; US: ultrasound; CNB: core needle biopsy; H&E: hematoxylin and eosin.

standardized breast NM lexicon was not assessed. Elastography, which complements the characterization of breast NM, was not included.

CONCLUSION

In our study, the ultrasonographic features of breast NM were defined using a standardized lexicon. Echogenic rind, hypervascularity, and calcifications were predictors for malignant breast NM. All breast NMs should be considered suspicious for malignancy and classified as category 4. In the presence of predictive features for malignancy, they should be classified at least as category 4B. For all breast NMs, biopsy is recommended for histopathologic confirmation of the diagnosis due to the possibility of malignancy. Interpretation of the ultrasonographic features of breast NM using a standardized lexicon can help radiologists describe them accurately and systematically.

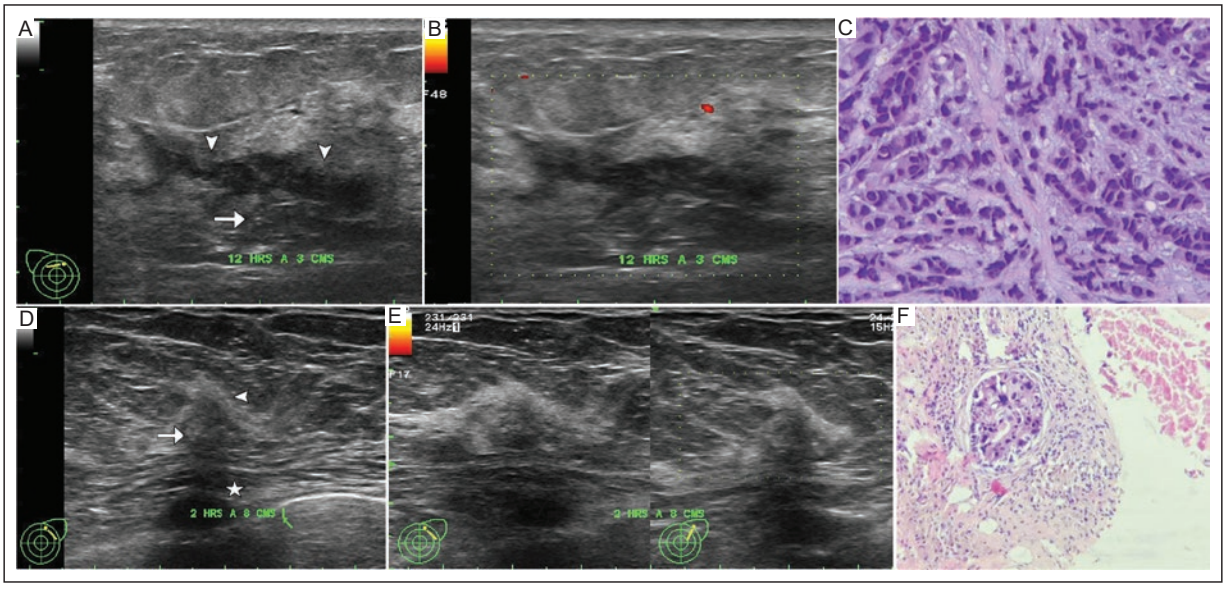

Figure 7. A 34-year-old woman with a screening examination. **A:** US in grayscale showing segmental, hypoechoic, parallel breast NM with echogenic rind, architectural distortion, posterior shadowing, ductal extension (arrowheads), associated with microcalcifications (arrow). **B:** breast US Doppler power with peripheral vascularity. **C:** CNB. Malignant neoplasm of the primary epithelial lineage of the mammary gland composed of nests, cords and tubular formation of less than 5%, H&E 400×. Histopathological diagnosis of invasive ductal carcinoma. A 52-year-old woman with screening examination. **D:** US in grayscale with focal breast NM, mixed echogenicity, antiparallel with echogenic rind (arrowhead), architectural distortion, posterior shadowing (star), associated with microcalcifications (arrow). **E:** US power Doppler shows avascular breast NM. **F:** CNB. Epithelial malignant neoplasm, of ductal origin, with a predominantly solid pattern and scarce glandular formations, located in the mammary ducts, H&E 100×. Histopathological diagnosis of ductal carcinoma in situ.

NM: nonmass; US: ultrasound; BAG: core needle biopsy; H&E: hematoxylin and eosin.

Acknowledgments

The authors thank Professor Ana M. Contreras-Navarro for her guidance in preparing and writing this scientific paper. Thesis in Radiology Specialty participating in the Primera Convocatoria Nacional 2023 “Las Mejores Tesis para Publicar en el JMeXFRI”.

Funding

None

Conflicts of interest

The authors declare no conflicts of interest.

Ethical disclosures

Protection of individuals: this study was conducted according to the Declaration of Helsinki (1964) and its subsequent amendments and the Mexican General Health Law on Research.

Confidentiality of information. The protocol of this hospital center was followed to anonymize patient data.

Right to privacy and informed consent. Informed consent was not required for this retrospective study.

REFERENCES

1. Choe J, Chikarmane SA, Giess CS. Nonmass findings at breast US: definition, classifications, and differential diagnosis. RadioGraphics. 2020;40(2):326-335. doi: 10.1148/rg.2020190125.
2. Kim YR, Kim HS, Kim HW. Are irregular hypoechoic breast masses on ultrasound always malignancies?: A pictorial essay. Korean J Radiol. 2015;16(6):1266-1275. doi: 10.3348/kjr.2015.16.6.1266.
3. Uematsu T. Non-mass lesions on breast ultrasound: why does not the ACR BI-RADS breast ultrasound lexicon add the terminology? J Med Ultrason. 2023. doi: 10.1007/s10396-023-01291-1.
4. Kim SJ, Park YM, Jung HK. Nonmasslike lesions on breast sonography: comparison between benign and malignant lesions. J Ultrasound Med. 2014;33(3):421-430. doi: 10.7863/ultra.33.3.421.
5. Giess CS, Chesebro AL, Chikarmane SA. Ultrasound features of mammographic developing asymmetries and correlation with histopathologic findings. AJR Am J Roentgenol. 2018;210(1):W29-W38. doi: 10.2214/AJR.17.18223.
6. Park JW, Ko KH, Kim EK, Kuzmiak CM, Jung HK. Non-mass breast lesions on ultrasound: final outcomes and predictors of malignancy. Acta Radiol. 2017;58(9):1054-1060. doi: 10.1177/0284185116683574.
7. Shin HJ, Kim HH, Kim SM, Kwon GY, Gong G, Cho OK. Screening-detected and symptomatic ductal carcinoma in situ: differences in the sonographic and pathologic features. AJR Am J Roentgenol. 2008; 190(2):516-525. doi: 10.2214/AJR.07.2206.

8. Ko KH, Jung HK, Kim SJ, Kim H, Yoon JH. Potential role of shear-wave ultrasound elastography for the differential diagnosis of breast non-mass lesions: preliminary report. Eur Radiol. 2014;24(2):305-311. doi: 10.1007/s00330-013-3034-4.
9. Uematsu T. Non-mass-like lesions on breast ultrasonography: a systematic review. Breast Cancer. 2012;19(4):295-301. doi: 10.1007/s12282-012-0364-z.
10. Lee J, Lee JH, Baik S, Cho E, Kim DW, Kwon HJ, et al. Non-mass lesions on screening breast ultrasound. Med Ultrason. 2016;18(4):446-451. doi: 10.11152/mu-871.
11. Ko KH, Hsu HH, Yu JC, Peng YJ, Tung HJ, Chu CM, et al. Non-mass-like breast lesions at ultrasonography: feature analysis and BI-RADS assessment. Eur J Radiol. 2015; 84(1):77-85. doi: 10.1016/j.ejrad.2014.10.010.
12. Wang ZL, Li Y, Wan WB, Li N, Tang J. Shear-wave elastography: could it be helpful for the diagnosis of non-mass-like breast lesions? Ultrasound Med Biol. 2017;43(1):83–90. doi: 10.1016/j.ultrasmedbio.2016.03.022.
13. Newell MS, Destounis S, Leung J, DeMartini W, Eby P. BI-RADS update: The edition formerly known as the 5th. Reston VA. USA. American College of Radiology (ACR); 2021.
14. Lin M, Wu S. Ultrasound classification of non-mass breast lesions following BI-RADS presents high positive predictive value. PLoS One. 2022;17(11):e0278299. doi: 10.1371/journal.pone.0278299.
15. Park KW, Park S, Shon I, Kim MJ, Han BK, Ko EY, et al. Non-mass lesions detected by breast US: stratification of cancer risk for clinical management. Eur Radiol. 2020;31(3):1693-1706. doi: 10.1007/s00330-020-07168-y.
16. Zhang W, Xiao X, Xu X, Liang M, Wu H, Ruan J et al. Non-mass breast lesions on ultrasound: feature exploration and multimode ultrasonic diagnosis. Ultrasound Med Biol. 2018;44(8):1703–1711. doi: 10.1016/j.ultrasmedbio.2018.05.005.
17. Purushothaman HN, Lekanidi K, Shousha S, Wilson R. Lesions of uncertain malignant potential in the breast (B3): what do we know? Clin Radiol. 2016;71(2):134-40. doi: 10.1016/j.crad.2015.10.008.
18. Forester ND, Lowes S, Mitchell E, Twiddy M. High risk (B3) breast lesions: What is the incidence of malignancy for individual lesion subtypes? A systematic review and meta-analysis. Eur J Surg Oncol. 2019;45(4):519-527. doi: 10.1016/j.ejso.2018.12.008.

JMeXFRI

Journal of the Mexican Federation of Radiology and Imaging

Check for updates

BRIEF RESEARCH ARTICLE

Structural MRI findings and postoperative prognosis in patients with temporal lobe epilepsy: a retrospective cohort study

Vanesa A. Cuellar-Figueroa[1,2a], Jaime I. Castro-Macias[3], Sara P. Perez-Reyes[3], and Omar Sanchez-Figueroa[1,2]*

[1]Departamento de Radiología e Imagen, Hospital Regional de Alta Especialidad del Bajio, Secretaria de Salud, Leon, Guanajuato; [2]Universidad Nacional Autonoma de Mexico. Mexico City; [3]Servicio de Neurociencias, Hospital Regional de Alta Especialidad del Bajío. Secretaria de Salud, Leon, Guanajuato. Mexico

ORCID: [a]0009-0001-1499-3053

ABSTRACT

The association between preoperative structural magnetic resonance imaging (MRI) and seizure freedom in Mexican patients with refractory temporal lobe epilepsy (TLE) undergoing surgery has not been reported. This study describes the hippocampal findings in preoperative structural MRI and their relationship with postoperative prognosis in Mexican patients with refractory TLE. This retrospective cohort study included patients older than 18 years with refractory TLE who underwent epilepsy surgery. The Harmonized Neuroimaging of Epilepsy Structural Sequences (HARNESS-MRI) protocol was used. Patients were followed for 24 months, and seizure freedom was determined based on the Engel classification. Forty-four patients with refractory TLE who underwent epilepsy surgery, 22 men and 22 women with a mean age of 35.2 ± 10.6 years (range 20 to 61), were assessed. Abnormal findings on preoperative structural MRI were identified in 36 patients. Hippocampal atrophy and increased signal on T2/FLAIR were the most common (n = 17, 47.2%). Seizure freedom was achieved in 30 (83.3%) of 36 patients. In contrast, only 4 (50%) of 8 patients with a normal preoperative structural MRI achieved seizure freedom (p = 0.042). This study is the first in Mexico that demonstrates the association between abnormal preoperative structural MRI findings and seizure freedom in patients with TLE undergoing epilepsy surgery.

Keywords: *Refractory temporal lobe epilepsy. Hippocampal sclerosis. Magnetic resonance imaging. Postoperative prognosis.*

INTRODUCTION

Structural magnetic resonance imaging (MRI) is crucial in the presurgical evaluation of refractory temporal lobe epilepsy (TLE). MRI identifies potentially epileptogenic brain structures, particularly in the temporal lobe (lesional epilepsy)[1]. Randomized clinical trials have reported that epilepsy surgery is more effective in controlling seizures than continued treatment with an antiseizure medication in patients with drug-refractory epilepsy[2]. Hippocampal sclerosis (HS) is the most common histologic abnormality in patients with refractory TLE[3,4]. Typical MRI findings of HS are atrophy, loss of internal structure, decreased T1-weighted, and increased T2-weighted signal intensity in the hippocampus[1]. Other features that may occur as secondary findings are atrophy of the ipsilateral fornix, mammillary body, and ipsilateral temporal lobe, especially the temporal pole[1,5]. Hippocampal atrophy suggestive of HS found on preoperative structural MRI is the most important prognostic factor for achieving seizure freedom after surgery[3,6-8].

Approximately 30% of patients with refractory TLE have a normal MRI on visual analysis (MRI-negative TLE), indicating the absence of an epileptogenic zone (nonlesional epilepsy)[3]. A normal or negative preoperative structural MRI in patients with TLE is associated with a less favorable postoperative outcome[3,6].

Corresponding author:
Vanesa A. Cuellar-Figueroa
E-mail: vcuellarf@hotmail.com

Received for publication: 11-02-2023
Accepted for publication: 27-03-2023
DOI: 10.24875/JMEXFRI.M23000050

Available online: 13-07-2023
J Mex Fed Radiol Imaging. 2023;2(2):126-132
www.JMeXFRI.com

The postoperative clinical course and the relationship of structural MRI findings with seizure freedom have not been described in Mexican patients with refractory TLE. This study describes the hippocampal findings on preoperative structural MRI and their relationship with seizure freedom in Mexican patients with refractory TLE.

MATERIAL AND METHODS

This retrospective cohort study was conducted from January 2015 to December 2020 at the Department of Imaging and Epilepsy Clinic of the Neuroscience Service of the Hospital Regional de Alta Especialidad del Bajio, Secretaria de Salud in Leon, Guanajuato, Mexico. The study included patients over 18 years with refractory TLE who underwent epilepsy surgery. Patients with incomplete examinations (no MRI) or a tumor, vascular malformation, encephalomalacia, gliosis, or cortical dysplasia were excluded. Patients who did not complete the 24-month postoperative follow-up were also excluded. Informed consent was not required for data collected as part of routine medical care. The protocol was approved by the institutional ethics and research committees.

Study development and variables

The clinical records of patients with refractory TLE who underwent epilepsy surgery were retrospectively reviewed. The indication for refractory TLE surgery was based on a complete diagnostic protocol that included a neurological physical examination, neuropsychological assessment, surface electroencephalogram, a functional MRI, the Wada test, positron emission tomography, and interictal cerebral single-photon emission computed tomography to determine the etiology and epileptogenic zone. Selective amygdalohippocampectomy was performed in patients with an epileptogenic zone in the dominant lobe with a good intelligence Quotient (IQ). Anterior temporal lobectomy was performed in patients with an epileptogenic zone in the non-dominant lobe or mental retardation in the dominant lobe. This study focuses only on reporting structural MRI findings.

The recorded variables included age, sex, duration of epilepsy in months, type of surgery, and laterality. Postoperative follow-up was conducted in the epilepsy clinic for a minimum of 24 months. Seizure outcome was assessed annually after the surgery date. Patients' seizure classifications could change over the course of 24 months.

Table 1. Abnormal hippocampal findings on preoperative structural MRI in patients with refractory TLE undergoing epilepsy surgery

Typical findings	n (%)
Atrophy and increased T2/FLAIR signal intensity	17 (47.2)
Hippocampal atrophy	14 (38.9)
Increased T2/FLAIR signal intensity	5 (13.9)
Total	36 (100)
Other findings	**n (%)**
Atrophy of the fornix	12 (33.3)
Loss of GM-WM differentiation at the temporal lobe	6 (16.6)
Atrophy of mammillary bodies	5 (13.9)
Loss of hippocampal head digitations	2 (5.6)
None	11 (30.6)
Total	36 (100)

MRI: magnetic resonance imaging; T2: weighted turbo-spin-echo sequence; FLAIR: fluid-attenuated inversion recovery; GM: gray matter; WM: white matter.

Definitions

Refractory TLE, according to the International League Against Epilepsy (ILAE), is "that in which there has been a failure of two trials of antiseizure medication, in monotherapy or combination, tolerated, appropriately chosen and adequately used to achieve the sustained absence of crises[9]."

Postoperative seizure freedom was based on the Engel classification of seizures[10].

Acquisition and analysis protocol

MRI was performed with a Magnetom Avanto 1.5 T unit (Siemens Healthcare, Erlangen, Germany) using the Harmonized Neuroimaging of Epilepsy Structural Sequences (HARNESS-MRI) protocol[11] with T1 and FLAIR-weighted sequences in axial, sagittal, and coronal views, and T2 in coronal view. MRI findings were described based on the Blümcke/ILAE classification[4,12].

The structural MRI was assessed by a board-certified neuroradiologist (OSF) with 15 years of experience. The clinical follow-up was conducted by a neurologist (JICM) specializing in epilepsy with 20 years of experience.

Statistical analysis

Quantitative variables are reported as means, standard deviations, and ranges. The chi-square test was

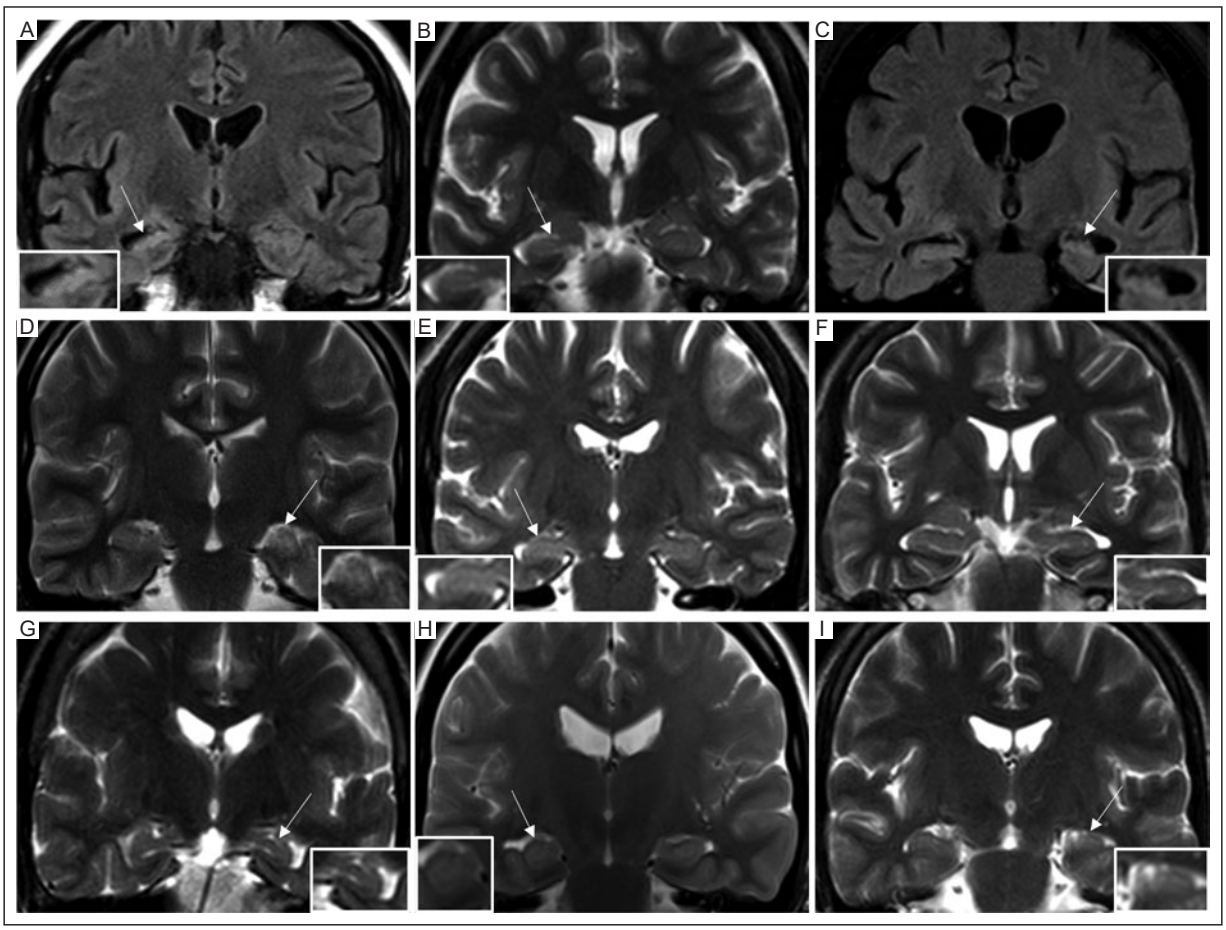

Figure 1. Examples of typical findings on preoperative structural MRI in patients with refractory TLE showing volume and signal abnormalities in the hippocampus. Magnified views are shown. **A:** coronal FLAIR view of a 38-year-old woman with atrophy and increased signal intensity in the right hippocampus (arrow). **B:** coronal T2-weighted view of a 36-year-old woman with atrophy and increased signal intensity in the right hippocampus (arrow). **C:** coronal FLAIR view of a 43-year-old woman with atrophy and increased signal intensity in the left hippocampus (arrow). **D:** coronal T2-weighted view of a 33-year-old man with atrophy and increased signal intensity in the left hippocampus (arrow). **E:** coronal T2-weighted view of a 27-year-old woman with normal volume and increased signal intensity of the right hippocampus (arrow). **F:** coronal T2-weighted view of a 32-year-old man with atrophy and normal signal intensity of the left hippocampus (arrow). **G:** coronal T2-weighted view of a 35-year-old woman with atrophy and normal signal intensity in the left hippocampus (arrow). **H:** coronal T2-weighted view of a 21-year-old woman with atrophy and normal signal intensity in the right hippocampus (arrow). **I:** coronal T2-weighted view of a 35-year-old man with atrophy and normal signal intensity in the left hippocampus (arrow).

MRI: magnetic resonance imaging; TLE: temporal lobe epilepsy; T2: weighted turbo-spin-echo sequence; FLAIR: fluid-attenuated inversion recovery.

used to compare frequencies and nominal data. The chi-square test compared a normal or abnormal MRI and seizure freedom. A p-value <0.05 was considered statistically significant. The data were analyzed using SPSS version 23.0 (IBM Corp., Armonk, NY, USA).

RESULTS

Fifty-three patients with refractory TLE who underwent epilepsy surgery were evaluated. Nine patients with other MRI-proven diagnoses were excluded: three with tumors, two with vascular malformations, two with encephalomalacia, one with gliosis, and one with cortical dysplasia. Forty-four patients, 22 men and 22 women, with a mean age of 35.2 ± 10.6 years (range 20 to 61), were evaluated. The mean duration of epilepsy was 254.7 ± 127.6 months (range 36-636). Selective amygdalohippocampectomy + anterior temporal lobectomy was performed in 39 patients, while three underwent amygdalohippocampectomy and two anterior temporal lobectomy. Epilepsy surgery was performed on the right side in 28 patients and on the left side in 16.

The preoperative structural MRI was normal in 8 patients, while abnormal MRI findings were observed

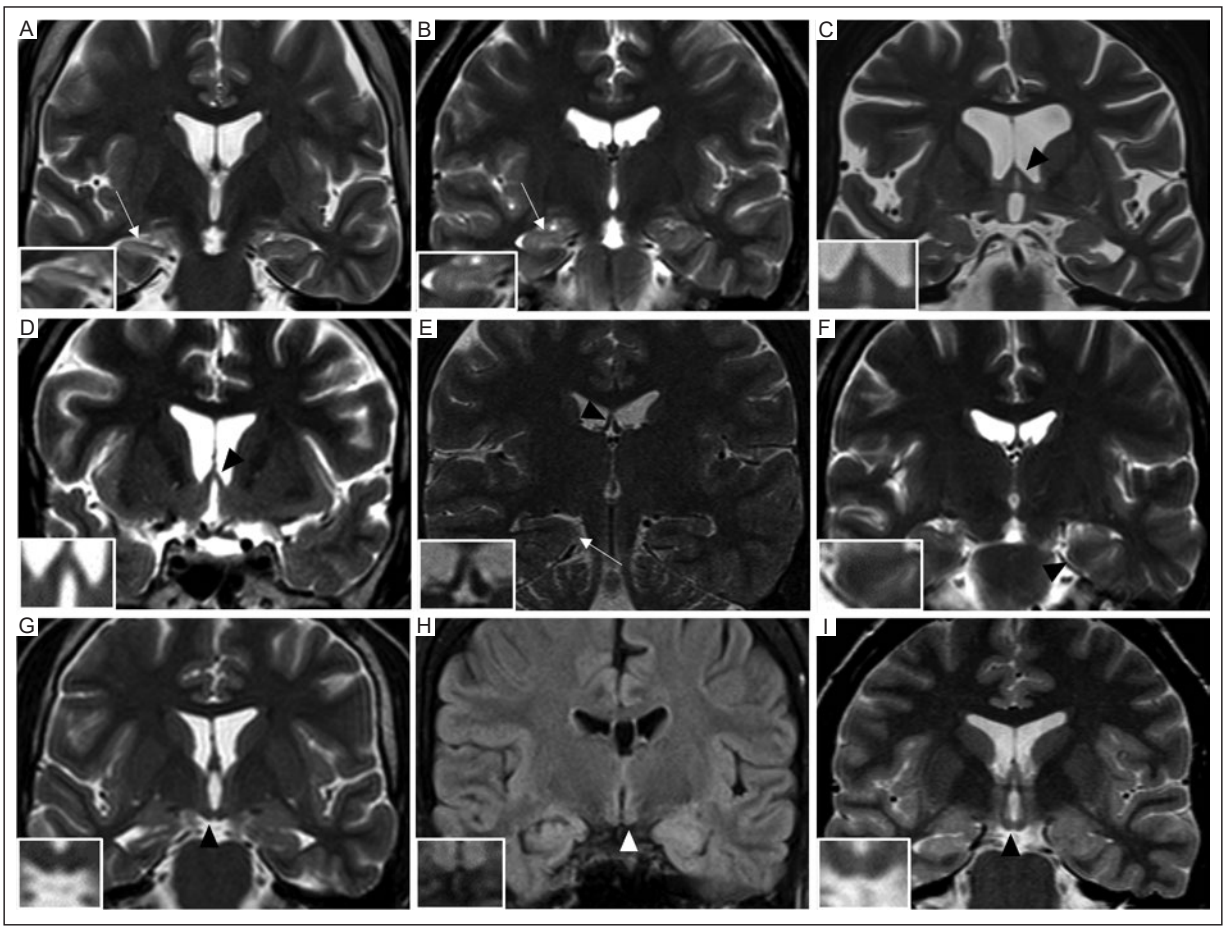

Figure 2. Examples of other abnormal findings on a preoperative structural MRI of patients with refractory TLE. Magnified views are shown. **A:** coronal T2-weighted view of a 34-year-old man with a loss of hippocampal head digitations in the right hippocampus (arrow). **B:** coronal T2-weighted view of a 21-year-old man with a loss of hippocampal head digitations in the right hippocampus (arrow). **C:** coronal T2-weighted view of a 37-year-old woman with atrophy of the left fornix (black arrowhead). **D:** coronal T2-weighted view of a 39-year-old man with atrophy of the left fornix (arrowhead). **E:** coronal T2-weighted of a 29-year-old woman with a loss of grey-white matter differentiation in the temporal lobe (black arrow) and atrophy of the right fornix (black arrowhead). **F:** coronal T2-weighted view of a 35-year-old man with a loss of grey-white matter differentiation in the left temporal lobe (black arrowhead). **G:** coronal T2-weighted view of a 21-year-old man with atrophy of the right mammillary body (black arrowhead). **H:** coronal FLAIR view of a 44-year-old woman with atrophy of the left mammillary body (black arrowhead). **I:** coronal T2-weighted view of a 21-year-old man with atrophy of the right mammillary body (black arrowhead).

MRI: magnetic resonance imaging; TLE: temporal lobe epilepsy; T2: weighted turbo-spin-echo sequence; FLAIR: fluid-attenuated inversion recovery.

in 36 patients (Table 1). The most common typical findings were hippocampal atrophy and increased T2/FLAIR signal, present in 17 (47.2%) of the 36 patients with an abnormal preoperative structural MRI. Hippocampal atrophy was found in 14 (38.9%) patients and increased T2/FLAIR signal in 5 (13.9%). Other findings such as atrophy of the fornix (n = 12, 33.3%) was the most common, followed by a loss of gray matter (GM)–white matter (WM) differentiation in the temporal lobe in 6 (16.6%) patients, atrophy of the mammillary bodies in 5 (13.9%) patients, and loss of the hippocampal head digitations in two (5.6%) patients.

Figure 1 shows typical findings on structural MRI in patients with refractory TLE with volume and signal abnormalities in the hippocampus. Figure 2 shows examples of other structural MRI findings in patients with refractory TLE. Figure 3 shows pre- and postoperative findings of abnormal and normal structural MRI in two and one patient with TLE, respectively.

At the 24-month follow-up, 30 (83.3%) patients with an abnormal preoperative structural MRI achieved complete seizure control (Engel IA, completely seizure-free since surgery), while only 4 (50%) of 8 patients with a normal MRI were classified as Engel IA ($p = 0.042$). Two (5.6%) of 36 patients were classified

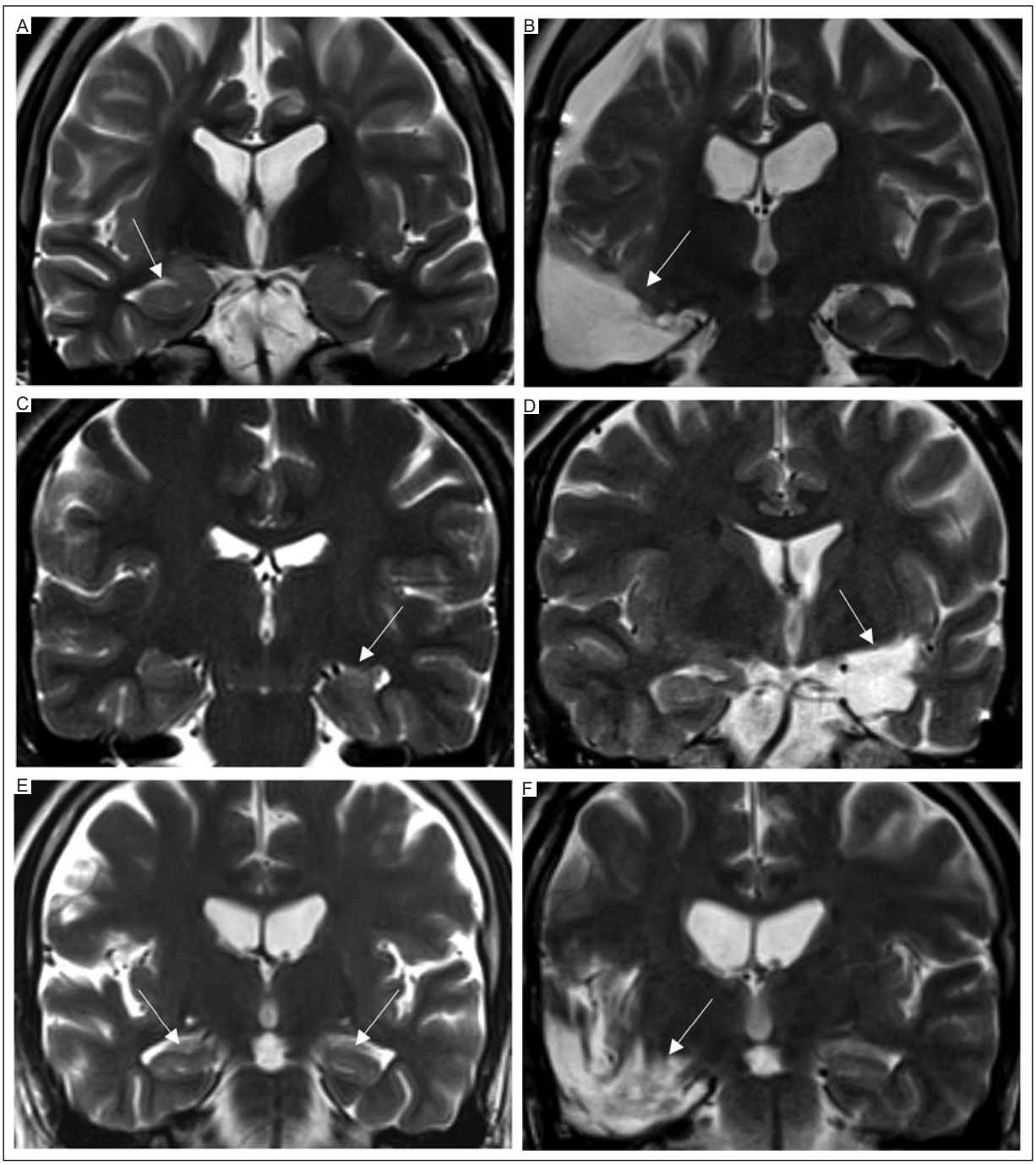

Figure 3. Preoperative and postoperative MRI findings of the patients with refractory TLE who underwent epilepsy surgery. **A:** abnormal preoperative coronal T2-weighted view of a 21-year-old man with atrophy and increased signal intensity in the right hippocampus (arrow). **B:** postoperative coronal T2-weighted view with changes secondary to right temporal lobectomy with right amygdalohippocampectomy. A residual hygroma is seen in the subarachnoid space of the frontal and temporal convexity (arrow). **C:** abnormal preoperative coronal T2-weighted view of a 32-year-old woman with atrophy and increased signal intensity of the left hippocampus (arrow). **D:** postoperative coronal T2-weighted view with changes secondary to amygdalohippocampectomy with an area of encephalomalacia and areas of gliosis at the left temporal level (arrow). **E:** normal preoperative coronal T2-weighted view of a 58-year-old man with normal volume and signal intensity in the bilateral hippocampus (arrow). **F:** postoperative coronal T2-weighted view with an area of encephalomalacia and gliosis in the right temporal level (arrow).

MRI: magnetic resonance imaging; TLE: temporal lobe epilepsy; T2: weighted turbo-spin-echo sequence.

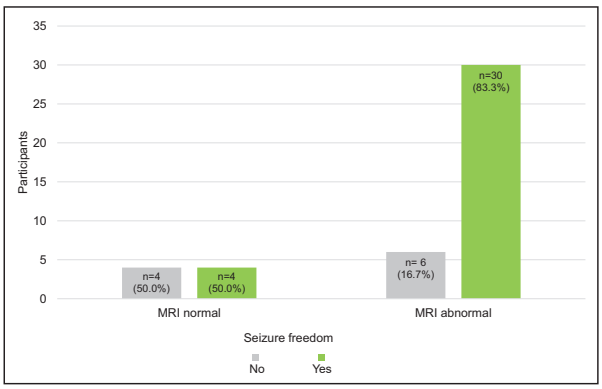

Figure 4. Comparison of normal or abnormal preoperative structural MRI with seizure freedom at 24-month follow-up after epilepsy surgery in patients with refractory TLE. Patients with an abnormal preoperative structural MRI had a significant difference in seizure freedom (n = 30, 83.3%) compared to patients with a normal MRI (n = 4, 50%) (p = 0.042). MRI: magnetic resonance imaging; TLE: temporal lobe epilepsy.

as Engel IB (non-disabling simple partial seizures only since surgery). Four (11.1%) of 36 patients with an abnormal MRI and 4 (50%) of 8 patients with a normal MRI were Engel IIA (rare disabling seizures, almost seizure free: initially free of disabling seizures but has rare seizures now). The mean duration of TLE was 233.65 ± 112.23 months in 34 patients with Engel IA, compared to 326.40 ± 155.82 months in the 10 patients with other categories (p = 0.586).

Postoperative complications included choroidal artery infarction in two patients and one with VI cranial nerve palsy.

DISCUSSION

This study is the first in Mexico that demonstrates an association between abnormal preoperative structural MRI findings and seizure freedom in patients with TLE undergoing epilepsy surgery. Abnormal findings in the hippocampus on preoperative structural MRI were associated with a favorable postoperative prognosis.

Preoperative structural MRI is the only imaging modality with a prognostic impact in patients with refractory TLE who undergo epilepsy surgery[6]. In our study, abnormal structural MRI findings in the hippocampus were associated with a favorable postoperative prognosis of seizure freedom in 30 (83.3%) with refractory TLE. In contrast, patients with a normal structural MRI showed a less favorable prognosis, with only 4 (50%) achieving seizure freedom. Lesional epilepsy detected by abnormal MRI findings is associated with a better outcome than nonlesional epilepsy. A systematic review and meta-analysis by Téllez-Zenteno et al.[7] that included 40 articles involving 697 patients with nonlesional epilepsy and 2860 patients with lesional epilepsy found that patients with lesions on MRI or histopathology were 2.5 times more likely to be seizure-free after surgery (OR 2.5, 95% CI, 2.1-3.0, p < 0.001). Furthermore, a meta-analysis[13] of 38 studies with a total of 84,703 patients demonstrated that an abnormal MRI is a favorable predictor of seizure freedom in epilepsy surgery. Our study provides evidence in Mexican patients with results comparable to studies that included a large patient series.

Patients with refractory TLE and normal MRI who undergo epilepsy surgery tend to have a less favorable postoperative outcome. In our study, 50% of patients with a normal MRI were seizure-free after surgery. Bell et al.[14], in a study of 44 patients with TLE and a normal MRI, 26 (60%) were seizure-free after anterior temporal lobectomy, and 15% had a decrease in seizure frequency (Engel II). Wang et al.[15], in a systematic review and meta-analysis of 18 studies with a total of 391 patients, reported that a normal MRI was associated with seizure freedom after temporal lobe surgery in 51% of cases. Muhlhofer et al.[3] reported that a normal MRI with no abnormalities in the temporal region was associated with seizure freedom in 51% of patients with TLE who underwent surgery. Therefore, a normal preoperative structural MRI is considered a less favorable predictor of postoperative seizure freedom in patients with refractory TLE.

The strengths of the study include its cohort design and the performance of preoperative and postoperative structural MRI with follow-up in all patients. However, the study is limited by its small sample size from a single center. Additionally, visual volume analysis of the hippocampus was used, which is less accurate than manual or automated volumetry[11]. The histopathological results of hippocampal sclerosis were not included. On the other hand, other clinical factors, such as mental retardation and generalized tonic-clonic seizures, which may impact postoperative seizure outcomes, were not recorded.

CONCLUSION

Our study showed that hippocampal abnormalities on preoperative structural MRI in Mexican patients with

refractory TLE predicted a favorable prognosis with seizure freedom in 4 out of 5 patients who underwent epilepsy surgery. Identifying an epileptogenic lesion provides a surgical target and increases the likelihood of achieving seizure freedom after surgery for eligible patients. Therefore, performing MRI examinations early in the clinical course using an optimized protocol (HARNESS-MRI)[1,11] is crucial. Future studies with a larger number of patients from multiple centers and a prospective design are needed to minimize bias and further investigate the postoperative prognosis in Mexican patients with refractory TLE.

Acknowledgments

The authors thank Professor Ana M. Contreras-Navarro for her guidance in preparing and writing this scientific paper. This thesis in the field of Radiology Specialty was awarded at the Primera Convocatoria Nacional 2023 “Las Mejores Tesis para Publicar en el JMeXFRI”.

Funding

This research received no external funding.

Conflicts of interest

The authors declare no conflicts of interest.

Ethical disclosures

Protection of Individuals. This study complied with the Declaration of Helsinki (1964) and subsequent amendments.

Confidentiality of Data. The authors declare they followed their center’s protocol for sharing patient data.

Right to privacy and informed consent. Informed consent was not required for this retrospective cohort study of information collected during routine clinical care.

REFERENCES

1. Wang I, Bernasconi A, Bernhardt B, Blumenfeld H, Cendes F, Chinvarun Y, et al. MRI essentials in epileptology: a review from the ILAE Imaging Taskforce. Epileptic Disorders. 2020;22(4):421–437. doi: 10.1684/epd.2020.1174.
2. Jobst BC, Cascino GD. Resective epilepsy surgery for drug-resistant focal epilepsy: a review. JAMA. 2015;313(3):285–293. doi: 10.1001/jama.2014.17426.
3. Muhlhofer W, Tan Y, Mueller SG, Knowlton R. MRI-negative temporal lobe epilepsy-What do we know? Epilepsia. 2017;58(5):727–742. doi: 10.1111/epi.13699.
4. Urbach H. Hippocampal Sclerosis. In Urbach H. MRI in Epilepsy. Freiburg. Springer, 2013:91–100. doi: 10.1007/978-3-642-25138-2.
5. Dekeyzer S, De Kock I, Nikoubashman O, Vanden Bossche S, Van Eetvelde R, De Groote J, et al. “Unforgettable”-a pictorial essay on anatomy and pathology of the hippocampus. Insights Imaging. 2017;8(2):199–212. doi: 10.1007/s13244-016-0541-2.
6. Jones AL, Cascino GD. Evidence on use of neuroimaging for surgical treatment of temporal lobe epilepsy: a systematic review. JAMA Neurol. 2016;73(4):464–470. doi: 10.1001/jamaneurol.2015.4996.
7. Téllez-Zenteno JF, Ronquillo LH, Moien-Afshari F, Wiebe S. Surgical outcomes in lesional and non-lesional epilepsy: a systematic review and meta-analysis. Epilepsy Res. 2010;89(2-3):310–318. doi: 10.1016/j.eplepsyres.2010.02.007.
8. Hagemann A, Bien CG, Kalbhenn T, Hopf JL, Grewe P. Epilepsy Surgery in Extratemporal vs Temporal Lobe Epilepsy: Changes in Surgical Volumes and Seizure Outcome Between 1990 and 2017. Neurology. 2022;98(19):1902–1912. doi: 10.1212/WNL.0000000000200194.
9. Kwan P, Arzimanoglou A, Berg AT, Brodie MJ, Allen Hauser W, Mathern G, et al. Definition of drug resistant epilepsy: consensus proposal by the ad hoc Task Force of the ILAE Commission on Therapeutic Strategies. Wiley Online Library; 2010. doi: 10.1111/j.1528-1167.2009.02397.x.
10. Wieser HG, Blume WT, Fish D, Goldensohn E, Hufnagel A, King D, et al. Proposal for a new classification of outcome with respect to epileptic seizures following epilepsy surgery. Epilepsia. 2001;42(2):282–286.
11. Bernasconi A, Cendes F, Theodore WH, Gill RS, Koepp MJ, Hogan RE, et al. Recommendations for the use of structural magnetic resonance imaging in the care of patients with epilepsy: a consensus report from the International League Against Epilepsy Neuroimaging Task Force. Epilepsia. 2019;60(6):1054–1068. doi: 10.1111/epi.15612.
12. Blümcke I, Thom M, Aronica E, Armstrong DD, Bartolomei F, Bernasconi A, et al. International consensus classification of hippocampal sclerosis in temporal lobe epilepsy: a Task Force report from the ILAE Commission on Diagnostic Methods. Epilepsia. 2013;54(7):1315–1329. doi: 10.1111/epi.12220.
13. Alim-Marvasti A, Vakharia VN, Duncan JS. Multimodal prognostic features of seizure freedom in epilepsy surgery. J Neurol Neurosurg Psychiatry. 2022;93(5):499–508. doi: 10.1136/jnnp-2021-327119.
14. Bell ML, Rao S, So EL, Trenerry M, Kazemi N, Matt Stead S, et al. Epilepsy surgery outcomes in temporal lobe epilepsy with a normal MRI. Epilepsia. 2009;50(9):2053–2060. doi: 10.1111/j.1528-1167.2009.02079.x.
15. Wang X, Zhang C, Wang Y, Hu W, Shao X, Zhang J, et al. Prognostic factors for seizure outcome in patients with MRI-negative temporal lobe epilepsy: a meta-analysis and systematic review. Seizure. 2016;38:54–62. doi: 10.1016/j.seizure.2016.04.002.

JMeXFRI

Journal of the Mexican Federation of Radiology and Imaging

Check for updates

BRIEF RESEARCH ARTICLE

Standardized structured report for Doppler duplex ultrasound of lower extremity venous insufficiency and thrombosis: a technical note

Mauricio Figueroa-Sanchez[1,2,3,a], Simmons D. Gough[1,2], M. Fernanda Lopez-Mendoza[1,2] and Aldo A. Montero-Cedeño[4]*

[1]Radiology and Imaging Department, Antiguo Hospital Civil of Guadalajara "Fray Antonio Alcalde"; [2]University Center of Health Sciences, Universidad of Guadalajara; [3]Laboratorio Vascular S.C., Guadalajara, Jalisco; [4]Radiology and Imaging Department, Hospital General de Durango, Secretaria de Salud. Durango, Durango. Mexico

ORCID: [a]0000-0001-7042-5221

ABSTRACT

A standardized structured Doppler duplex ultrasound (US) report format for lower extremity venous system assessment has not been previously described. This technical note proposes a standardized, structured report for a complete Doppler duplex US protocol for evaluating lower extremity venous insufficiency and thrombosis. The protocol begins in the upper abdomen with an assessment of the heart, the ostium of the inferior vena cava (IVC), the caval hiatus, the entire course of the IVC, the iliac veins on both sides, and the entire course of the superficial and deep, perforator, and reticular venous system of the lower extremities. The diameter, compressibility, permeability, competence, velocity, thrombosis, or endothelial thickening in the transverse plane with compression maneuvers, the Valsalva maneuver, respiratory variation, and augmentation of one or both lower extremities are described according to the referring physician's request. Additional pathologic findings of varicose plexuses, incompetent perforating veins, thrombi, or surgical changes are reported. The proposed standardized structured report format, developed for educational purposes for radiologists and residents, is intended to improve accuracy and consistency of information. It also facilitates effective communication by providing relevant information to clinicians and patients.

Keywords: *Structured standardized report. Venous insufficiency. Duplex ultrasonography. Thrombosis.*

INTRODUCTION

The assessment of venous insufficiency and thrombosis of the lower extremities is one of the most common indications for Doppler duplex ultrasound (US) worldwide. The prevalence of venous insufficiency varies from 5% to 30% of the adult population with a female-to-male ratio of 3 to 11[1]. It affects approximately 20 million Americans each year[2]. Lower extremity venous insufficiency was found in 231 (66.0%) women and 119 (34.0%) men (2:1 ratio) in a preliminary report of 350 Mexican patients (personal communication). Clinical manifestations can be due to venous obstruction or valvular insufficiency[3], causing pain, swelling, edema, skin changes, and ulceration. Primary venous insufficiency is not associated with thrombosis, while secondary insufficiency is associated with obstruction and/or thrombosis; reflux leads to chronic venous hypertension in both types.

The venous system is, in many ways, far more complicated than the arterial system[4]. Effective venous return from the lower extremities requires the interaction of the heart, a pressure gradient, peripheral muscle pumps of the leg, and competent venous valves[3]. The venous system of the lower extremities includes the deep veins, which lie beneath the muscle fascia and

***Corresponding author:**
Mauricio Figueroa-Sanchez
E-mail: figueroa_sanchez@hotmail.com

Received for publication: 07-03-2023
Accepted for publication: 27-03-2023
DOI: 10.24875/JMEXFRI.M23000045

Available online: 13-07-2023
J Mex Fed Radiol Imaging. 2023;2(2):133-141
www.JMeXFRI.com

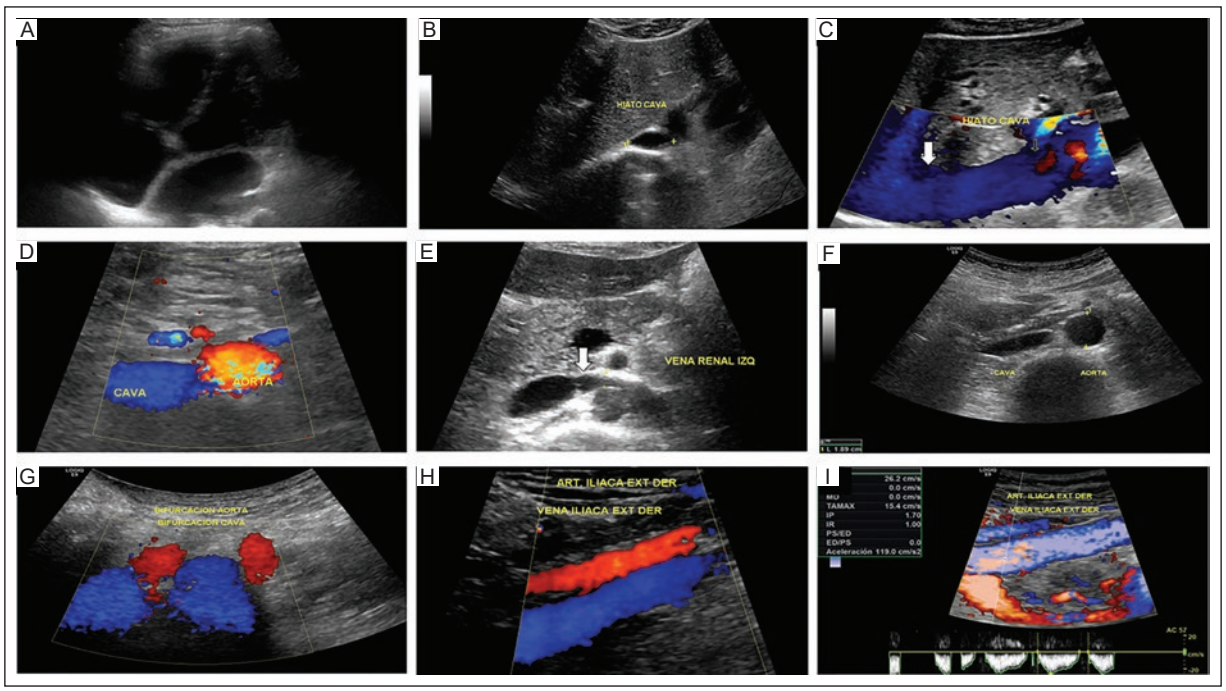

Figure 1. A: grayscale US subxiphoid approach showing the four chambers of the heart. **B:** transverse view, grayscale US showing the vena cava hiatus (3.54 cm, not shown). **C:** sagittal view, color Doppler US of the vena cava hiatus (arrow) to the root of the IVC (right atrium). **D:** transverse view, color doppler US showing normal aorta, IVC, superior mesenteric artery, and vein. **E:** transverse view, grayscale US showing the normal left renal vein (5 mm, not shown) at the junction of the aorta and superior mesenteric artery (arrow) and its junction with the normal IVC. **F:** transverse view, grayscale US of the normal aorta (1.89 cm) and IVC. **G:** transverse view, color Doppler US showing the bifurcation of the aorta and the IVC with normal patency and flow direction. **H:** sagittal view, color Doppler US of the right external iliac artery and vein showing normal patency and flow direction. **I:** sagittal view, color Doppler US and spectrum of the right external iliac vein with normal spectral morphology and velocity (26.2 cm/sec).

IVC: inferior vena cava; US: ultrasound.

drain the muscles of the lower extremities; the superficial veins, which are above the deep fascia and drain the cutaneous microcirculation; and the perforating veins, which penetrate the muscular fascia and connect the superficial and deep veins[3]. The communicating veins connect the veins within the same compartment[3].

Several authors have emphasized the importance of a standardized structured radiology report[5-7], and Mexican radiologists prefer a standardized structured report[7]. A standardized structured report of quantitative ultrasound findings, which may help to systematize the evaluation, diagnosis, and follow-up of patients with pelvic congestion syndrome or asymptomatic pelvic venous congestion, was recently published[8]. There is no standardized structured reporting format for ultrasound-based lower extremity venous system assessment. On the other hand, there is also no consensus on a defined examination protocol. The American College of Radiology recommends performing the imaging examination from the thigh to the ankle and independently assessing venous insufficiency or thrombosis[9]. Another protocol describes only examining in the standing position[10]. This technical note proposes a standardized structured report of Doppler duplex US based on a complete protocol for the assessment of venous insufficiency and thrombosis of the lower extremity.

US DUPLEX DOPPLER ACQUISITION PROTOCOL

Lower extremity venous system assessment is performed with a complete US examination protocol using different modalities: grayscale, Doppler duplex, color Doppler, power Doppler, and, more recently, B-Flow. A vascular presetting is used in the abdomen and the lower extremity venous system. The approximate duration of the full protocol is approximately 60 minutes per extremity. The complete examination protocol was developed by a radiologist (MFS) with 30 years of experience in vascular imaging.

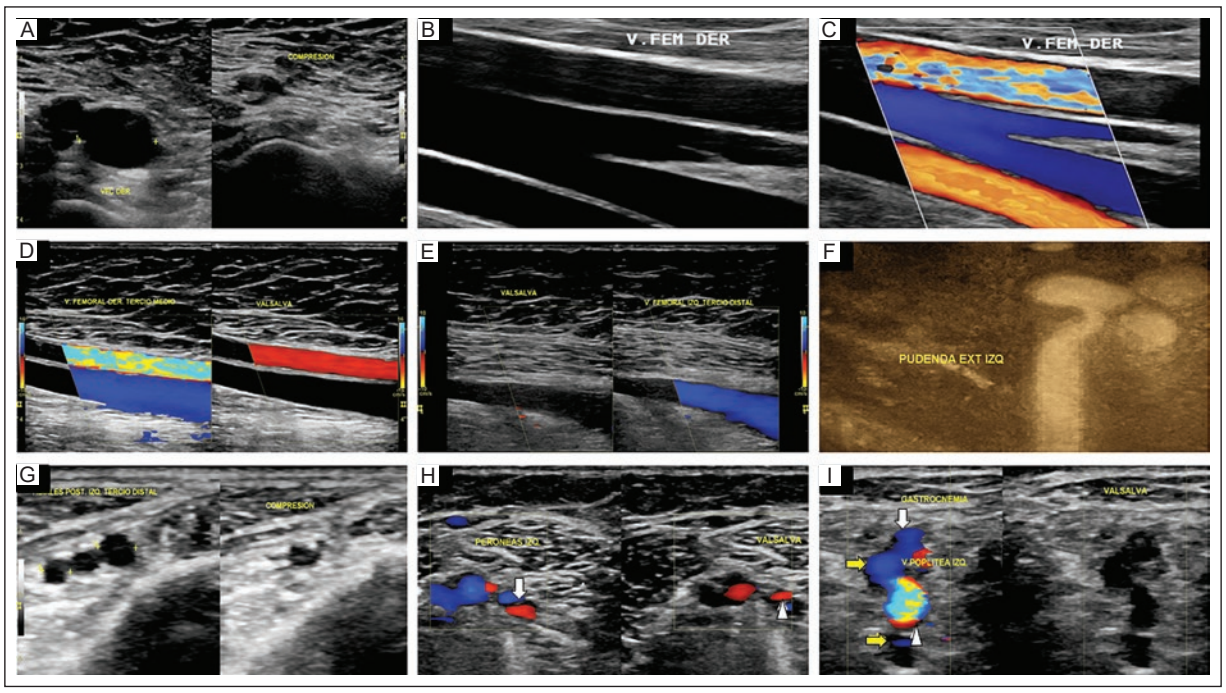

Figure 2. A: transverse view, grayscale US, the right common femoral vein is identified, with normal morphology and compressibility. **B-C:** sagittal view, the bifurcation of the common femoral vein is identified with grayscale and color Doppler US showing normal patency and flow direction. **D:** sagittal view, color Doppler US of the middle third of the right common femoral vein with normal patency and flow direction; there is no reflux during the Valsalva maneuver. **E:** sagittal view, color Doppler US of the left femoral vein in its distal third with no reflux with the Valsalva maneuver. **F:** transverse view, B-Flow US showing dilated external pudendal vein (8 mm, not shown) with retrograde flow. **G:** transverse view, grayscale US of the distal third of the left posterior tibial veins with diameters of 3.4 and 2.5 mm (not shown), normal with a complete compression maneuver. **H:** transverse view, color Doppler US of the left peroneal veins with a transverse echogenic band (arrow) in a peroneal vein, secondary to chronic thrombosis. Reflux is seen with the Valsalva maneuver (arrowhead). **I:** transverse view, color Doppler US showing the popliteal vein with a normal bifid segment (yellow arrows) and left gastrocnemius (white arrow). No reflux is observed during the Valsalva maneuver. A normal popliteal artery is seen (arrowhead).

US: ultrasound.

Respiratory variation and Valsalva maneuvers are used to evaluate the abdominal venous system with compression maneuvers in the transverse plane; augmentation, and Valsalva are performed in the reverse Trendelenburg position[4]. For insufficiency examination, the legs must be positioned below the level of the patient's head to maximize venous filling and optimize assessment of reflux[4].

The thigh and leg are examined in bipedestation when no reflux is demonstrated. All vessel diameters are recorded in the transverse plane and after the Valsalva maneuver.

Definitions

Venous reflux: retrograde flow associated with dilation during the Valsalva maneuver. A spectral inversion of > 1-second duration and a change from blue to red on color Doppler are demonstrated[11].

Incompetent perforating vein: dilatation > 3 mm with flow inversion with an abnormal direction from the deep to the superficial system.

Reverse Trendelenburg: the 45-to-60-degree tilt of the examination table in the caudal direction.

Color Doppler: the estimation and display of mean velocities relative to the direction of the ultrasound beam, interpreted as a color overlay on grayscale images.

Power Doppler: the display of scattering velocities relative to the direction of the interrogating ultrasound beam at positions throughout the image field, ignoring velocity and estimating only the strength. No direction is given.

Spectral Doppler: visual display of the audible velocity and directional shifts in blood flow.

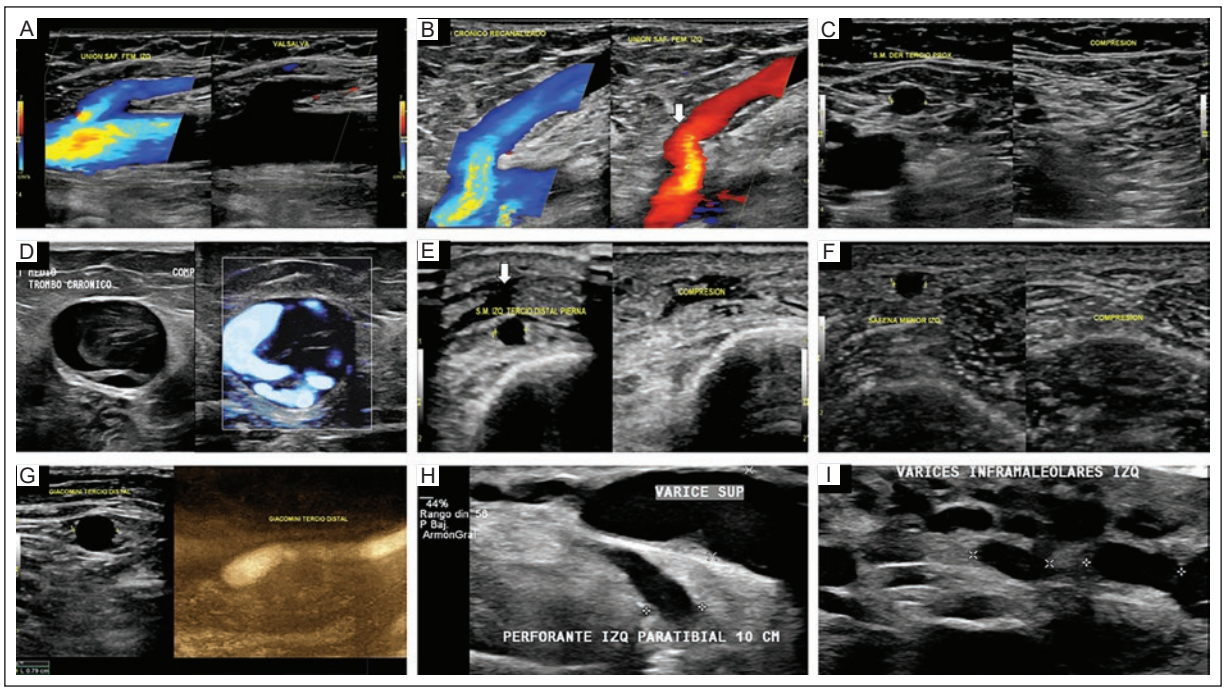

Figure 3. A: sagittal view, color Doppler US of the left saphenous-femoral junction, showing patency and flow direction. No reflux is observed with the Valsalva maneuver. **B:** sagittal view; color Doppler US of the left saphenous-femoral junction with patency and normal flow direction. Reflux is observed with the Valsalva maneuver (arrow). **C:** transverse view, grayscale US of the right great saphenous vein in the proximal third of the thigh with a diameter of 7.2 mm (not shown) and complete compressibility maneuver. **D:** transverse view, grayscale and color Doppler US of the left great saphenous vein in the middle third of the thigh with echogenic material corresponding to a chronic thrombus with partial recanalization <50%. **E:** transverse view, grayscale and color Doppler US of the left great saphenous vein in the distal third of the leg with a diameter of 4.3 mm (not shown) and complete compression maneuver. There is also mild edema of the subcutaneous tissue (arrow). **F:** transverse view, grayscale US of the left lesser saphenous vein with a diameter of 4 mm (not shown) in the middle third with complete compression maneuver. **G:** transverse view, US grayscale and sagittal view in B-Flow showing a variant of Giacomini's vein with a 7.9-mm (not shown) diameter and normal patency in B-Flow US. **H:** transverse view, grayscale US showing the left paratibial perforating vein with a diameter of 4.57 mm, located 10 cm from the inferior border of the lateral malleolus. It drains into a dilated superficial varicose vein (8.14 mm, not shown). **I:** transverse view, grayscale US of the left inframalleolar variceal bundle with 8- and 9-mm (not shown) diameters.

US: ultrasound.

B-Flow: blood flow with grayscale or B-mode US, digitally encoded wide band pulses transmitted and received to differentiate soft tissue from blood. No velocity or direction is given.

STANDARDIZED STRUCTURED REPORT FORMAT

The proposed standardized structured report format is shown in Table 1. In the case of a bilateral examination, the left lower extremity is recorded first. In the case of a unilateral examination, information on the corresponding extremity is recorded. The entire abdominal and pelvic region is always examined bilaterally, regardless of whether the lower extremity is examined unilaterally or bilaterally. The editable format of the standardized structured ultrasound report is available as a at DOI: 10.24875/JMEXFRI.M23000045.

Patient data and relevant clinical information are recorded in the report format. It is recommended that the clinician record the clinical, etiological, anatomical, and pathophysiological (CEAP) classification[6].

The assessment includes the heart, the ostium of the inferior vena cava (IVC), the suprahepatic, and entire course of the IVC, the left renal vein, the bifurcation and formation of the primitive, external, and hypogastric iliac veins; a bilateral examination is always performed in the pelvis (Figure 1). The diameter, permeability, velocity, and presence of thrombi or endothelial thickening are recorded in transverse and sagittal projections, excluding obstruction and/or extrinsic compression. The heart is examined in a transverse four-chamber plane with a subxiphoid approach because effective venous return from the lower extremities requires interaction with the heart[3]. Findings, such as thrombi, pericardial effusion, and myxomas.

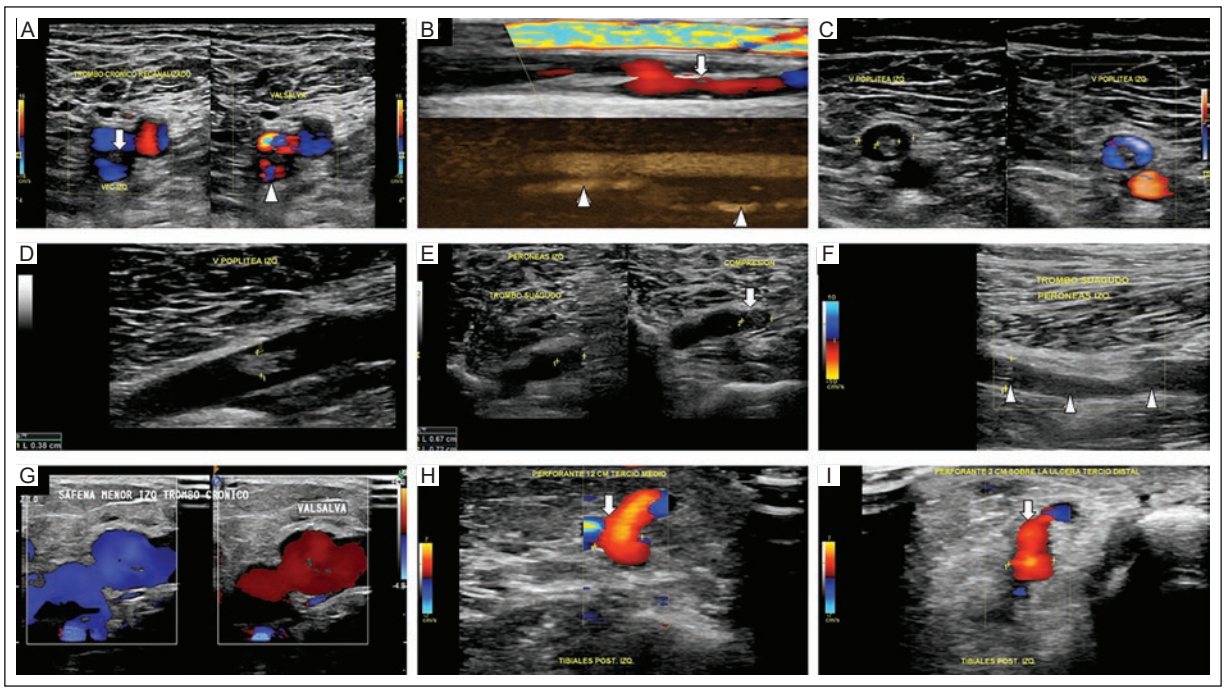

Figure 4. A: transverse view, color Doppler US of the left common femoral vein with central endoluminal echogenic material (arrow). Valsalva maneuver shows reflux secondary as a sequel of chronic thrombosis (arrowhead). **B:** sagittal view (upper image) color Doppler US of the left femoral vein in the middle third with thick endoluminal echogenic bands, central, fixed to the inferior wall due to chronic thrombosis with valvular damage and reflux (arrow). B-Flow (lower image) showing recanalization of the femoral vein (arrowheads) **C:** transverse view, grayscale US, and **D:** sagittal view, color Doppler US of the left popliteal vein with fixed central echogenic material secondary to a chronic recanalized thrombus. **E:** transverse view, grayscale US, and **F:** sagittal view, color Doppler US of the left peroneal veins with hyperechogenic, heterogeneous material in one of the noncompressible peroneal veins (arrow). Absence of flow in relation to a subacute thrombus with complete obstruction (arrowheads). **G:** transverse view, color Doppler US shows left lesser saphenous vein dilated with a 10-mm diameter (not shown). Reflux is observed with the Valsalva maneuver. **H:** transverse view, color Doppler US showing a dilated and incompetent perforator with a diameter of 6.1 mm (not shown) located 12 cm from the inferior border of the medial malleolus. **I:** transverse view, color Doppler US showing a dilated and incompetent perforating vein with a 5.8 mm (not shown) diameter, located 2 cm from the inferior border of the medial malleolus.

US: ultrasound.

The examination continues along the entire deep (Figure 2) and superficial venous systems (Figure 3). Assessment of the deep, superficial, perforating, and reticular venous systems in the thigh continues with assessment of the diameter, compressibility, permeability, competence, velocity, and presence of thrombi or endothelial thickening (Figure 3). The maximum diameter of the vessels is described in the transverse plane and after the Valsalva maneuver. Perforating veins in the thigh are designated as anteromedial, anterolateral, or posterolateral depending on their location, as is their distance in centimeters from an anatomic reference point such as the popliteal fossa. The popliteal fossa is examined with the knee flexed and in the sitting or prone position. In the leg, the location of the perforating system is described in the same way, and the distance to the medial and lateral malleolus in the ankle is determined.

Because of the complex anatomic variations of the lower venous system, it is important to know the most common variations to not confuse benign findings with pathologic changes.

Additional pathologic findings of the heart, abdomen, pelvis, and superficial and deep venous systems of the lower extremities, such as varicose veins, their location, diameter, communication with perforating veins, and thrombosis, are specifically described. In the case of abnormal perforating veins, their location and diameter are assessed. Some examples are shown in Figure 4.

The pathological findings of the abdominal region, the presence or absence of insufficiency and/or thrombosis of the deep and/or superficial venous system, and a brief description of other pathological findings are recorded as conclusions at the end of the standardized structured report format.

STANDARDIZED STRUCTURED ULTRASOUND REPORT FOR LOWER EXTREMITY VENOUS INSUFFICIENCY OR THROMBOSIS[a]

Table 1. Ultrasound examination of the venous system of the lower extremities is performed in the supine, reverse Trendelenburg, and upright positions. The following ultrasound modes are used: real time mode B, Doppler duplex, color, and power Doppler in the transverse and longitudinal planes. The following maneuvers are performed: 1. Compression in the transverse plane, 2. Valsalva maneuver, 3. Respiratory variation, and 4. Augmentation. [a]The editable format of the standardized structured report is available as a digital appendix at www.jmexfri.com.

Patient name: _____ Sex: _____ Age: _____ Date: _____

Clinical Data (CEAP)[12]:

0	1	2	3	4	5	6

Clinical diagnosis: _____

Previous procedures and examinations of the lower extremities: _____

ABDOMEN AND PELVIS

Vein	Diameter (mm)	Compressibility[a] (Yes/No)	Permeability (Yes/No)	Competence[b] (Yes/No)	Velocity (cm/sec)	Thrombosis or Endothelial thickening (Yes/No)
Inferior vena cava[c]						
Right primitive iliac						
Left primitive iliac						
Right external iliac						
Left external iliac						

[a] Since the inferior vena cava and the primitive iliac veins are deep in the abdomen, compressibility is not evaluated.
[b]Since the inferior vena cava and the primitive and external iliac veins lack valves, competence is not evaluated.
[c]The evaluation of the heart is done in a transverse 4-chamber plane and only pathological findings (thrombus, pericardial effusion, myxoma, etc.) are recorded in the additional findings section.

DEEP VENOUS SYSTEM OF THE LEFT LOWER EXTREMITY

Vein	Diameter (mm)	Compressibility (Yes/No)	Permeability (Yes/No)	Competence[a] (Yes/No)	Velocity (cm/sec)	Thrombosis or endothelial thickening (Yes/No)
Common femoral						
Deep femoral						
Proximal third femoral						
Middle third femoral						
Distal third femoral						
Popliteal[b]						
Anterior tibialis						
Posterior tibialis						
Peroneals						
Main gastrocnemic						

[a]If "yes," record the total time of reflux in seconds followed by "/" and the maximum velocity of reflux in cm/sec (example, 5 sec/20 cm/sec) [b]The popliteal vein is assessed with the patient in the prone position at the end. The patient is asked to lift the foot and rest on the toes.

SUPERFICIAL VENOUS SYSTEM OF THE LEFT LOWER EXTREMITY

Vein	Diameter (mm)	Compressibility (Yes/No)	Permeability (Yes/No)	Competence[a] (Yes/No)	Velocity (cm/sec)	Thrombosis or endothelial thickening (Yes/No)
Femoral-saphenous junction						
Greater saphenous vein						
Segment 1						
Segment 2						
Segment 3						
Segment 4						
Segment 5						
Segment 6						
Lesser saphenous vein						
[a]If "yes," record the total time of reflux in seconds followed by "/" and the maximum velocity of reflux in cm/sec (example, 5 sec/20 cm/sec).						

ADDITIONAL PATHOLOGICAL FINDINGS OF THE LEFT LOWER EXTREMITY

VARICOSE PLEXUS: indicate the presence or lack of varicose plexuses. If they exist, describe their location and if patent or thrombosed.

PERFORATING VEINS: indicate the existence or lack of incompetent perforators. Describe their maximum diameter in mm and location on the limb.

DEEP VENOUS SYSTEM OF THE RIGHT LOWER EXTREMITY

Vein	Diameter (mm)	Compressibility (Yes/No)	Permeability (Yes/No)	Competence[a] (Yes/No)	Velocity (cm/sec)	Thrombosis or endothelial thickening (Yes/No)
Common femoral						
Deep femoral						
Proximal third femoral						
Middle third femoral						
Distal third femoral						
Popliteal						
Anterior tibialis						
Posterior tibialis						
Peroneals						
Main gastrocnemic						
[a]If "yes," record the total time of reflux in seconds followed by "/" and the maximum velocity of said reflux in cm/sec (example, 5 sec/20 cm/sec).						

SUPERFICIAL VENOUS SYSTEM OF THE RIGHT LOWER EXTREMITY

Vein	Diameter (mm)	Compressibility (Yes/No)	Permeability (Yes/No)	Competence[a] (Yes/No)	Velocity (cm/sec)	Thrombosis or endothelial thickening (Yes/No)
Femoral-saphenous junction						
Greater saphenous vein						
Segment 1						
Segment 2						
Segment 3						
Segment 4						
Segment 5						
Segment 6						
Lesser saphenous vein						

[a]If "yes," record the total time of reflux in seconds followed by "/" and the maximum velocity of said reflux in cm/sec (example, 5 sec/20 cm/sec).

ADDITIONAL PATHOLOGICAL FINDINGS OF THE RIGHT LOWER EXTREMITY

VARICOSE PLEXUS: : indicate the presence or lack of varicose plexuses. If they exist, describe their location and if patent or thrombosed.

PERFORATING VEINS: indicate the existence or lack of incompetent perforators. Describe their maximum diameter in mm and location on the limb.

CONCLUSIONS:

- Abdominal pathological findings (no, or if yes, describe):
- Left lower extremity
  1. Deep venous system: competent or incompetent (describe pathological segments).
  2. Superficial venous system: competent or incompetent (describe pathological segments).
  3. Additional pathological findings: varicose plexus, incompetent perforating veins, thrombus, surgical changes, etc.
- Right lower extremity
  4. Deep venous system: competent or incompetent (describe pathological segments).
  5. Superficial venous system: competent or incompetent (describe pathological segments).
  6. Additional pathological findings: varicose plexus, incompetent perforating veins, thrombus, surgical changes, etc.

CONCLUSION

In this technical note, we propose for the first time a structured standardized reporting format for ultrasonographic examination of venous insufficiency and thrombosis of the lower extremities based on a complete protocol with different US modalities. A thorough knowledge of the anatomy and hemodynamics of the lower extremity venous system is essential for optimal examination. The described protocol allows obtaining a complete vascular map with morphologic and hemodynamic information about the sites of retrograde flow and venous leakage, enabling the referring clinician and surgeon to determine therapy based on the standardized structured report findings with precise and reproducible language for multicenter studies and research purposes. The standardized structured report format is intended for educational purposes to assist the radiologists and residents in performing a systematic, complete, and reproducible examination of the venous system of the lower extremities to achieve clear, accurate, and complete communication with the referring clinician and patients.

Supplementary data

Supplementary data are available online in the Journal of the Mexican Federation of Radiology and Imaging online (DOI: 10.24875/JMEXFRI.M23000045). These data are provided by the corresponding author and published online for the reader's benefit. The contents of supplementary data are the sole responsibility of the authors.

Acknowledgments

The authors thank Professor Ana M. Contreras-Navarro for her guidance in writing this scientific paper.

Funding

The authors declare that they received no funding or support for this article.

Conflicts of interest

The authors declare no conflicts of interest.

Ethical disclosures

Protection of Individuals: This study complied with the Declaration of Helsinki (1964) and subsequent amendments.

Confidentiality of Data. The authors followed their center's protocol for sharing patient data.

Right to privacy and informed consent. The authors declare no ethical responsibilities since humans' confidential information was not used.

REFERENCES

1. Eberhardt RT, Raffetto JD. Chronic Venous Insufficiency. Circulation. 2005;111(18):2398-2409. doi: 10.1161/01.CIR.0000164199.72440.08.
2. Sumpio BJ, Png CYM, Harrington A, Root D, McLaughlin R, Manchester S, et al. Utility of unilateral versus bilateral venous reflux studies for venous insufficiency. J Vasc Surg Venous Lymphat Disord. 2021;9(5):1297-1301. doi: 10.1016/j.jvsv.2021.01.004.
3. Meissner MH, Moneta G, Burnand K, Gloviczki P, Lohr JM, Lurie F, et al. The hemodynamics and diagnosis of venous disease. J Vasc Surg. 2007;46 Suppl S:4S-24S. doi: 10.1016/j.jvs.2007.09.043.
4. Adler C, Mousa A, Rhee A, Patel MD. Varicose Veins of the Lower Extremity: Doppler US Evaluation Protocols, Patterns, and Pitfalls. RadioGraphics. 2022;42(7):2184-2000. doi: 0.1148/rg.220057.
5. Larson DB, Towbin AJ, Pryor RM, Donnelly LF. Improving consistency in radiology reporting through the use of department-wide standardized structured reporting. Radiology. 2013;267(1):240-250. doi: 10.1148/radiol.12121502.
6. Martí-Bonmati L. The importance of a structured radiological report. J Mex Fed Radiol Imaging. 2023; 2(1):1-3. doi:10.24875/JMEXFRI.M23000036.
7. Garcia-Moreno C, Ricardo Jimenez-De La O R, Herrera-Sanchez A. Mexican radiologists' and referring clinicians' preference for a standardized structured radiology report: qualities and content. J Mex Fed Radiol Imaging. 2022;1(1):13-22. doi.10.24875/JMEXFRI.M21000001.
8. Figueroa-Sanchez M, Garcia-Colmenero ML, Sanchez-Rueda MA. Ultrasound diagnostic criteria and grades of pelvic congestion syndrome and asymptomatic pelvic venous congestion: a structured report. J Mex Fed Radiol Imaging. 2022;1(4):222-235. doi: 10.24875/JMEXFRI.M22000035.
9. AIUM Practice Parameter for the Performance of a Peripheral Venous Ultrasound Examination. J Ultrasound Med. 2020;39(5): E49-E54. doi: 10.1002/jum.15263.
10. Coleridge-Smith P, Labropoulos N, Partsch H, Myers K, Nicolaides A, Cavezzi A. Duplex Ultrasound Investigation of the Veins in Chronic Venous Disease of the Lower Limbs-UIP Consensus Document. Part I. Basic Principles. Eur J Vasc Endovasc Surg. 2006;31(1):83-92. doi: 10.1016/j.ejvs.2005.07.019.
11. Evans CJ, Allan PL, Lee AJ, Bradbury AW, Ruckley CV, Fowkes FG. Prevalence of venous reflux in the general population on duplex scanning: the Edinburgh vein study. J Vasc Surg. 1998;28(5):767-776. doi: 10.1016/s0741-5214(98)70051-5.
12. Lurie F, Passman M, Meisner MH, Dalsing M, Masuda E, Welch H, et al. The 2020 update of the CEAP classification system and reporting standards. J Vasc Surg Venous Lymphat Disord. 2020;8(3):342-352. doi: 10.1016/j.jvsv.2019.12.075. Erratum in: J Vasc Surg Venous Lymphat Disord. 2021;9(1):288.

JMeXFRI

Journal of the Mexican Federation of Radiology and Imaging

Check for updates

CASE REPORT

Metaplastic breast cancer mimicking a benign finding on mammography: a case report and literature review

Karen A. Rojas-Galeana[1,a], Benjamin Conde-Castro[2], Juan I. Morales-Ramirez[3], Cecilia Ortiz-De Iturbide[4] and Yhovanna Y. Gonzalez del Toro[5]*

[1]Department of Radiology and Imaging, Hospital Juarez de Mexico, Mexico City; [2]Imaging Research Department, Salud Digna, Mexico City; [3]Department of Radiology and Imaging, Hospital "Lic. Adolfo López Mateos", Toluca, State of Mexico; [4]Department of Breast Imaging and Intervention, Hospital Ángeles del Pedregal, Mexico City; [5]Department of Pathological Anatomy, Hospital Centro Médico Nacional "20 de Noviembre", Mexico City. Mexico

ORCID: [a]0000-0002-6085-1697

ABSTRACT

Metaplastic breast carcinoma (MBC) may present nonspecific imaging findings that mimic benignity. This case report describes a 77-year-old woman with MBC who initially presented with dystrophic calcification on mammography. A screening mammogram and US examination performed in 2020 showed dystrophic calcification in the left breast, BI-RADS 2. In 2021, screening mammography and US showed the previously detected dystrophic calcification with an increase in size compared to previous examinations, BI-RADS Category 2. Eight months later, she had a rapidly growing mass in the left breast. Mammography and US examination showed a mass abutting into the dystrophic calcification with suspected malignancy, BI-RADS 4B. An excisional biopsy was histopathologically diagnosed as MBC with malignant bone formation and chondroid components. Neoplastic cells were positive for P53 and CK AE1/AE3. Estrogen, progesterone, and HER2/neu receptors were negative. This case report is the first in the literature on MBC initially presenting as dystrophic calcification mimicking benignity. It is published for educational purposes to show mammographic and US findings.

Keywords: *Dystrophic calcification. BI-RADS. Metaplastic breast carcinoma. Mammography. Ultrasound.*

INTRODUCTION

Metaplastic breast carcinoma (MBC) is a heterogeneous group of neoplasms that share metaplastic changes of non-glandular components of the breast tissue[1]. According to the World Health Organization classification of tumors of the breast,[2] MBC is classified into four histopathological types: adenosquamous, fibromatosis-like, squamous and spindle cell, and mesenchymal metaplastic carcinoma with chondroid and bone metaplasia.

MBC is a rare breast neoplasia[3]. Its different histopathological types are associated with variable and nonspecific imaging findings on mammography and ultrasound (US)[1,4]. Calcifications in MBC are observed in the osteoclastic type[1,2]. Malignant calcifications are usually pleomorphic, clustered, linear or segmental. This report describes a woman with MBC with dystrophic calcification on mammography and US.

CASE DESCRIPTION

The patient is a 77-year-old woman of Japanese origin with a history of a sister diagnosed with infiltrating ductal breast carcinoma. The patient was referred for annual mammography and US screening. In 2020, she

***Corresponding author:**
Karen A. Rojas-Galeana
E-mail: kandrearg37956@gmail.com

Received for publication: 03-03-2023
Accepted for publication: 21-03-2023
DOI: 10.24875/JMEXFRI.M23000046

Available online: 13-07-2023
J Mex Fed Radiol Imaging. 2023;2(2):142-146
www.JMeXFRI.com

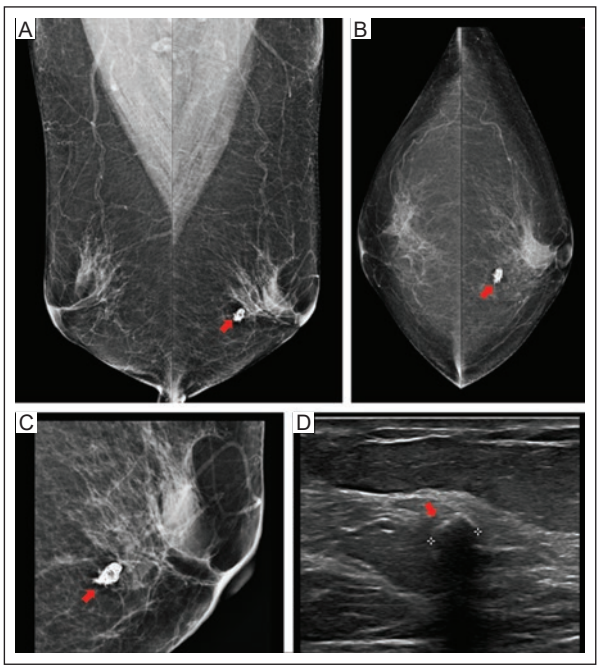

Figure 1. A 77-year-old asymptomatic woman with a screening examination. **A-B:** mammography in MLO and CC views showing dystrophic calcification (arrow) in the lower-inner quadrant of the middle third of the left breast. **C:** magnification cone of the left breast that delineates the dystrophic calcification. Suspicious findings of malignancy were ruled out. **D:** US at 7 o'clock of the left breast, 5-mm dystrophic calcification with an acoustic shadow is observed; BI-RADS Category 2.

BI-RADS: Breast Imaging Reporting and Data System; MLO: medial-lateral oblique; CC: craniocaudal; US: ultrasound.

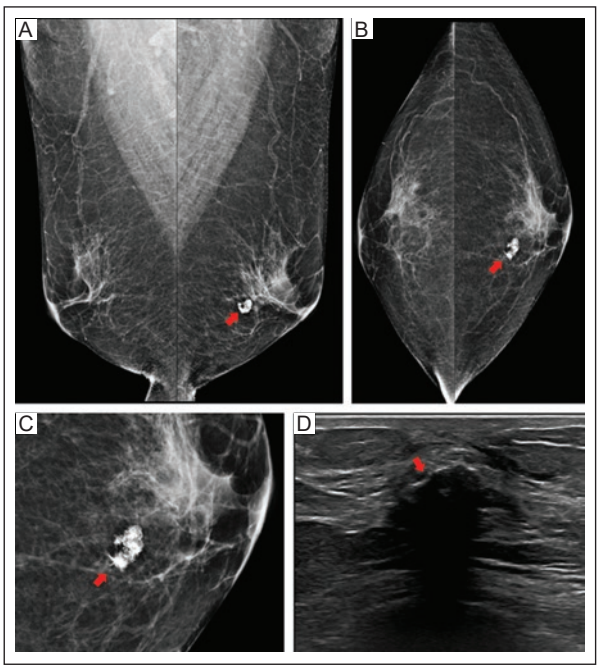

Figure 2. A 77-year-old asymptomatic woman with a screening examination one year later. **A-B:** mammography in MLO and CC views showing dystrophic calcification (arrow) in the lower quadrant of the middle third of the left breast with an increase in size compared with previous screening examinations. **C:** magnification of the dystrophic calcification, with no finding suspicious for malignancy. **D:** US examination at 7 o'clock of the left breast, focusing on the dystrophic calcification, unchanged from the previous examination; BI-RADS Category 2.

BI-RADS: Breast Imaging Reporting and Data System; MLO: medial-lateral oblique; CC: craniocaudal; US: ultrasound.

was asymptomatic. Her mammography showed dystrophic calcification in the lower inner quadrant of the middle third of the left breast (Figure 1). US showed a 5-mm calcification with acoustic shadowing, BI-RADS Category 2. In 2021, she came for a breast examination. She was asymptomatic. Screening mammography and US showed the previously detected dystrophic calcification with an increase in size compared to previous examinations, BI-RADS Category 2 (Figure 2). Eight months later, she had a palpable, painful, rapidly growing mass in the left breast. Mammography of the left breast showed an irregular, indistinct, hyperdense mass abutting the dystrophic calcification detected on previous examinations (Figure 3). US showed a calcified, irregular mass with complex echogenicity and combined pattern, BI-RADS Category 4B.

An excisional biopsy was performed. Histopathologic findings were MBC with chondroid and metaplastic bone consisting mostly of osteoid with focal mineralization (Figure 4). P53 and CK AE1/AE3 were positive in the neoplastic cells. Estrogen, progesterone, and human epithelial growth factor receptor 2 (HER2/neu) receptors were negative. The patient had no metastases and underwent a left mastectomy with a good postoperative outcome.

DISCUSSION

This case report describes a 77-year-old woman diagnosed with MBC who initially had dystrophic calcification that mimicked benignity on mammography. This report is the first of a bone-forming MBC with malignant dystrophic calcification and is published for educational purposes to show the findings on mammography and US.

There are no specific imaging findings for MBC, and it may simulate benign lesions[1]. Table 1 shows several reports in the literature describing MBC imaging findings on mammography, US, and magnetic resonance imaging (MRI)[1-3,5]. MBC is often a large, firm, rapidly growing mass. On mammography, it may present an irregular, oval mass circumscribed or not with or without calcifications[1-3,5]. On US images, it is a variable-shaped (round, oval, lobulated) circumscribed and hypoechoic

Table 1. Literature review of MBC and current case

Author	Country	n	Age, years	Clinical presentation	Mammography	Ultrasound	Magnetic resonance imaging	Immuno histochemistry
Toumi[4]	Japan	1	78	2 cm firm, palpable mass	Circumscribed mass	Round, circumscribed, hypervascularized mass.	N/A	ER positive PR negative HER2/neu negative
Kim[3]	Korea	5	51.6 (46-55)	Palpable mass (80% of cases)	Circumscribed, dense, noncalcified mass	Complex, lobulated mass	T1: rounded, circumscribed, hypointense mass T2: hyperintense mass Gd: heterogeneous peripheral enhancement Type II curve	ER negative PR negative HER2/neu positive or negative
Donato[1]	Portugal	11	65 (30-86)	Palpable mass (45%) Screening (36%) Distant metastases (18%)	Dense oval mass (56%) Uncircumscribed margins (67%) Calcifications (pleomorphic and coarse heterogeneous) (44%) Skin thickening and retraction (11%) Asymmetry 22%	Oval mass (64%) Circumscribed (55%) Non-circumscribed (45%) Parallel (45%) Non-parallel (18%) Complex echogenicity (82%) Hypoechoic (18%) Acoustic reinforcement (55%)	T1: hypointense and heterogeneous mass. T2: hyperintense mass Gd: heterogeneous reinforcement Type I curve Type III curve peripheral enhancement	ER negative PR negative HER2/neu negative or positive
Jia[2]	China	19	55 (28-75)	Palpable 1-6 cm (mean 3 cm) mass	Oval mass (54.5%) Indistinct margin (45.5%) Hyperdense (72.7%)	Oval mass (57%) Hypoechoic areas (85%)	T2: Heterogeneous mass with central hyperintensity (100%). indistinct margin (75%) Gd: peripheral enhancement (58.3%). Type III curve (91.7%) DWI: restriction of diffusion	ER negative PR negative HER2/neu negative
Kimura[5]	Japan	1	70	Fast-growing, palpable mass	Irregular, microlobulated, hyperdense mass	Heterogeneous lobulated mass with mixed posterior pattern.	T2: irregular, heterogeneous mass	N/A
Current case	Mexico	1	77	Palpable, painful, rapidly growing mass	Irregular[a] indistinct, hyperdense mass with dystrophic calcification	Irregular mass[a] with calcification and combined pattern[a].	N/A	ER negative PR negative HER2/neu negative

MBC: metaplastic breast carcinoma; n: number of subjects; ER: estrogen receptor; PR: progesterone receptor; HER2/neu: human epithelial growth factor receptor 2; NA: not available. [a]Mammography and US findings when excisional biopsy was performed.

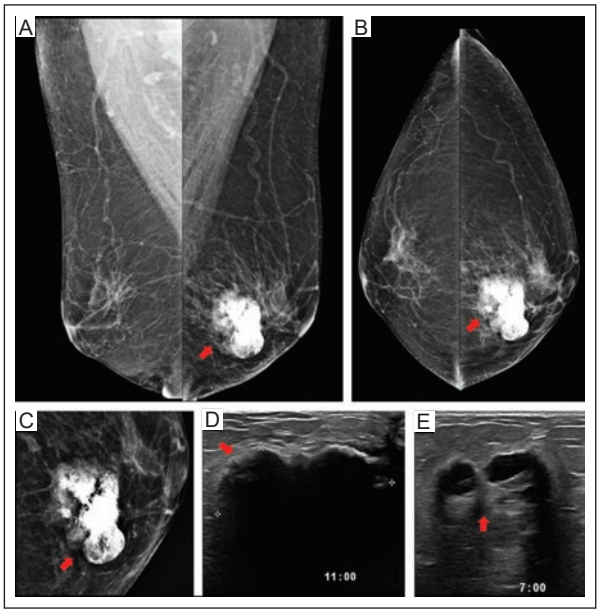

Figure 3. A 77-year-old woman with a rapidly growing painful mass in her left breast. **A-B:** mammography in MLO and CC projection shows an irregular, indistinct, and hyperdense mass (arrow) in the lower inner quadrant of the middle third of the left breast associated with the dystrophic calcification noted in previous examinations. **C:** magnification cone of the left breast shows enlarged dystrophic calcification associated with an irregular, microlobulated, and hyperdense mass in the lower-inner quadrant. **D:** US shows an enlargement of the calcification in the left breast. **E:** US focused on the 7 o´clock of the left breast with an irregular, microlobulated mass parallel to the coronal plane, with complex echogenicity and combined pattern (arrow); BI-RADS Category 4B.

BI-RADS: Breast Imaging Reporting and Data System; MLO: medial-lateral oblique; CC: craniocaudal; US: ultrasound.

mass that is less commonly heterogeneous, with non-circumscribed margins or complex echogenicity and acoustic shadow or enhancement[1-3,5]. Donato et al.[1] reported two MBC cases with pleomorphic and heterogeneous thick calcifications consistent with a histopathological image of bone matrix forming. In contrast, the calcifications in our case were dystrophic and developed insidiously with a malignant rapidly-growing mass. Calcifications in the breast are the most common abnormal radiographic findings detected on screening mammography[6]. Mammographic calcifications may be the only radiographic manifestation of breast cancer[7]. Therefore, one must be aware of the appearance of these calcifications, and if there are unusual changes or additional findings, a histopathological examination is warranted to detect malignancy.

MBC usually behaves as a highly malignant neoplasm with a large mass[8]. Diagnosis of the specific MBC type is based on co-expression of mesenchymal and epithelial cell markers[1]. It is often negative for hormone receptors, limiting therapeutic targets[8]. The two cases with pleomorphic and coarse heterogeneous calcification reported in the literature had a diagnosis of MBC and were bone-forming[1]. On the other hand, only one case with a solid tumor and pleomorphic calcification diagnosed as a bone matrix-producing MBC was documented by Ebrahim[6]. A case of a woman with a high-grade carcinoma *in situ* associated with a benign dystrophic calcification into in a small oil cyst surrounded by neoplasia was also reported[6]. In contrast, the dystrophic calcification in our case corresponded to malignant calcification, and its association with a benign lesion by histopathology was ruled out. The diagnosis of calcified MBC was confirmed in relation to a carcinoma producing a bone matrix. In this case, the histopathologic diagnosis was MBC with heterologous chondroid and bone components.

Dystrophic calcifications are associated with benign processes such as fat necrosis, a history of trauma and surgery, irradiated breasts, or dystrophic subcutaneous dermatomyositis. Benign calcifications may coexist in breast tissue, abutting or incorporated into the malignant tumor as it grows[6]. The differential imaging diagnosis of malignant dystrophic breast calcification includes infiltrating ductal carcinoma[6], low-grade ductal carcinoma in situ, and bone-producing tumors, such as bone metaplasia in a phyllodes tumor, primary breast sarcoma, mixed mammary fibromatosis,[6] and osteosarcoma. In our case report, malignant dystrophic calcification was the initial presentation of MBC bone formation.

CONCLUSION

In this case report, we present the radiological and histopathological correlation with a confirmed diagnosis of malignant calcification due to a bone matrix-forming MBC. A limitation is that MRI was not performed as a complementary examination. The radiologist should be familiar with malignant calcifications associated with various forms of breast cancer, as there are rare variants, such as MBC, with nonspecific imaging findings that may mimic benignity.

Acknowledgments

The authors thank Professor Ana M. Contreras-Navarro for her noble and invaluable work as our mentor in writing scientific research papers and stimulating and promoting radiology research in our country. Special thanks to Dr. Cecilia Gallegos Garza, Head of the Department of Pathology at Hospital Ángeles del Pedregal.

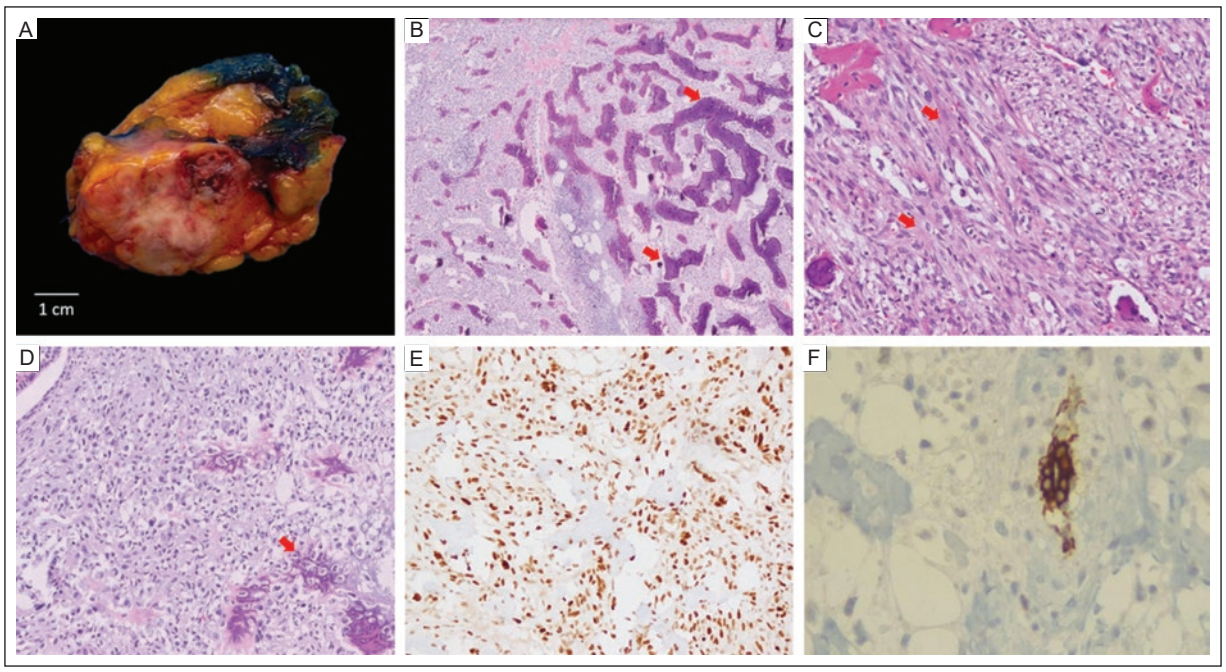

Figure 4. A: left breast tumor with heterogeneous appearance. **B:** areas of mature bone tissue (arrowheads) are seen, H&E (20x). **C:** fusiform areas with a storiform pattern of long fascicles (arrowheads), H&E (40x). **D:** a mature chondroid element (arrowhead), H&E (40x). **E:** immunoreactive P53 in neoplastic cells, H&E (40x). **F:** immunoreactive CK AE1/AE3 in neoplastic cells, H&E (40x). The histopathological diagnosis was MBC with bone and chondroid components.

H&E: hematoxylin and eosin; MBC: metaplastic breast carcinoma; x: microscopy magnification number.

Funding

This research received no external funding.

Conflicts of interest

The authors declare that they have no conflicts of interest.

Ethical disclosures

Protection of human and animal subjects. The authors declare that the procedures of this case report were conducted in compliance with the Declaration of Helsinki (1964) and its subsequent amendments.

Confidentiality of data. The authors declare that they followed the protocols of their work center on the publication of patient data.

Right to privacy and informed consent. Informed consent was not required for this case report of information collected during routine clinical care.

REFERENCES

1. Donato H, Candelária I, Oliveira P, Gonçalo M, Caseiro-Alves F. Imaging Findings of Metaplastic Carcinoma of the Breast with Pathologic Correlation. J Belg Soc Radiol. 2018;102(1):46. doi:10.5334/jbsr.1386.
2. Jia Y, He C, Liu L, Sun L, Chen Y, Luo Y, et al. A Retrospective Study of the Imaging and Pathological Features of Metaplastic Breast Carcinoma and Review of the Literature. Med Sci Monit. 2019; 25:248. doi: 10.12659/MSM.912107.
3. Kim HJ, Kim SY, Huh S. Multimodality Imaging Findings of Metaplastic Breast Carcinomas A Report of Five Cases. Ultrasound Q. 2018;34(2):88–93. doi:10.1097/ruq.0000000000000340.
4. Toumi Z, Bullen C, Tang ACS, Dalal N, Ellenbogen S. Metaplastic breast carcinoma: A case report and systematic review of the literature. Pathol Int. 2011;61(10):582-588. doi:10.1111/j.1440-1827.2011.02698.
5. Kimura F, Kawamoto A, Sato E, Orimoto K, Miyahara K, Kawate T, et al. A case of metaplastic breast carcinoma with cartilaginous differentiation: comparison with the histology and tissue characterizations of an ultrasound image. J Med Ultrason. 2022;49(2):313–314. doi:10.1007/s10396-021-01182-3.
6. Ebrahim L, Dissanayake D, Metcalf C, Wylie E. Screen-detected breast carcinoma with macroscopic dystrophic calcification: A pictorial essay with radiologic pathologic correlation. J Med Imaging Radiat Oncol. 2016;60(2):216-223. doi:10.1111/1754-9485.12426.
7. Choi BB, Shu KS. Metaplastic carcinoma of the breast: multimodality imaging and histopathologic assessment. Acta Radiol. 2012;53(1):5–11. doi:10.1258/ar.2011.110341.
8. Altaf FJ, Mokhtar GA, Emam E, Bokhary RY, Mahfouz NB, Al Amoudi S, et al. Metaplastic carcinoma of the breast: an immunohistochemical study. Diagn Pathol Open Access. 2014;9(1):139. doi:10.1186/1746-1596-9-139.
9. D'Orsi C, Sickles EA, Mendelson EB, Morris EA. Breast Imaging Reporting and Data System: ACR BI-RADS breast imaging atlas. 5th Edition. Reston, VA, USA American College of Radiology, 2013.

JMeXFRI

Journal of the Mexican Federation of Radiology and Imaging

Check for updates

IMAGES IN RADIOLOGY

MR imaging of primary muscular hydatid cysts

Carmen Popa[1,a], Andrei Moisin[2,3], Ciprian Tanasescu[2,3]*

[1]Department of Radiology, Sibiu County Emergency Clinical Hospital; [2]Department of Surgery, Sibiu County Emergency University Clinical Hospital; [3]Department of Surgery, Faculty of Medicine, 'Lucian Blaga' University. Sibiu, Romania

ORCID: [a]0000-0002-7053-5633

We examined a 44-year-old patient who presented to us with a deformity of the right thigh. A magnetic resonance (MR) imaging of the lower extremity was performed, which showed a multicystic lesion involving the right adductor magnus muscle, with a hypointense T1 signal, moderate signal intensity in PD (proton density sequence), hyperintense in T2 and STIR (Figure 1) with a size of 64.1 × 75.7 × 130 mm (antero-posterior/lateral/longitudinal diameter) and a compressive effect on the vascular bundle. The imaging findings correlated with biological analysis and confirmed the diagnosis of a primary muscular hydatid cyst.

Hydatid cyst is a parasitic disease caused by *Echinococcus granulosus,* and is endemic to the Mediterranean region, Africa, and Asia[1]. Muscular hydatidosis is rare and accounts for approximately 3-5% of all hydatidosis cases, likely due to the fact that the cyst requires oxygen for growth, while muscle typically contains lactic acid[2]. The most typical treatment for a simple muscular hydatid cyst is surgical removal. Drug treatment with albendazole is an alternative for inoperable cases[1,2].

Funding

This paper received no external funding.

Conflicts of interest

The authors declare that they have no conflicts of interest.

Ethical disclosures

Protection of Individuals: This study was conducted in compliance with the Declaration of Helsinki (1964) and its subsequent amendments.

Data Confidentiality. The authors declare they followed their center's protocol for sharing patient data.

Right to privacy and informed consent. Informed consent was not required to analyze and publish routinely acquired clinical and imaging data.

REFERENCES

1. Tekin R, Avci A, Tekin RC, Gem M, Cevik R. Hydatid cysts in muscles: clinical manifestations, diagnosis, and management of this atypical presentation. Rev Soc Bras Med Trop. 2015;48(5):594–598. doi: 10.1590/0037-8682-0197-2015.
2. Gougoulias NE, Varitimidis SE, Bargiotas KA, Dovas TN, Karydakis G, Dailiana ZH. Skeletal muscle hydatid cysts presenting as soft tissue masses. Hippokratia. 2010;14(2):126–130.

***Corresponding author:**
Carmen popa
E-mail: carmen.popa3694@gmail.com

Received for publication: 04-02-2023
Accepted for publication: 12-05-2023
DOI: 10.24875/JMEXFRI.23000004

Available online: 13-07-2023
J Mex Fed Radiol Imaging. 2023;2(2):147-148
www.JMeXFRI.com

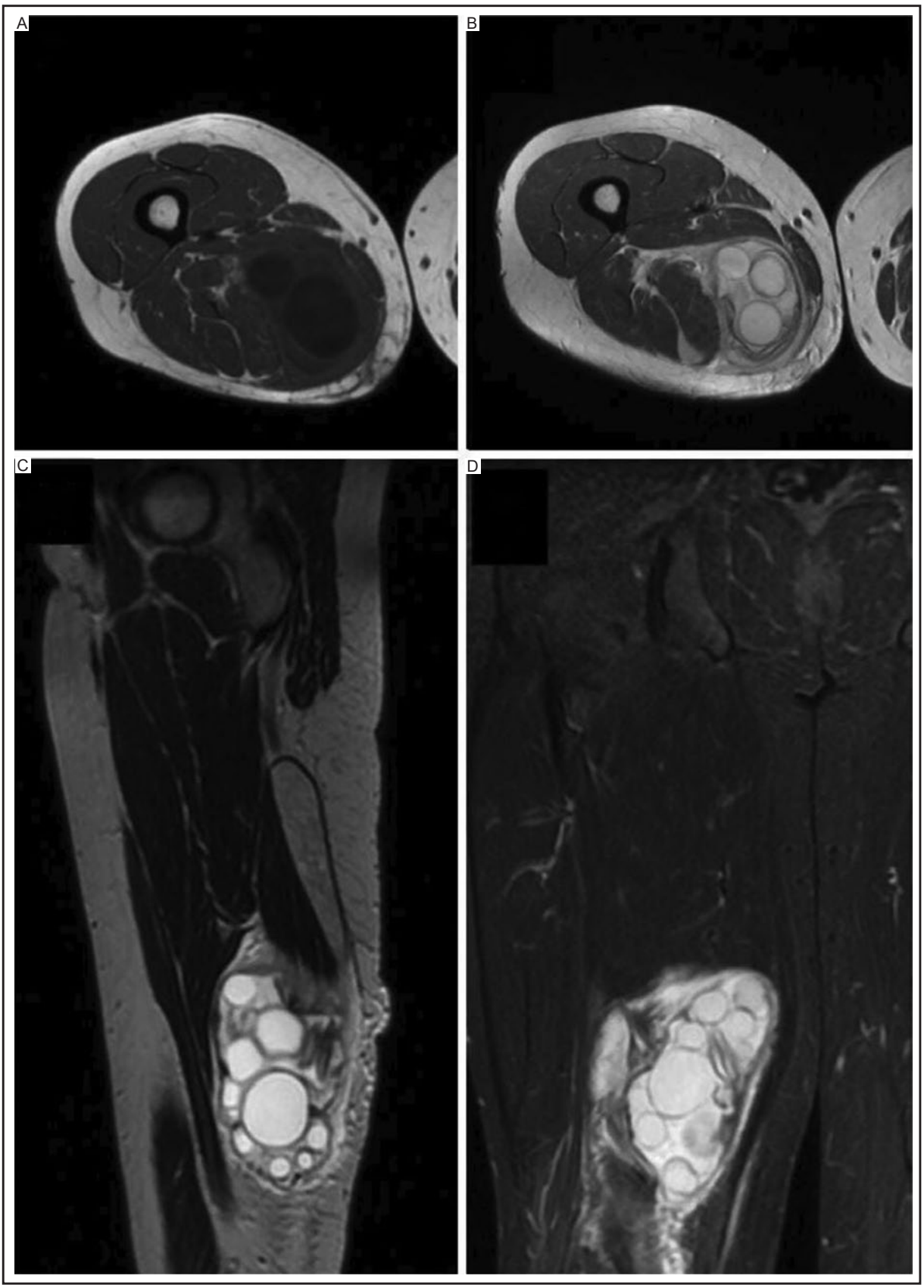

Figure 1. MR imaging of a 44-year-old patient with a deformity of the right thigh. **A:** multicystic lesion with T1 hypointensity. **B:** PD moderate signal intensity. **C:** T2 hyperintensity. **D:** STIR hyperintensity.

MR: magnetic resonance; PD: proton density.